HIGH STRENGTH CERAMICS

Final Report Submitted to the

Office of Naval Research, Metallurgy Program

Contract No. N00014-67-A-0385-0004, ONR 032-509

H. A. McKinstry and W. R. Buessem

30 March 1972

THE MATERIALS RESEARCH LABORATORY

THE PENNSYLVANIA STATE UNIVERSITY

UNIVERSITY PARK, PENNSYLVANIA

DISCLAIMER NOTICE

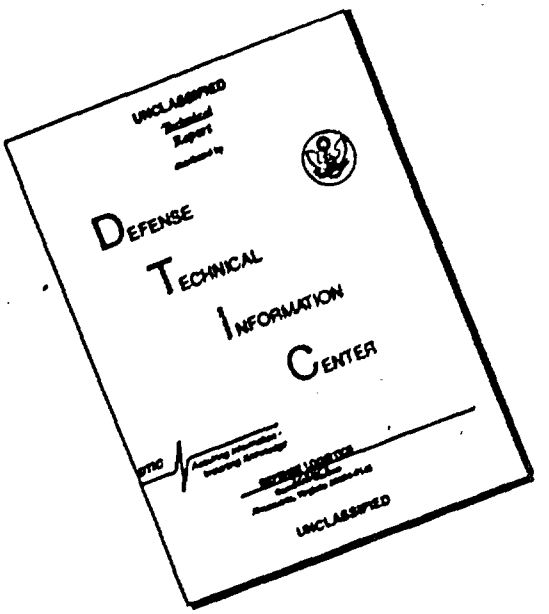

THIS DOCUMENT IS BEST QUALITY AVAILABLE. THE COPY FURNISHED TO DTIC CONTAINED A SIGNIFICANT NUMBER OF PAGES WHICH DO NOT REPRODUCE LEGIBLY.

HIGH STRENGTH CERAMICS

Final Report Submitted to the

Office of Naval Research, Metallurgy Program
Contract No. N00014-67-A-0385-0004, ONR 032-509

H. A. McKinstry and W. R. Buessem

30 March 1972

The Technical Reports, Numbers 3, 4 and 5 constitute the major part of the final report for project N00014-67-A-0385-0004, ONR 032-509, since they contain the findings that have been achieved with the finite element method. In summary these are:

STRESS RAISER

The anisotropic elastic properties of a material can act as a stress raiser. The elastic constants used for study were derived from the measured elastic compliances for alumina. In other materials the degree of anisotropy may be larger and hence more important since alumina is not the most anisotropic material. The direction of maximum anisotropy for alumina is, in terms of angles defined in Reports 3 and 4, $\alpha = 0$, $\beta = 55°$.

NOTCH FACTOR

The notch factor as calculated by Neuber for hyperbolic cross section specimens does not apply when the material is anisotropic. Instead of 1.45, the FEM value is 1.82. This latter value may not be correct since there are some obvious deficiencies in the model used. It may be even higher since the stress gradients were greater than the model was designed to handle.

NON-UNIFORM STRESS STATE

The stress increase for a bicrystal in tension was found to yield stress concentrations at the boundary as high as 1.5. It is thus seen that the assumption of uniform stress states in bicrystal mechanical response is not generally accurate.

MODEL FOR CERAMIC BODIES

A model for the study of the mechanical behavior of a polycrystalline ceramic body has been proposed. For certain selected orientations the model generates results that are consonate with reality and shows that the position of maximum shear can be shifted by a change in anisotropy. There seems to be a limit to the effect anisotropy can make on a system after the degree of anisotropy has passed a certain value.

When the model was subjected to the case of different orientation for each crystal the stress gradients which resulted were higher than could be adequately studied by the model. A further modification of the model would be necessary for the proper characterization of a ceramic body by this method.

A further technical report will be submitted when the measurements of the strain distribution in an alumina bicrystal have been completed. Thus far, the "d" spacing for the (054) diffraction peak has been measured at systematically selected points over the surface of the bicrystal. The residual strain has in this way been partially measured. Similar data are being obtained for the (330) diffraction peak. Preliminary measurements with an applied tensile stress have shown a linear relationship between applied stress and the interplanar spacing. Thus, the apparatus is seen to be in good operating condition. With additional time, the measured strain in a bicrystal of alumina under tensile loading should be completed. A request for a no-cost extension has been made.

STRESS CONCENTRATION IN ELASTICALLY ANISOTROPIC BICRYSTAL TENSILE SPECIMENS

Thomas Kovacs, Herbert A. McKinstry and W. R. Buessem

Technical Report Number 3

Office of Naval Research, Metallurgy Program
Contract No. N00014-67-A-0385-0004, ONR 032-509

30 March 1972

Materials Research Laboratory
The Pennsylvania State University
University Park, Pennsylvania 16802

Stress Concentration in Elastically Anisotropic Bi-crystal Tensile Specimens

A. Introduction

Ceramics are rapidly increasing their importance as technological materials in a number of important applications. Due to this increased interest and also because of the commercial availability of pure metal-oxide powders and single crystals, a great deal of new knowledge of their mechanical behavior is being collected. However, the progress in understanding some characteristics of the mechanical response of polycrystalline aggregates of metal oxides is seriously hampered by the inherent analytical difficulty encountered in modeling such systems.

In recent years, the problem was approached from the bi-crystal point of view [1,2,3] in order to gain insight into the process of brittle fracture at the grain boundaries. This form of failure is sometimes observed in polycrystalline metal oxides.

Brittle fracture may be induced in suitably shaped tensile specimens provided that a sufficiently high stress level is maintained in the gauge section of the specimen.

A tensile specimen generated either by a hyperboloid of revolution or by shaping the two opposing sides by hyperbolas as shown in Fig. 1, will display a substantial tensile stress at the focal plane while maintaining sufficiently low stresses at the gripping ends.

The hyperbolic tensile specimen shape was used in measuring the intrinsic brittle strength of single and bi-crystal MgO [1].

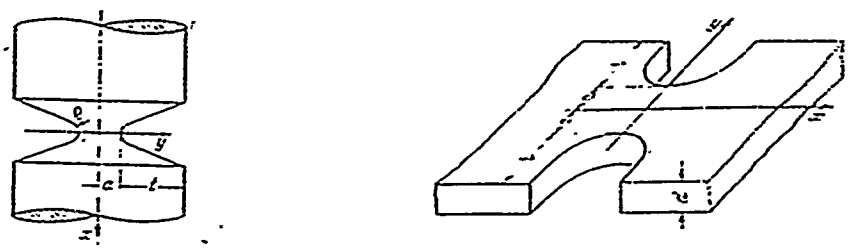

a) Axisymmetric b) Planar

Fig. 1. Hyperbolic Tensile Specimens.

The stress distribution in hyperbolic tensile specimens was studied by Neuber [4] and by Leven [5]. A stress concentration factor or notch factor for homogeneous and isotropic specimens was calculated from an exact theory and was experimentally confirmed to be accurate within a few percent.

Some recent investigations [6] however, considered the influence of elastic mismatch across a planar boundary in rectangular bi-crystal tensile specimens. It was shown that the anisotropy of elastic properties as well as the elastic mismatch produce similar effects to that of notches in the tensile specimens.

Various attempts have been made [7] to find an exact and general solution for the problem of stress distribution in anisotropic bodies bounded by cylindrical surfaces. The theoretical approach was successful only for infinitely large bodies bounded by planes or parabolic surfaces. The introduction of the necessary finite boundary conditions to delimit a finite body would prevent solution.

An attempt is made here to formulate the problem in such terms that an approximate method of analysis could be applied, which as a limit, would converge to the exact solution.

B. Method of Analysis

Since a closed form exact solution is not available for anisotropic finite bodies at the present time, a solution based on the calculated stiffness of the anisotropic finite continuum was sought. This method of analysis has been used in the past in various forms such as "Moment Distribution" or "Deflection Analysis" of structural elements. The Finite Element Method (F.E.M.) of analysis and its terminology was first formulated by M. J. Turner et al. [8] and it was first applied in its present form to an elastic continuum by R. W. Clough [9]. It has been shown repeatedly [10,11] that, while the method of analysis is approximate, it converges to the exact solution as the limiting value.

The first step of applying the F.E.M. analysis is to divide the finite elastic continuum into polygonal elements. The elements are usually triangular or quadrilateral in shape. The elements are considered to be jointed at their corners (the nodal points) and the stiffnesses of the individual elements are assumed to interact through these mutual nodal points.

The choice of element size requires some experience of the user so that the possible error in the calculations is minimized for a given number of elements. The model used is shown in Fig. 2.

It was shown by Wilson [12] that the error E for the displacements u_j of a nodal point j is:

$$E_{(u)_j} = \frac{1}{2}\left(x_j^2 \frac{\partial^2 u}{\partial x^2} + 2x_j y_j \frac{\partial^2 u}{\partial x \partial y} + y_j^2 \frac{\partial^2 u}{\partial y^2} \right) \qquad (1)$$

where x,y are the coordinates of the nodal point j.

The error term demonstrates the influence of both the element size and that of the rate of change of strain. Since the rate of change of strain is determined by the geometry of the problem, the proper choice of element size will improve accuracy.

While it is generally true that convergence of finite element solution increases with decreasing element size, the gain is sometimes offset by the increase in the "round-off" error resulting from the limited word length of electronic digital computers.

In the stiffness formulation of F.E.M. analysis the unknowns of the continuum are the nodal displacements. The basic equation which relates nodal displacements to the nodal forces F will always take the form [10] in matrix notation:

$$\{F\} = [K]\ \{u\} \tag{2}$$

where [K] is the stiffness matrix of the continuum. The global stiffness matrices are defined as:

$$[K] = [B]^T[D][B] \times \text{volume} \tag{3}$$

In Equation (3), [B] and [D] represent the displacement-strain and stress-strain matrices respectively.

The global stiffness matrix is symmetric and only the boundary conditions render it non-singular. Since the stiffness of a particular nodal point is defined by the combined effects of only those elements which contain that particular nodal point, the stiffness matrix is large and is very sparsely populated. An efficient computer storage scheme is a necessity to handle large problems successfully.

Once the global stiffness matrix is developed, the unknown nodal displacements are calculated from equation (2).

The element strains and stresses are computed from the relations:

$$[\varepsilon] = [B][u] \tag{4}$$

$$[\sigma] = [D][\varepsilon] \tag{5}$$

The continuity between the elements is assumed by a suitable linear polynomial expression for [B] to relate displacements within the triangular elements to that of stress.

The stress-strain relationship in terms of the principal technical constants E, G and U, (Young's modulus, shear modulus and Poisson's ratio respectively) is given in general form (6).

$$\begin{aligned}
\varepsilon_x &= \frac{1}{E_1}\sigma_x - \frac{\nu 21}{E_2}\sigma_y - \frac{\nu 31}{E_3}\sigma_z \\
\varepsilon_y &= \frac{-\nu 12}{E_1}\sigma_x + \frac{1}{E_2}\sigma_y - \frac{\nu 32}{E_3}\sigma_z \\
\varepsilon_z &= \frac{-\nu 13}{E_1}\sigma_x - \frac{\nu 23}{E_2}\sigma_y + \frac{1}{E_3}\sigma_z \\
\gamma_{xy} &= \frac{1}{G_{12}}\sigma_{xy}
\end{aligned} \tag{6}$$

Isotropy is re-established by the proper choice of the principal technical constants, i.e., $E_1=E_2=E_3 = E$; $\nu_{12}=\nu_{21}$ and $G_{12} = E/2(1+\nu)$.

An excellent description of this technique is given by Zienkiewicz and Chung in their book [10]. The actual matrix manipulations for any sizable finite body can only be accomplished by digital computers of storage capacity in excess of 100 Kbytes.

The computer program used in this investigation was written in its original form by H. D. Dahl [13] and was extensively modified for the present purpose. The program is written in FORTRAN IV language and consists of a main routine which in turn calls for subroutines during the processing of input data. The method of solution of the large number of simultaneous linear equations of expression (2) is an iterative technique based on the Gauss-Seidel over-relaxation method. The computer output consists of the re-print of input data, calculated nodal point displacements and of the stresses at the centroid of each element.

C. Stress Distribution in Isotropic Specimens

The nature of stress concentration in hyperbolic specimens is now well understood due to the pioneering work of Neuber in the early 1930's. It was shown [4] that in homogeneous and isotropic flat specimens under pure tension the principal stresses σ_u and σ_v may be calculated readily from the equations:

$$\sigma_u = \frac{A}{h^2} \cosh u \cos v \left(2 + \frac{\cos^2 v_o - \cos^2 v}{h^2}\right)$$

$$\sigma_v = \frac{A}{h^4} \cosh u \cos v \left(\cos^2 v - \cos^2 v_o\right) \qquad (7)$$

$$\text{where } A = P \frac{\sin v_o}{v_o + \sin v_o \cos v_o}$$

$$\text{and } h^2 = \sinh^2 u + \cos^2 v$$

u and v are elliptic coordinates, related to the cartesian coordinates by

$$x = \sinh u \cdot \cos v$$

$$y = \cosh u \cdot \sin v \qquad (8)$$

The curves with u = const. are ellipses, those with v = const. are hyperbolas.

The surface of the hyperbolic specimen is given by $v = \pm v_o$. The waist of the specimen is defined by

$$x = u = o$$

$$y_{v=v_o} = \sin v_o = a \tag{9}$$

Equation (7) gives the principal stresses in terms of p, the average axial stress in the focal plane of the specimen. It is obvious that both stresses have their maximum in the focal plane; the values follow from Equation (7) by setting u = 0. For axisymmetrical specimens generated by a hyperboloid of revolution the equations are slightly more complex and for the focal plane the stress equations can be written in the form:

$$(\sigma_u)_{u=o} = \frac{1}{h^2}\{B\cos v + C\,[1-(\alpha+2)]\cos v\} + \frac{\cos v}{h^4}\{B + C\cos^2 v - A\}$$

$$(\sigma_v)_{u=o} = \frac{1}{h^2}\{C\cos(\alpha-1) - A\frac{\cos v}{1+\cos v}\} + \frac{\cos v}{h^4}\{A - B - C\cos^2 v\} \tag{10}$$

$$(\sigma_w)_{u=o} = \frac{1}{h^2}\{A\frac{\cos\nu}{1+\cos\nu} - B\cos\nu + C\cos\nu\,(\alpha-2)\}$$

$$h^2 = \sinh^2 u + \cos^2 v$$

$$\alpha = 2(1-\nu)$$

$$A = C(\alpha-1)\,(1+\cos v_o)$$

$$B = A - C\cos^2 v_o$$

$$C = \frac{P}{2}\left(\frac{1+\cos v_o}{1+(2-\alpha)\cos v_o + \cos^2 v_o}\right)$$

ν = Poisson's ratio

The elliptic coordinates used here are defined by:

$x = \sinh u \cos v$

$y = \cosh u \sin v \cos w$

$z = \cosh u \sin v \sin w$

The surfaces with u = constant are ellipsoids,

those with v = constant are hyperboloids

and those with w = constant are planes through the x-axis.

The specimen is bounded by the hyperboloid $v = v_o$.

The photoelastic measurements of Leven (5) showed that the numerical values calculated from the above equations are within a few percent of those measured experimentally. In Fig. 3a and 3b, the axial and transverse stress distribution are plotted in terms of p, the maximum nominal stress. The parameters of the generating hyperbola for both flat and axisymmetrical specimens were chosen as 0.00098 for a^2 and 0.00124 for b^2 respectively, where a^2 and b^2 are the constants in the equation defining the surface of the flat specimen (hyperbola symmetrical to the y-axis)

$$\left(\frac{y}{a}\right)^2 - \left(\frac{x}{b}\right)^2 = 1 \tag{11}$$

Using Neuber's parameter, v_o, defining the same surface, one can write this equation

$$\left(\frac{y}{\sin v_o}\right)^2 - \left(\frac{x}{\cos v_o}\right)^2 = 1 \tag{12}$$

Since

$$\sin^2 v_o + \cos^2 v_o = 1 \tag{13}$$

one has to multiply a^2 and b^2 with a normalization factor, f^2, so that the last equation is satisfied. ($f^2 = 450$, $f = 21.5$) It follows that $\sin^2 v_o = 0.44$ and $\cos^2 v_o = 0.56$. Inserting v_o in Equation (7) gives the curve plotted in Fig. 3a as Nueber's exact solution.

The procedure for the axisymmetrical case, plotted in Fig. 3b, is analog.

The above analyses were repeated using the "Finite Element" method. For the purpose of analysis a model was constructed consisting of 288 elements and 175 nodal points to represent the transverse half of the tensile specimen as shown in Fig. 2. The numerical results of the F.E.M. analysis are also shown in Figs. 3a and 3b. It can be seen that the "Finite Element" analysis produces a very close set of results, within about 5 percent of the "exact" solution of Neuber. Some part of this error may be due to the fact that the triangular elements are finite in size and they are located slightly on one side of the focal plane. The other possible source of error is that the strain is considered constant in any one element. Since the rate of change of strain is large in the immediate vicinity of the focal section, even a small finite element size introduces some error in the actual numerical value. The accuracy may be increased, especially in the area near the edge of the specimen, by refining the triangular mesh used.

In this instance, however, the stress distribution follows a continuous and smooth curve, thus a relatively accurate extrapolation of F.E.M. data points to the hyperbolic boundary is possible.

The "exact" and F.E.M. analyses of isotropic tensile specimens served usefully for checking the relative accuracy of the crystal model and that of the computing process.

D. Stress Distribution in Anisotropic Single Crystal Tensile Specimens

Some previous investigations (6) showed that the anisotropy in elastic properties exerts considerable influence on the stress distribution within the anisotropic body.

The results of the investigation of the influence of anisotropic mechanical properties on the stress distribution are presented here for MgO

and Al_2O_3. The principal reason for choosing these two materials is the availability of reliable elastic data in the form of compliances. Also, the crystallographic symmetries of MgO and Al_2O_3 are representative of a large number of ceramic materials.

The values of the principal technical constants of MgO and Al_2O_3 were calculated [7] from the compliance matrices of Chung [14] and of Gieske [15] respectively.

Some selected values of Young's moduli of alumina are shown in Figs. 4a, 4b and 4c. In these polar diagrams the anisotropy in the Young's moduli are shown in the plane perpendicular to one of the two-fold axes. By a polar rotation of approximately 55° in alumina, the elastic axes may be brought into a position where the difference between the moduli in direction of the hexad axis and one of the diad axes is at a maximum. That it is a real maximum can be seen from Fig. 4b where the polar diagram of Young's moduli is shown in the plane perpendicular to that of the plane of Fig. 4a. The other point of significance may be that where the moduli show isotropy in the plane perpendicular to the tensile direction. This point is found at approximately 10° away from the original setting of axes. Similarly, in Fig. 4c the variation of Young's moduli is shown in the plane perpendicular to the plane of Fig. 4a and rotated by 10° from the original setting.

Similar diagrams are presented in Figs. 5a and 5b where the variation of Young's moduli of magnesia is shown. The maximum anisotropy occurs at 45° rotation between the <100> and <111> directions. The anisotropy in the plane perpendicular to that of Fig. 5a is indicated in Fig. 5b where it can be seen that while the absolute elastic values increase, the relative difference between them reduces. Based on this set of elastic data, a number of representative orientations was chosen to keep the computational work within manageable limits.

The calculated elastic properties and the corresponding orientations are tabulated in Table 1.

It must be mentioned at this stage, that the stress analysis of anisotropic specimens of axisymmetrical shape would require a full three-dimensional analysis to obtain meaningful results. This, however, is outside the capability of the present computer program used in these analyses. This work therefore is restricted to the analysis of flat-hyperbolic specimen shapes.

Figs. 6 and 7 show the results of analysis for the flat-hyperbolic specimens of alumina and magnesium-oxide, respectively. The stress distribution is again shown as a dimensionless stress concentration factor similar to the isotropic case. It can be seen that while the general appearance of the distribution curve is unchanged, the maximum stress concentration ranges from about 1.45 to approximately 1.32 depending on the selected combination of elastic constants.

Since the orientations were chosen to include the limiting maximum and minimum elastic properties, it is probable that the values of 1.45 and 1.82 are the minimum and maximum concentration factors for all orientations in alumina.

Similarly, the range of stress concentration factors in magnesium oxide is found between 1.45 and 1.65. It may be significant that the range of stress concentration factors for alumina and magnesia is somewhat in proportion to their relative degree of anisotropy.

E. Stress Distribution in Anisotropic Bi-crystal Tensile Specimens

For this part of the analysis the bi-crystal was assumed to be composed by joining a combination of single crystals whose anisotropic stress distribution was studied in the previous section. This would demonstrate the

TABLE 1

CRYSTAL ORIENTATION AND ELASTIC PARAMETERS FOR Al_2O_3 and MgO.

IDENTIFICATION	MATERIAL	$\alpha°$	$\beta°$	E_1 ($\times 10^6$ lb/in^2)	E_2 ($\times 10^6$ lb/in^2)	G ($\times 10^6$ lb/in^2)	μ_{21}	ν_{21}
A	Al_2O_3	0°	10°	61.73	64.93	22.80	0.271	0.258
B	"	0°	55°	61.73	59.00	19.80	0.114	0.119
C	"	0°	100°	61.73	64.93	21.76	0.212	0.201
D	"	0°	145°	61.73	49.05	25.50	0.271	0.340
E	"	0°	55°	49.05	61.73	25.50	0.340	0.271
F	"	0°	55°	49.05	59.00	28.01	0.335	0.278
G	"	0°	145°	59.00	61.73	19.80	0.119	0.114
H	MgO	0°	45°	36.23	46.46	22.57	0.312	0.243
J	"	0°	135°	46.46	36.23	22.57	0.243	0.312

influence of a boundary between two discretely adjoined anisotropic bodies. The bi-crystal boundary was chosen such that it lies perpendicular to the tensile axis and is located at the waist section.

In Table 2 the combination of the bi-crystals is presented together with a summary of the "Axial Notch Factor" and derived by FEM for each of the composing single crystals as calculated in Section D.

The analytical results are presented in graphical form in Figs. 8 and 9.

It is easily observed that the axial stress distribution along the focal plane is, with the exception of one case, unchanged compared to the axial stresses computed for individual single crystals. It appears in general, that the component of stress perpendicular to a boundary is largely defined by the elastic anisotropy of the crystals located at either side of the boundary, and it is influenced only to a small extent by the mutual restraining influence on each other at the boundary.

The transverse stress distribution in the bi-crystals is not as clear as was found for the normal stresses. For example, in the bi-crystal specimen A, the top half of the system showed a reduction in the maximum value of approximately 43%, allowing for a negative stress concentration at the outer edges of approximately 0.220. The lower half increased its maximum by about 18%.

A somewhat analogous situation was found in the bi-crystal specimen D, though the numerical values were not so extreme as in the case A discussed above. In both specimens B and C the transverse stress concentration was found unchanged.

Since there were only four combinations studied it could be dangerous to attempt wide generalizations. However, it appears that those bi-crystal specimens whose composing shear moduli are widely different will display changes in their tangential stress component, while those bi-crystals of approximately the same shear moduli will behave like two individual single crystals with no mutual influence.

Table 2. Tabulation of FEM Notch Factor

	Elastic Properties Identification from Table 1		Notch Factor		
	Upper Half	Lower Half	Upper Half		Lower Half
Single Crystal	Isotropic	Isotropic		1.45*	
	A	A		1.71	
	B	B		1.82	
	C	C		1.71	
	D	D		1.65	
	E	E		1.52	
	F	F		1.47	
	G	G		1.80	
Bicrystal	B	D	1.85		1.61
	B	G	1.82		1.82
	B	F	1.52		1.50
	B	F	1.79		1.61

*Same as Nueber's calculated value 1.454.

F. Discussion of Results

The results show that the elastic anisotropy of the material has an effect on the Neuber notch factor for samples with a hyperbolic cross section.

The maximum effect for constants derived from alumina, using values for maximum anisotropy, is 25% more than the Neuber value for an isotropic specimen. The use of two different crystals, top and bottom, does not enhance this value, and the two halves seem to act independently of each other. This latter result indicates what seems to be a deficiency in the model and led to the discovery of two other results that confirm this suspicion.

For two cases, Figs. 9a and 9d, the transverse forces do not come to zero at the edge of the model. This is a violation of the known boundary conditions and seems to indicate the presence of very much higher stress gradients than the present configuration of the model can cope with. There is another indication that a finer mesh model is needed: the integrated force, across the focal plane for the normalized force used, should equal one. This condition is satisfied only for the isotropic case where the FEM results agree with the Neuber result.

The model used as indicated in Fig. 2, is composed of 288 triangles but in the region of the focal plane from which the results are obtained there are only 6 triangles. It is likely that this is too coarse a mesh in this region so that the results are affected by this choice of model division.

The presence of an enhanced notch factor in these results seems to indicate that in a refined model the effect might be even more pronounced, since it is established that there are stress gradients present that are higher than this model can take into account.

G. Conclusions

The finite element method as applied to the study of ceramic materials offers a means of understanding the effect of elastic anisotropy and elastic

mismatch on a boundary. The use of the hyperbolic shape adds a complicating additional factor to the interpretation, since the shape effects the stress concentration more than the elastic properties do.

In order to evaluate the elastic effects in this configuration a finer mesh model should be used.

References

1. F. F. Lange and W. R. Buessem, "Intrinsic Brittle Strength of Magnesium Oxide Bi-Crystals," J. Appl. Phys., 38 [5] 2013-23 (1967).

2. R. J. Stokes, "Thermal-Mechanical History and the Strength of Magnesium Oxide Single Crystals: I, Mechanical Tests," J. Amer. Ceram. Soc., 48 [2] 60-67 (1965).

3. R. J. Stokes, "Dislocation Sources and Strength of Magnesium Oxide Single Crystal," Trans. AIME, 224, 1227-37 (1962).

4. N. Neuber, Kerbspannugslehre (English Trans: U.S. Atomic Energy Com. Trans. S. AEC-tr-4547), Springer-Verlag, Berlin (1937).

5. M. M. Leven, "A New Material for Three-Dimensional Photoelasticity," Proc. Soc. Exp. Stress Anal., 6 [1] 19-28 (1948).

6. J. E. Gagorik, R. A. Queeney and H. A. McKinstry, "Stress Distributions in Al_2O_3 Bi-Crystal Tensile Specimens," J. Amer. Ceram. Soc., 54 [12] 625-27 (1971).

7. S. G. Lekhnitskii, Theory of Elasticity of an Anisotropic Elastic Body. Holden-Day Inc., San Francisco, 1963.

8. M. J. Turner, R. W. Clough, H. C. Martin and L. J. Topp, "Stiffness and Deflection Analysis of Complex Structures," J. Aero. Sci., 23 [9] 805-23 (1956).

9. R. W. Clough, "The Finite Element Method in Plane Stress Analysis," Proc. 2nd ASCE Conf. on Electronic Computation, Pittsburgh, Pa. (1960).

10. O. C. Zienkiewicz and Y. K. Cheung, The Finite Element Method is Structural and Continuum Mechanics. McGraw-Hill Publishing Co. Ltd., New York, 1967.

11. P. Tong and T. H. H. Pian, "The Convergence of Finite Element Method in Solving Linear Elastic Problem," Int. J. Solids and Struct., 3 [5] 865-79 (1967).

12. E. L. Wilson, "Finite Element Analysis of Two-Dimensional Structures," Ph.D. Dissertation, University of California, Berkeley, (1963).

13. H. D. Dahl, "A Finite Element Model for Anisotropic Yielding in Gravity Loaded Rock," Ph.D. Dissertation, The Pennsylvania State University (1969).

14. D. H. Chung, "Elastic Anisotropy of Single-Crystals and the Polycrystalline Isotropic Elastic Moduli of Solids," Ph.D. Dissertation, The Pennsylvania State University (1966).

15. J. H. Gieske, "The Third Order Elastic Coefficients and Some Anharmonic Properties of Aluminum Oxide," Ph.D. Dissertation, The Pennsylvania State University (1968).

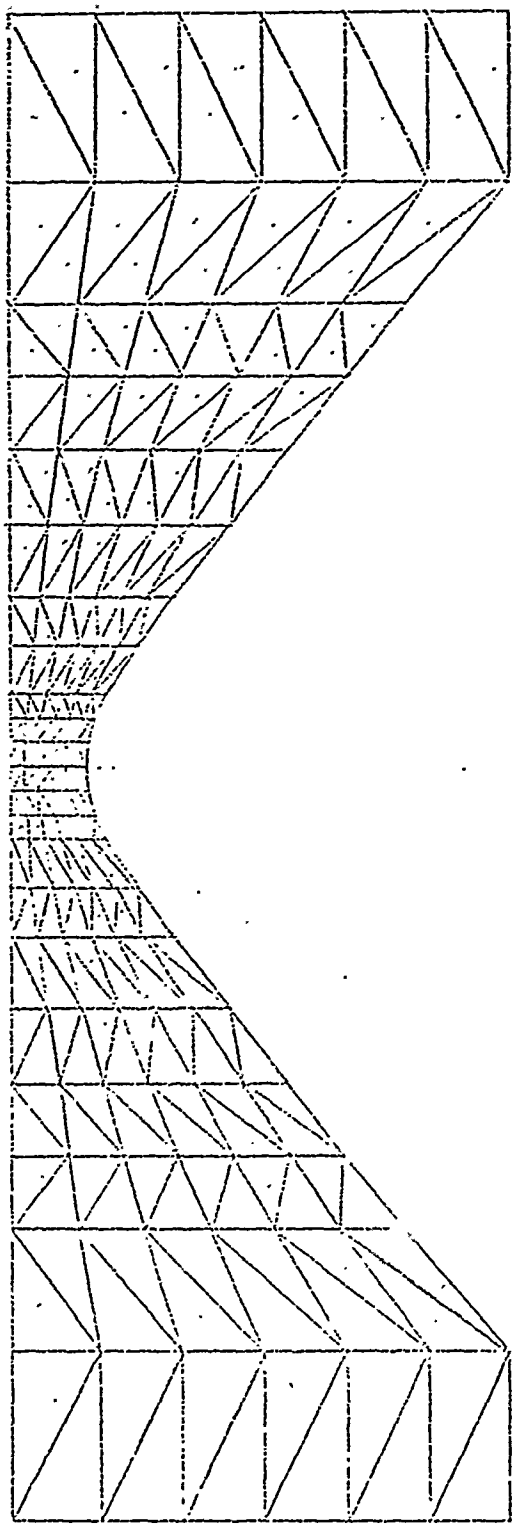

Fig. 2: The transverse half of the F.E.M. hyperbolic model.

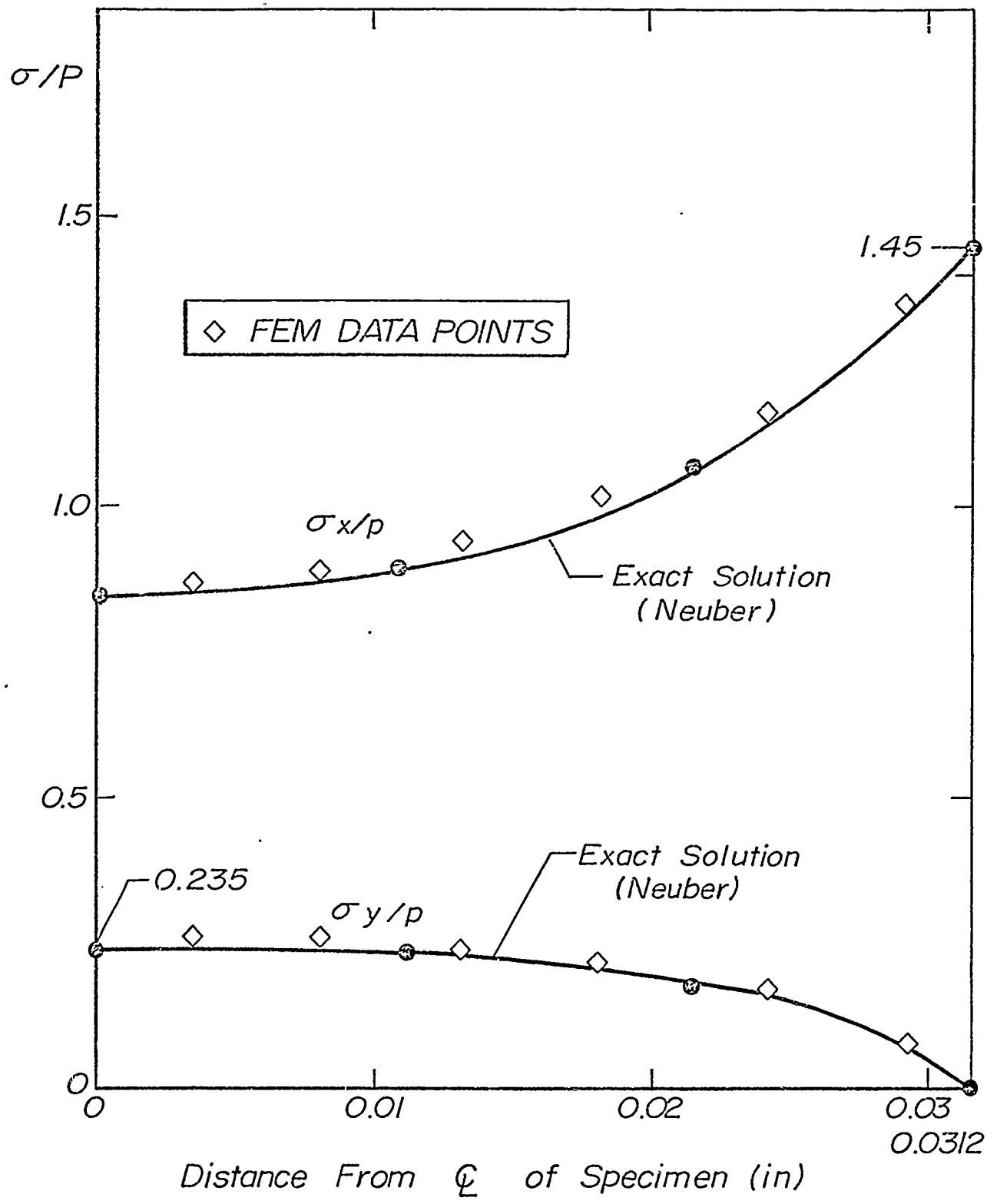

Fig. 3a: Comparison of Exact and F.E.M. Isotropic Solutions for Axial and Radial Stresses (Flat Hyperbolic Specimen).

Preceding page blank

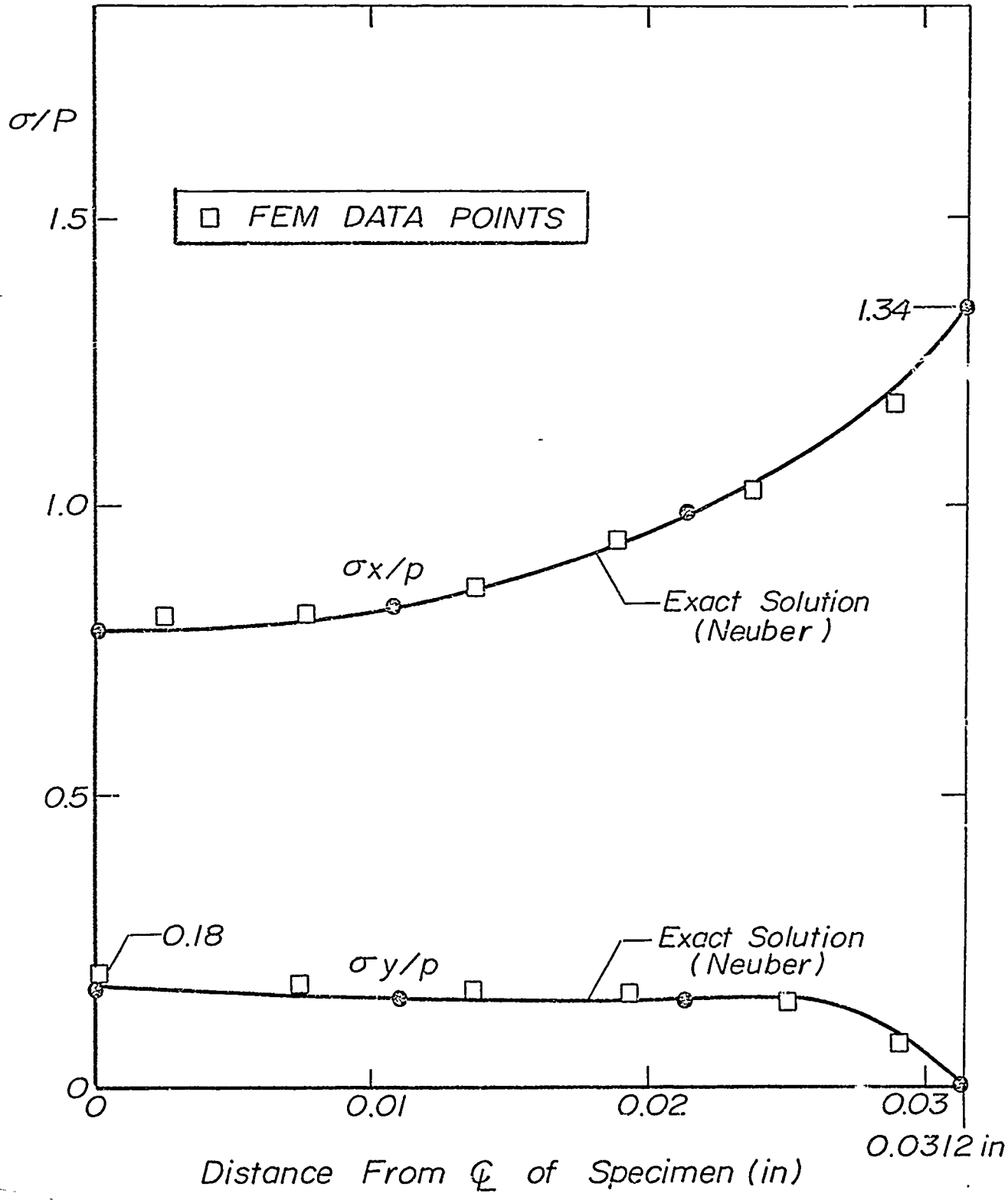

Fig. 3b: Comparison of Exact and F.E.M. Isotropic Solutions for Axial and Radial Stresses (Axisymmetric Specimen).

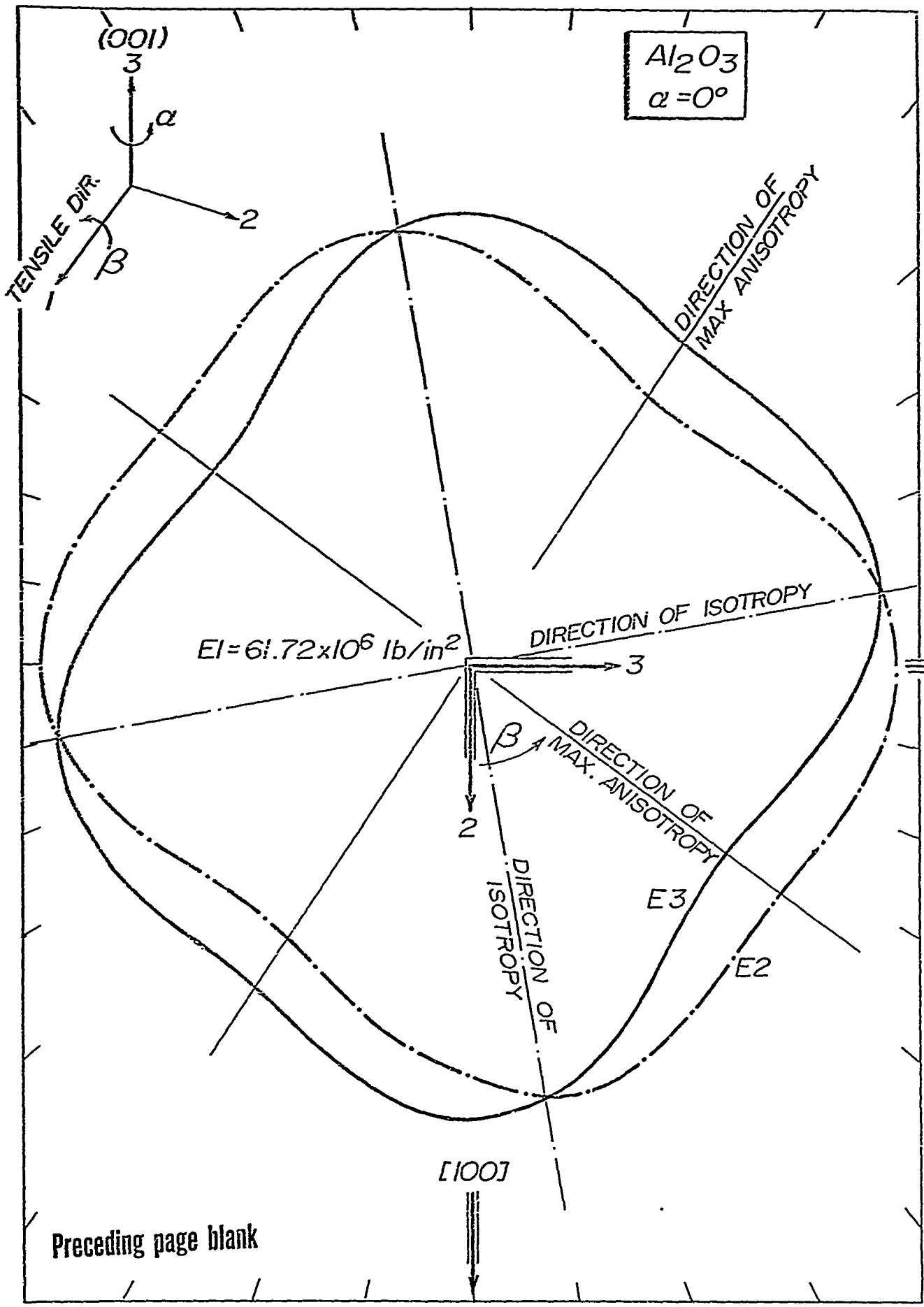

Preceding page blank

Fig. 4a: Variation of Young's moduli for alumina.

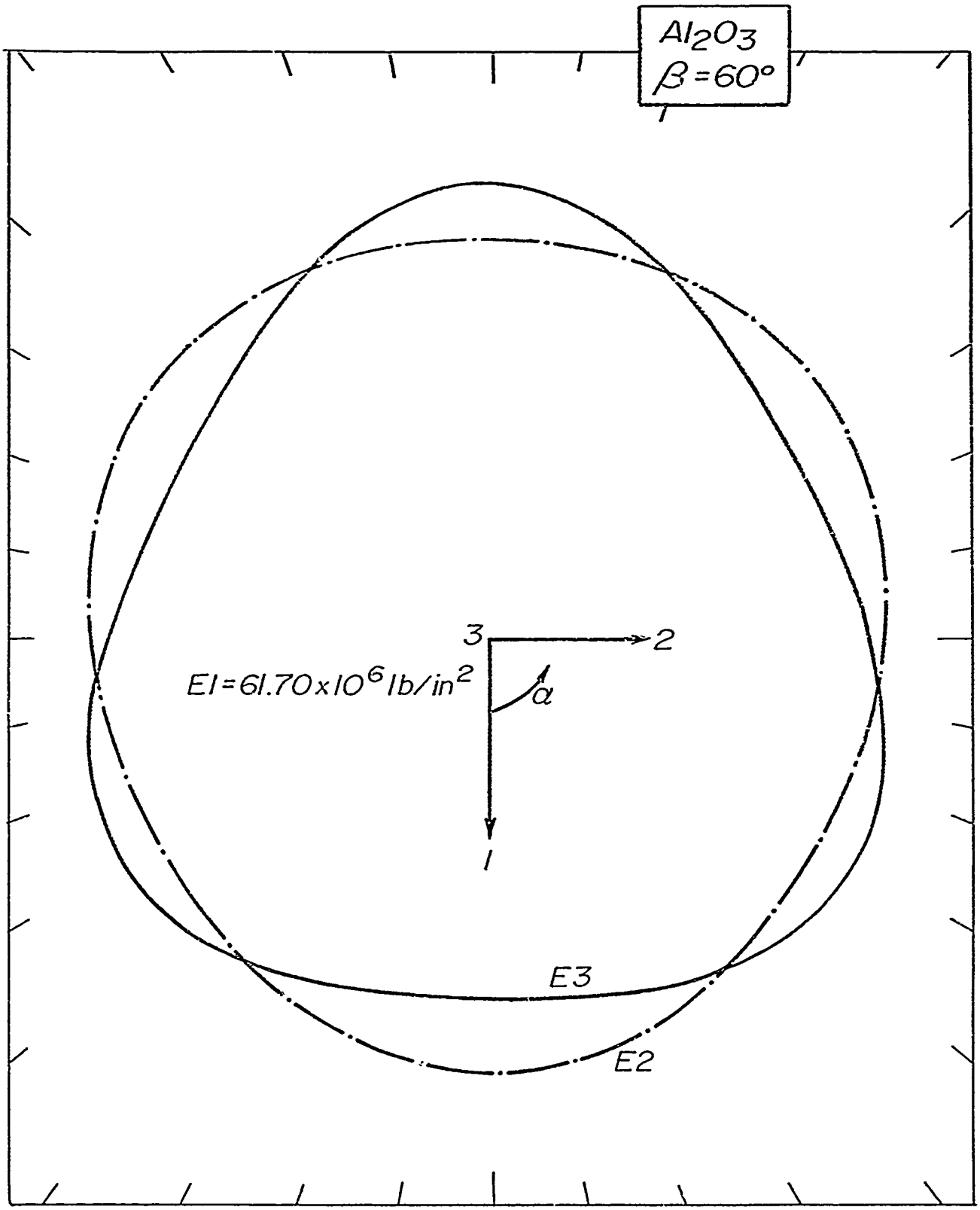

Fig. 4b: Variation of Young's moduli for alumina.

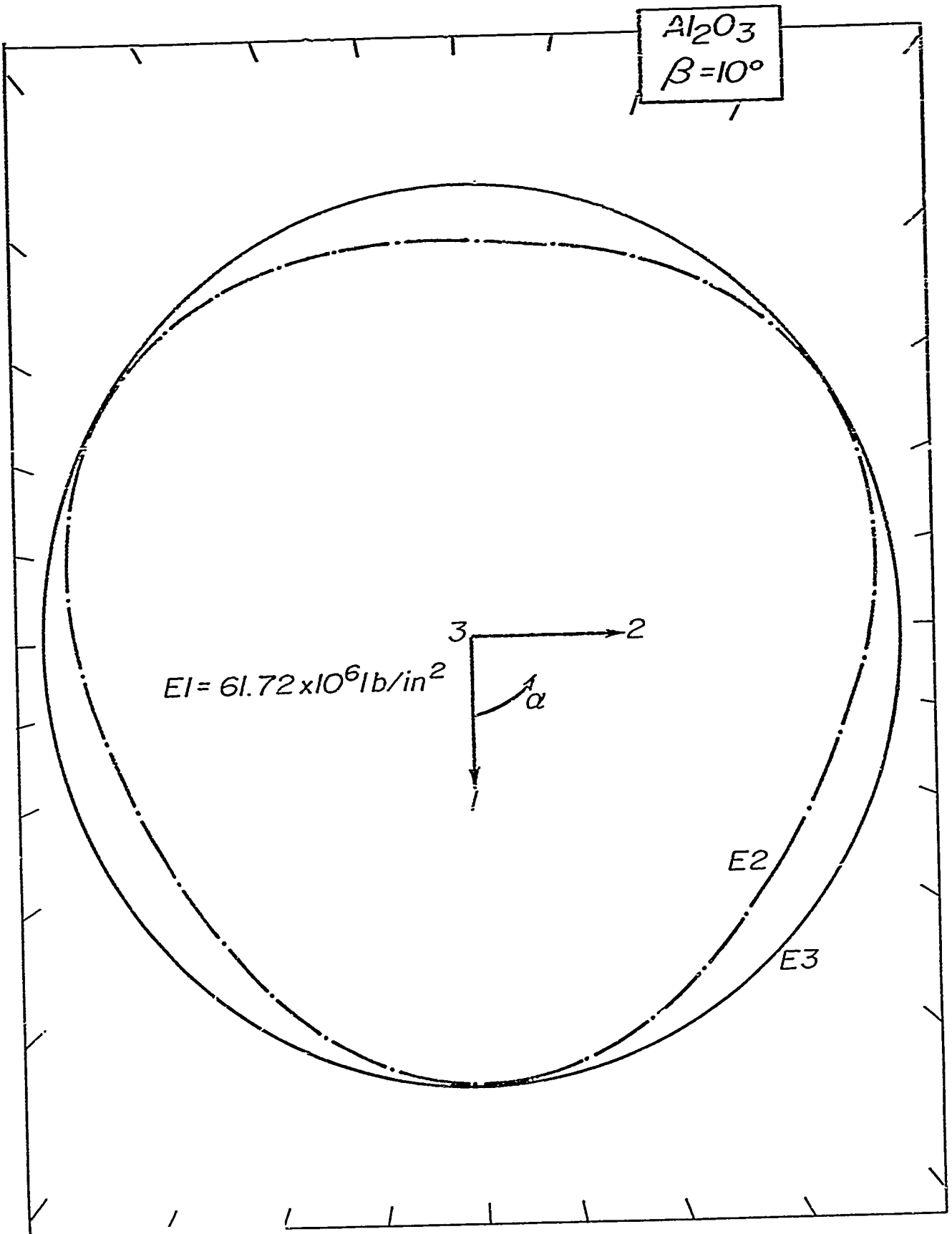

Preceding page blank

Fig. 4c: Variation of Young's moduli for alumina.

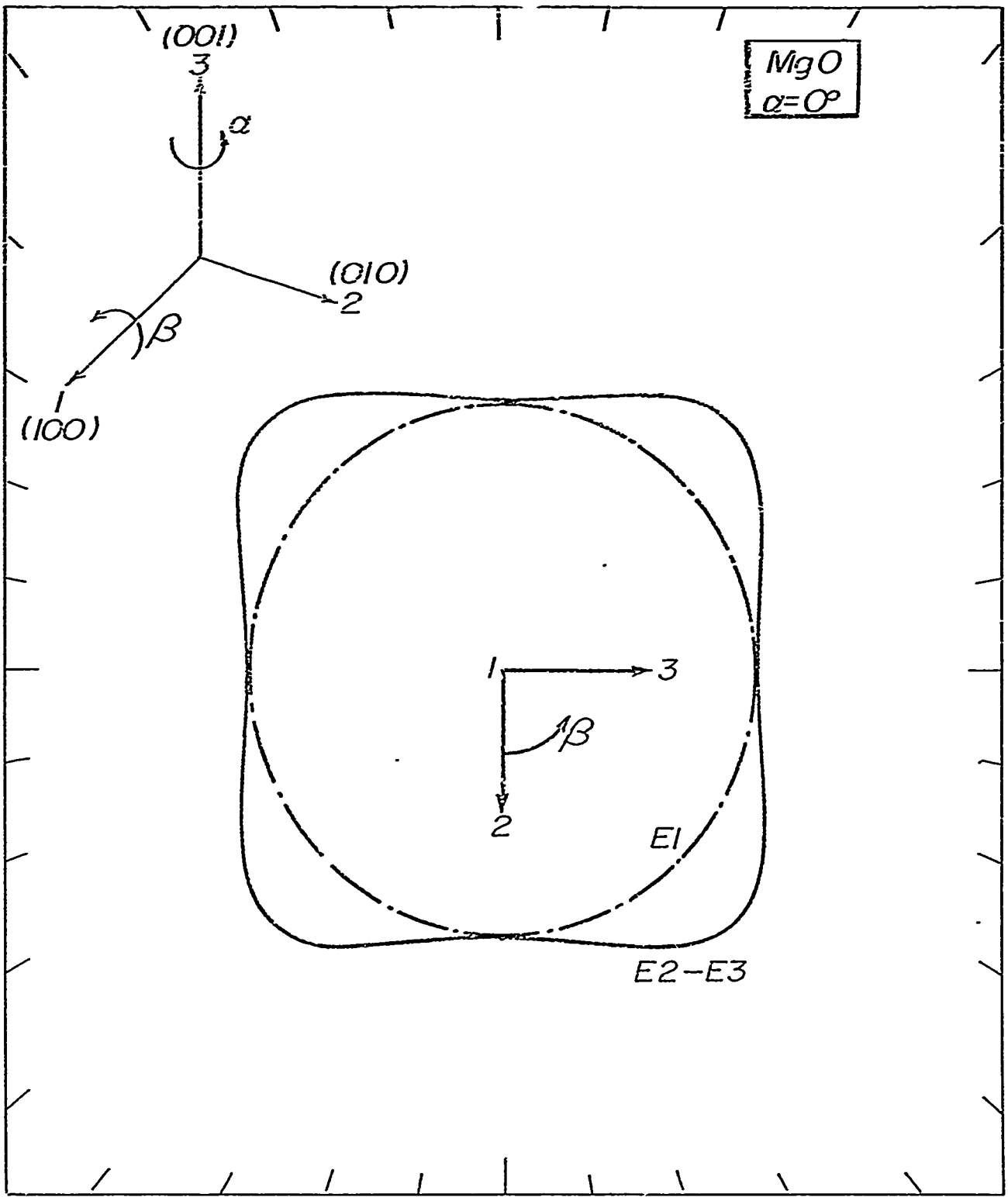

Fig. 5a: Variation of Young's moduli for magnesia.

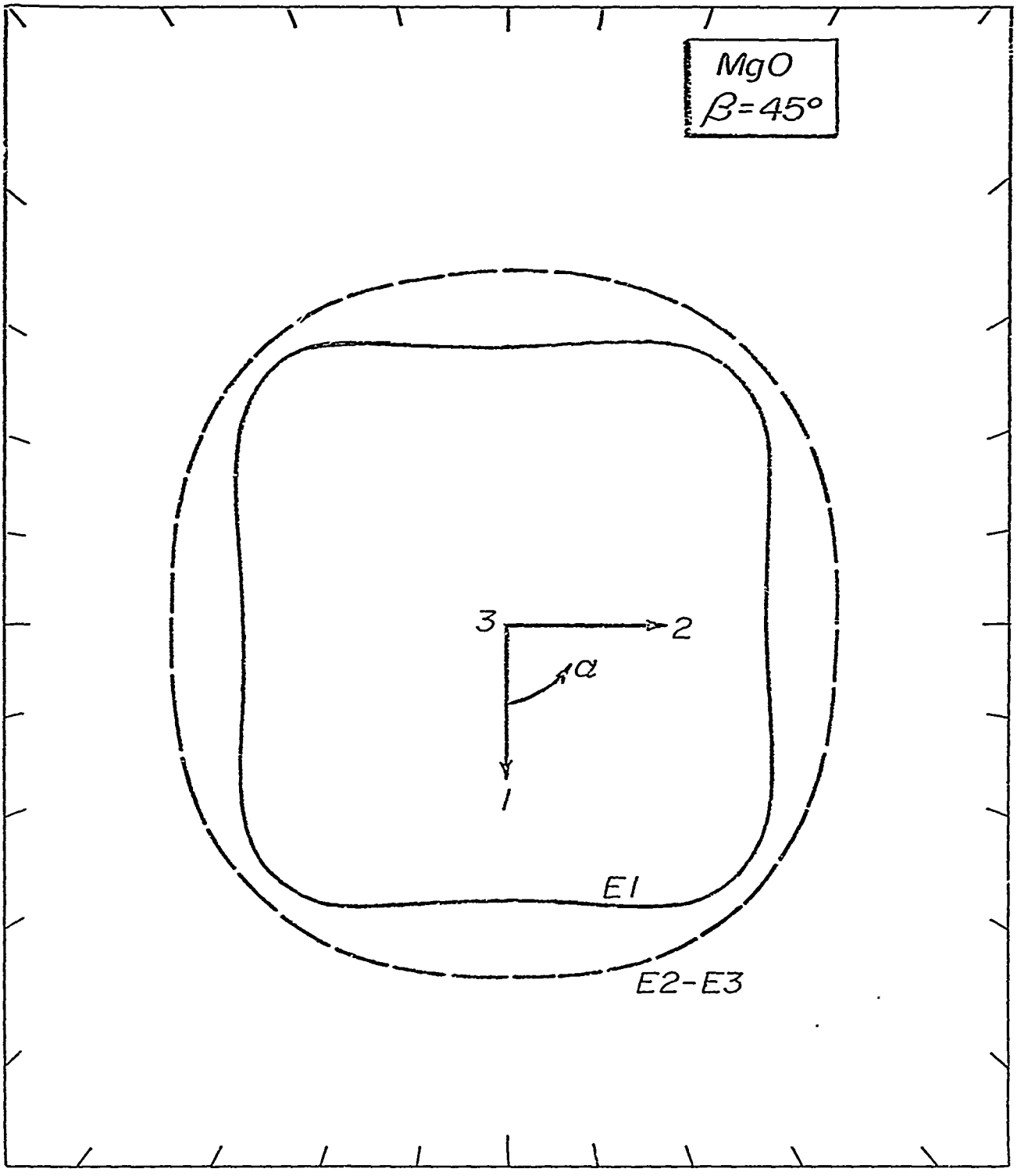

Fig. 5b: Variation of Young's moduli for magnesia.

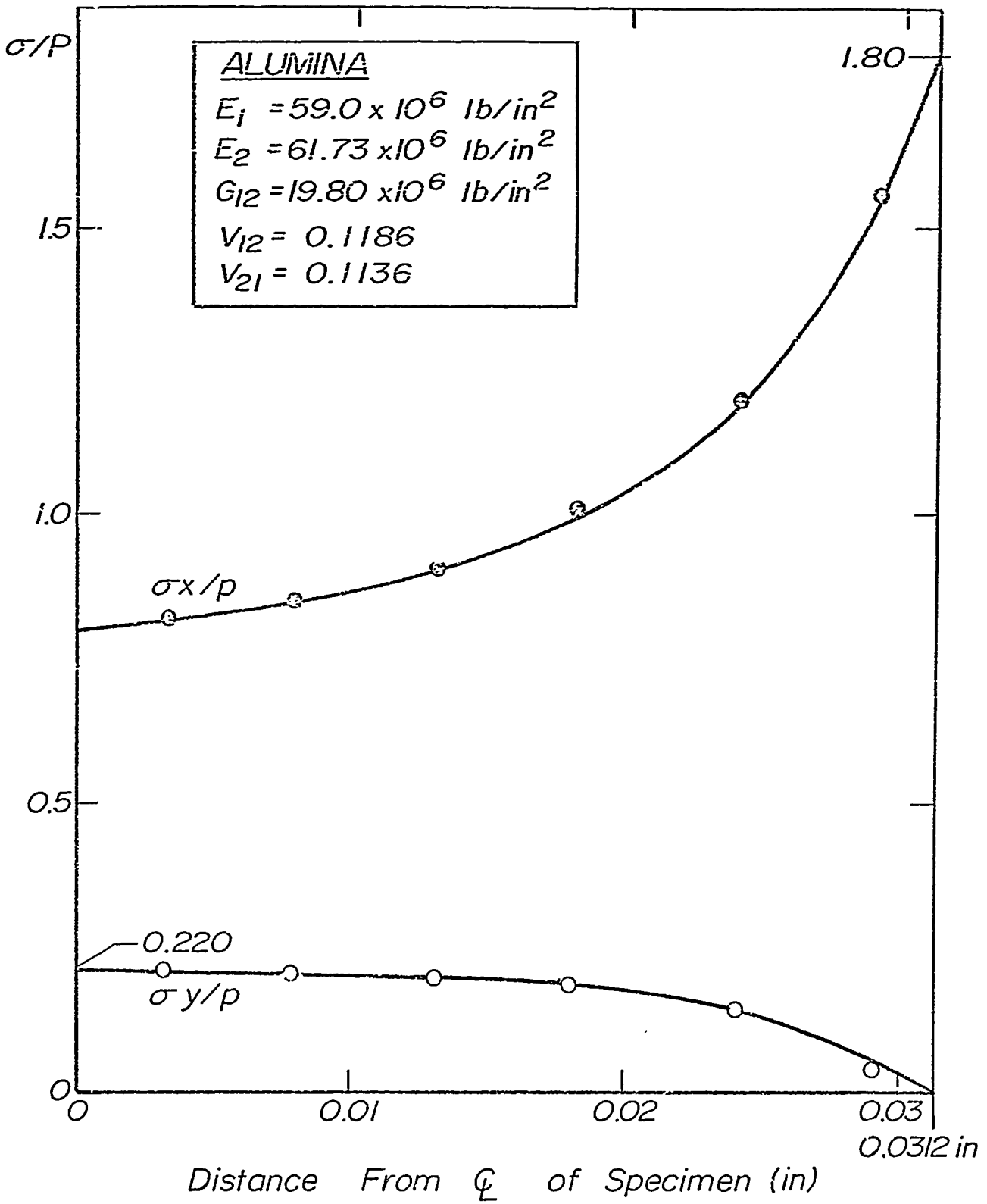

Fig. 6a: Stress distributions of the flat hyperbolic specimen of alumina. Both top half and bottom half of the model are the same anisotropic material. The curves for two different orientations were so similar they are plotted as one. The elastic parameters are those corresponding to identidications A and C in Table 1.

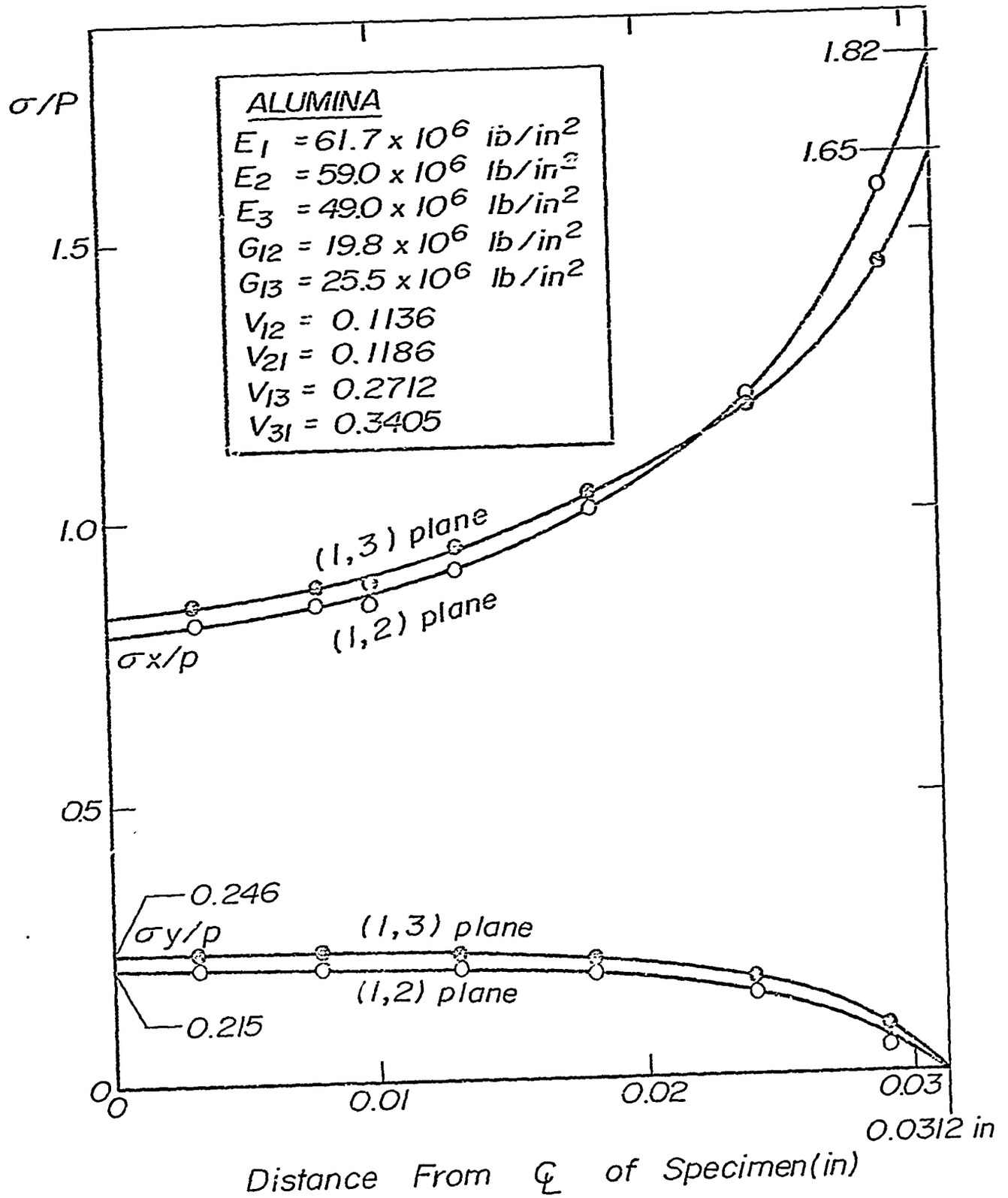

Fig. 6b: Stress distribution of the flat-hyperbolic specimens of alumina. Both top half and bottom half of the model are the same anisotropic material, Identification B in Table 1. (Maximum anisotropy)

Preceding page blank

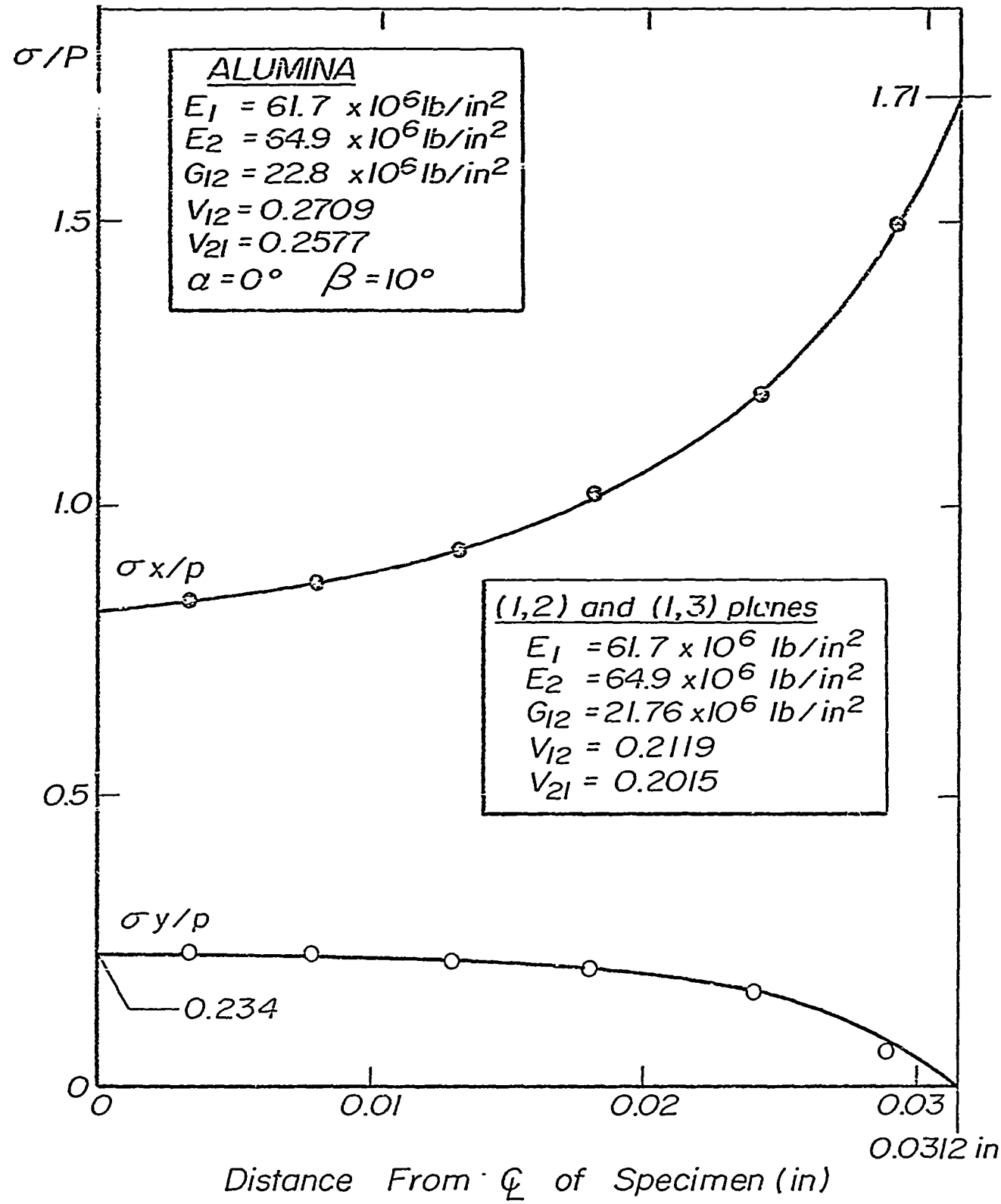

Fig. 6c: Stress distribution of flat-hyperbolic specimen of alumina. Both top half and bottom half are the same anisotropic material. "(1,2) plane" refers to Identification B and "(1,3) plane" refers to Identification D in Table 1.

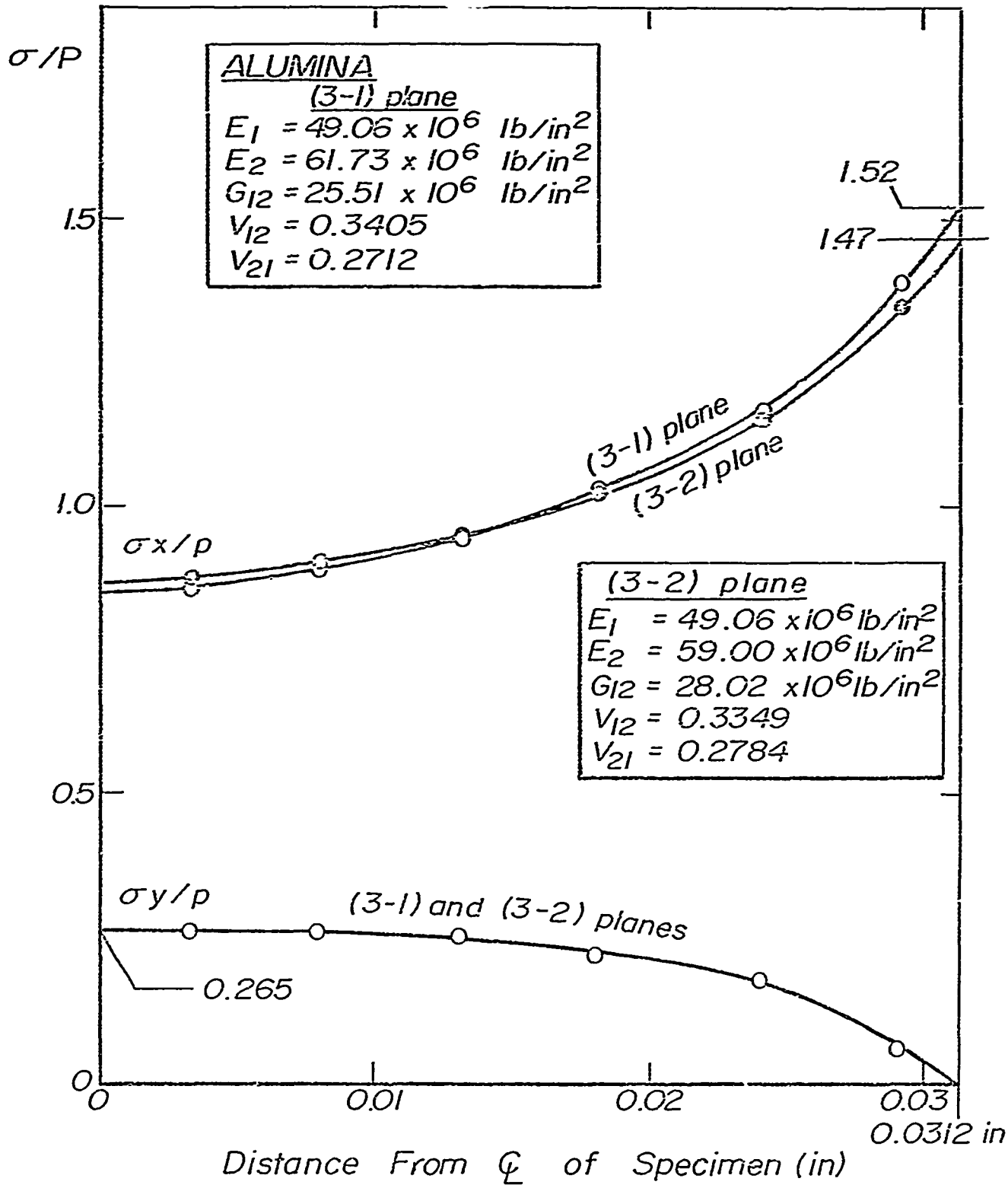

Fig. 6d: Stress distribution of flat-hyperbolic specimen of single crystal alumina. Both top half and bottom half are the same anisotropic material. "(3-1) plane" refers to Identification E and "(3-2) plane refers to Identification F of Table 1.

Preceding page blank

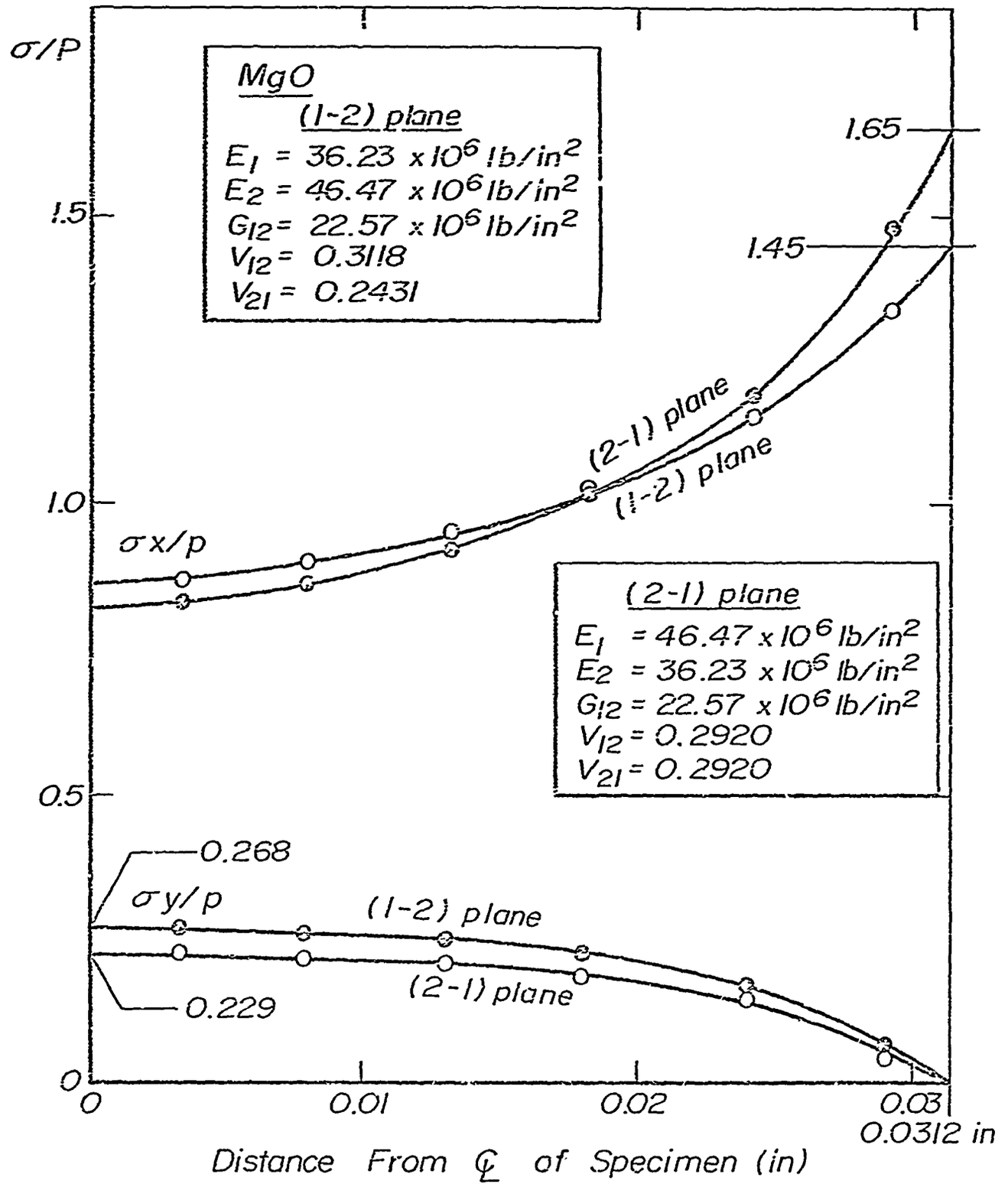

Fig. 7: Stress distribution of the flat-hyperbolic specimens of single crystal "(1-2) plane" and "(2-1) plane" correspond to identifications H and J respectively in Table 1.

Preceding page blank

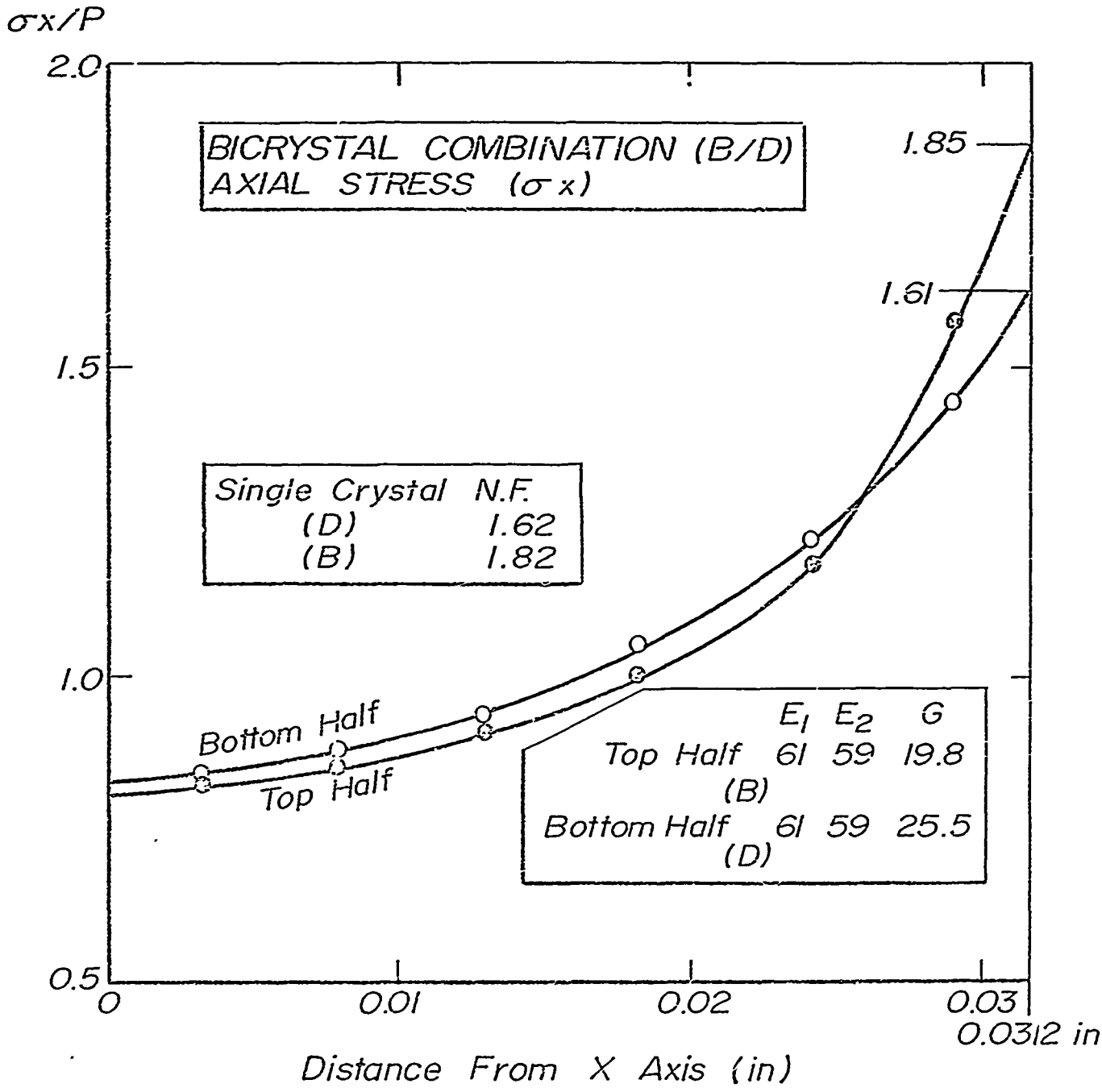

Fig. 8a: Stress distribution of the flat-hyperbolic bicrystal specimen of alumina. The notch factor for the bicrystal specimen exceeds slightly the values for each material separately. The materials are identifications B and D of Table 1.

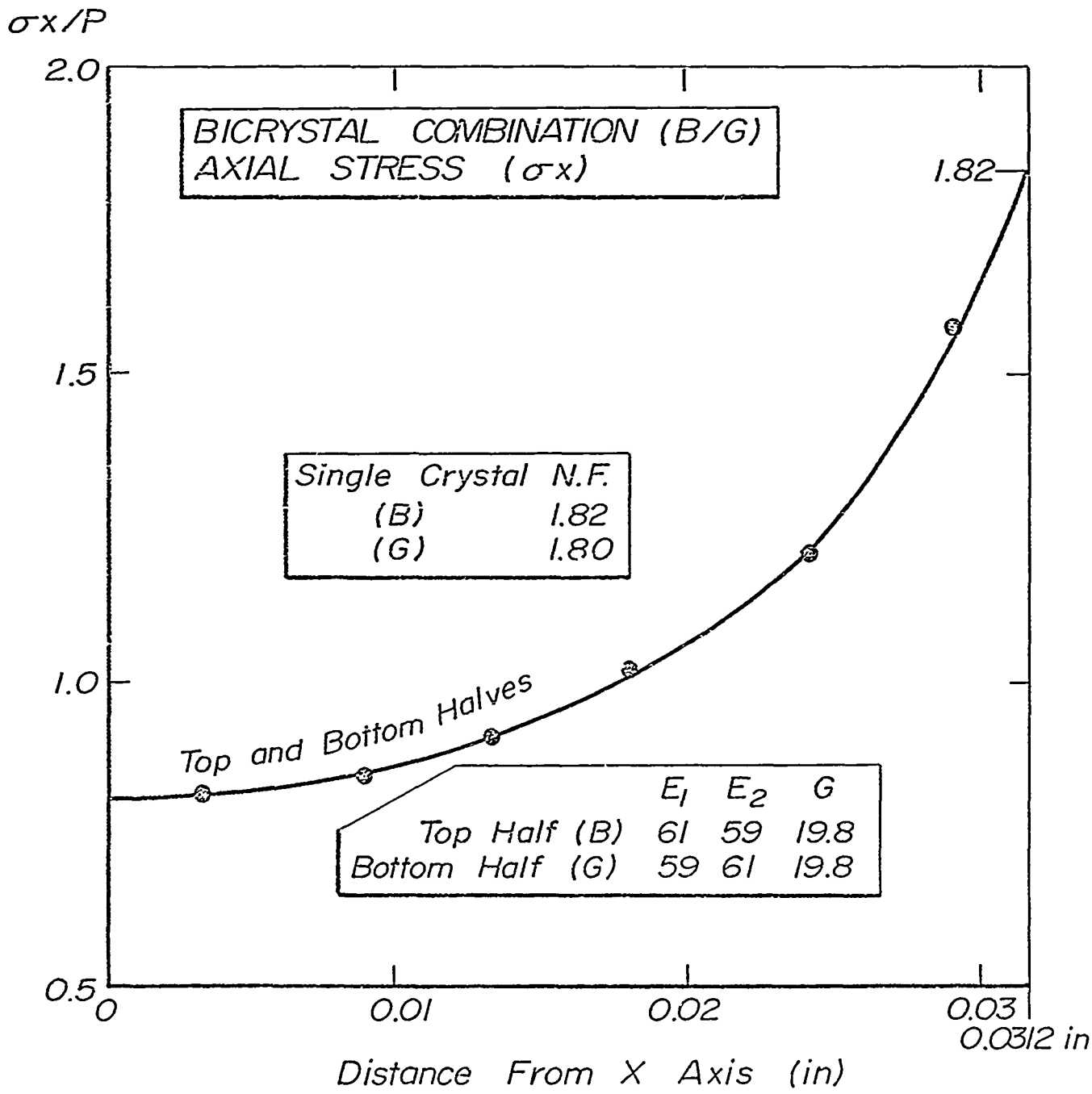

Fig. 8b: Stress distribution of the flat-hyperbola bicrystal specimen of alumina using the material properties of identifications B and G of Table 1. The notch factor of each separately is nearly the same as that for the bicrystal.

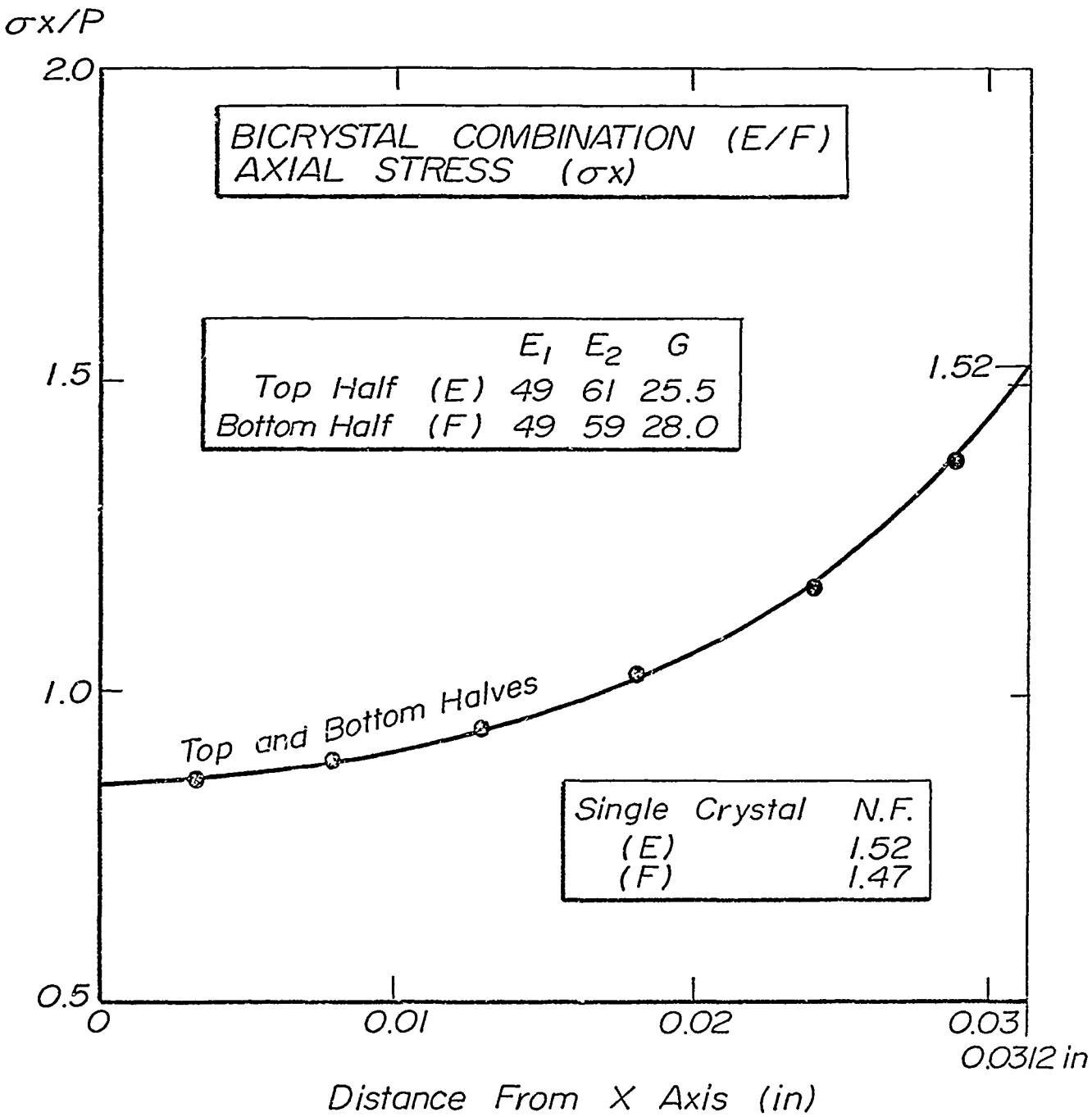

Fig. 8c: Stress distribution of the flat-hyperbola bicrystal specimen of alumina using the material properties of identifications E and F of Table 1. The notch factor of each separately is nearly the same as that for the bicrystal.

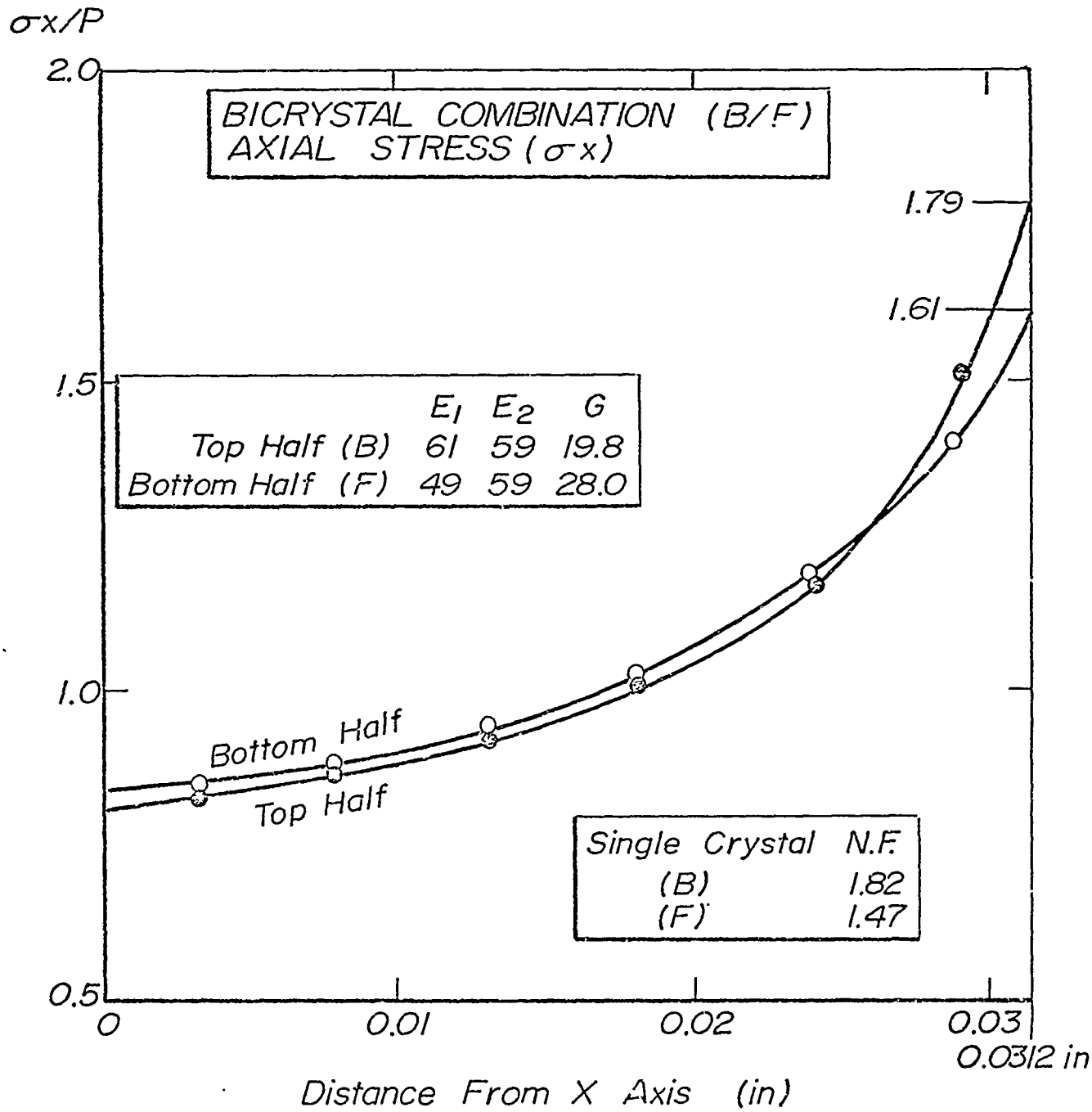

Fig. 8d: Stress distribution of the flat-hyperbola bicrystal specimen of alumina using the material properties of identifications B and F of Table 1. The notch factor for the bicrystal lies within the bounds for the single crystals. This is in contrast to the results in Fig. 8a.

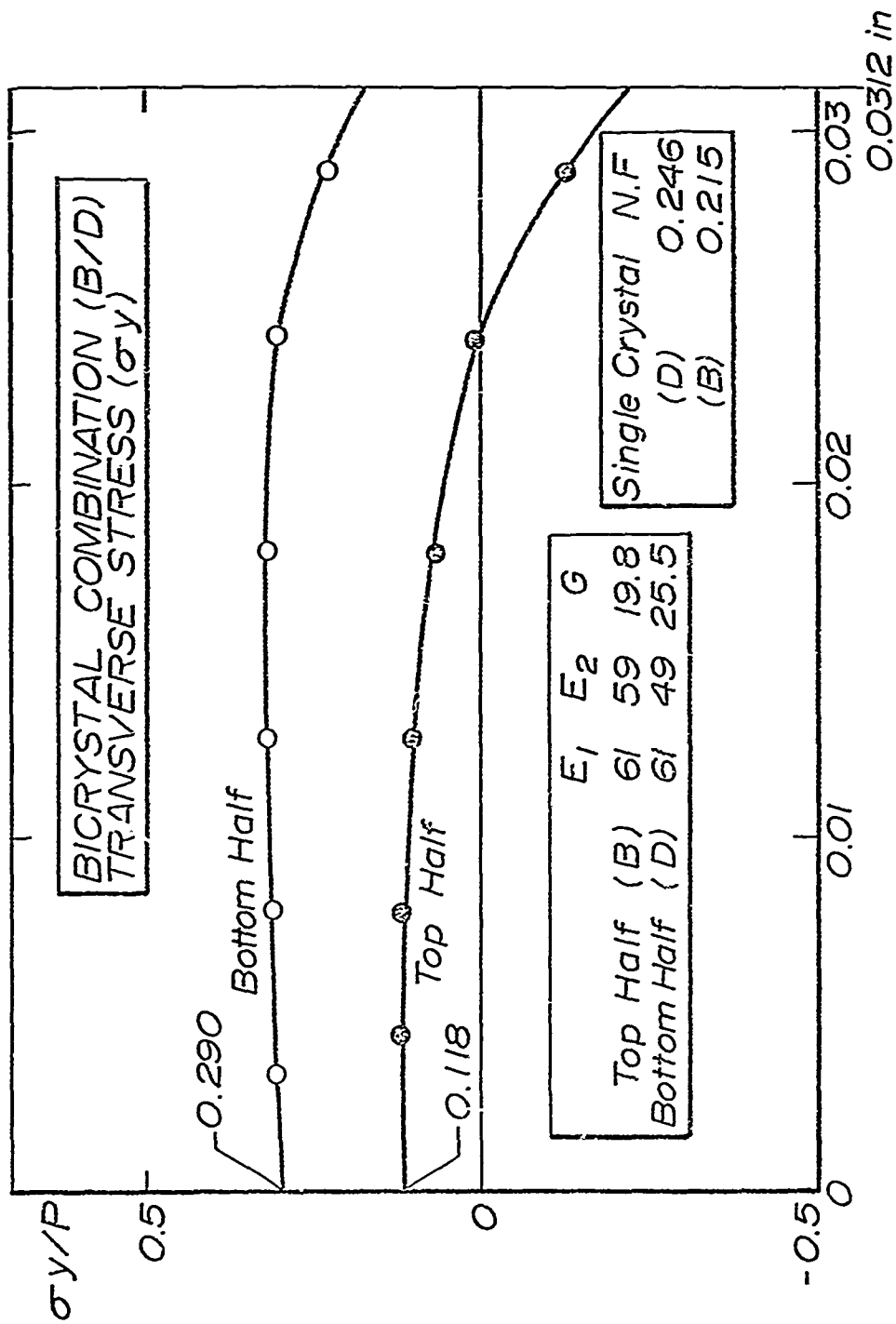

Fig. 9a: Transverse stress distribution of the flat-hyperbolic specimens of alumina. The materials are identifications B and D of Table 1.

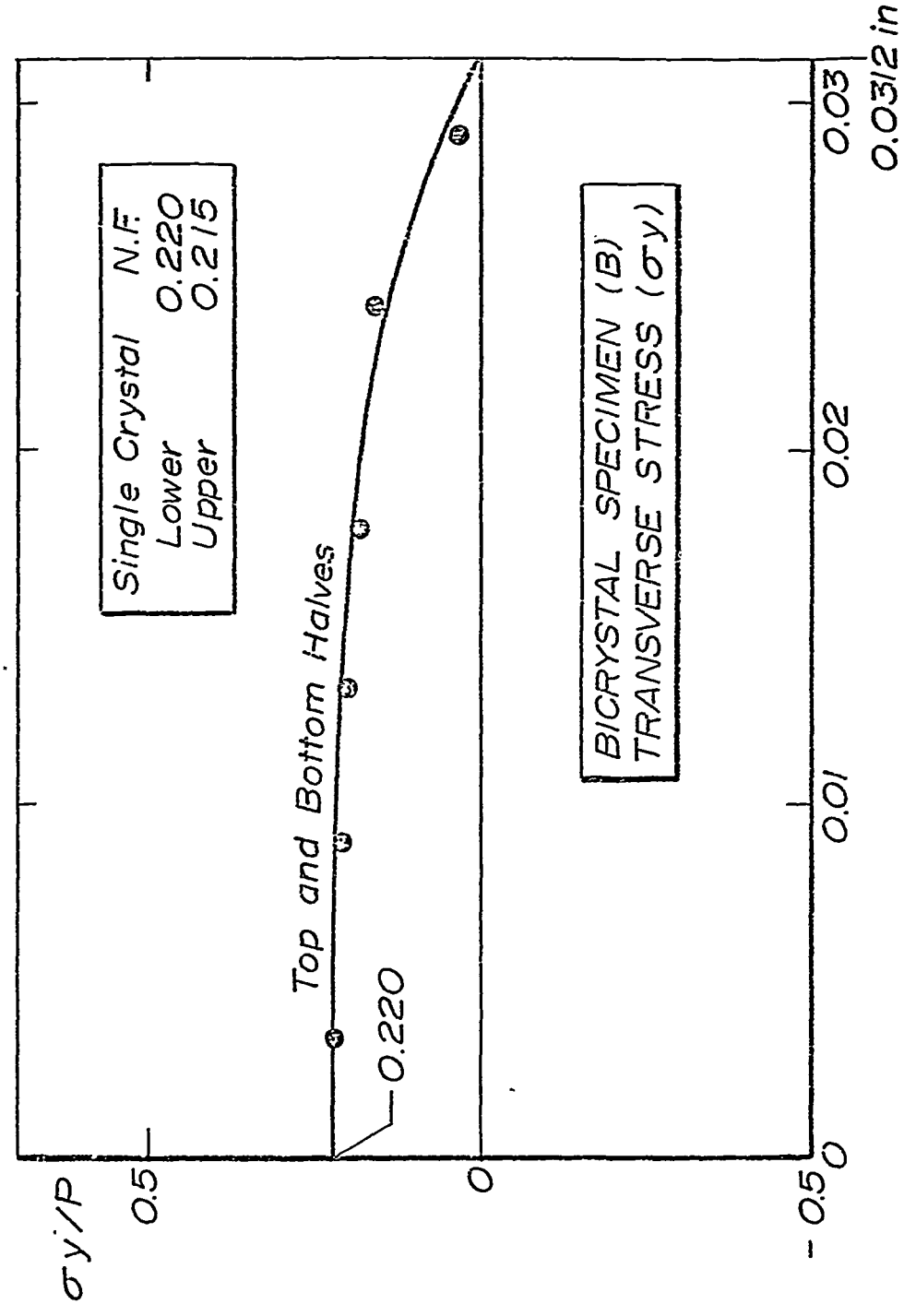

Fig. 9b: Transverse stress distribution of the flat-hyperbolic specimens of alumina. The materials are identifications B and G of Table 1.

Preceding page blank

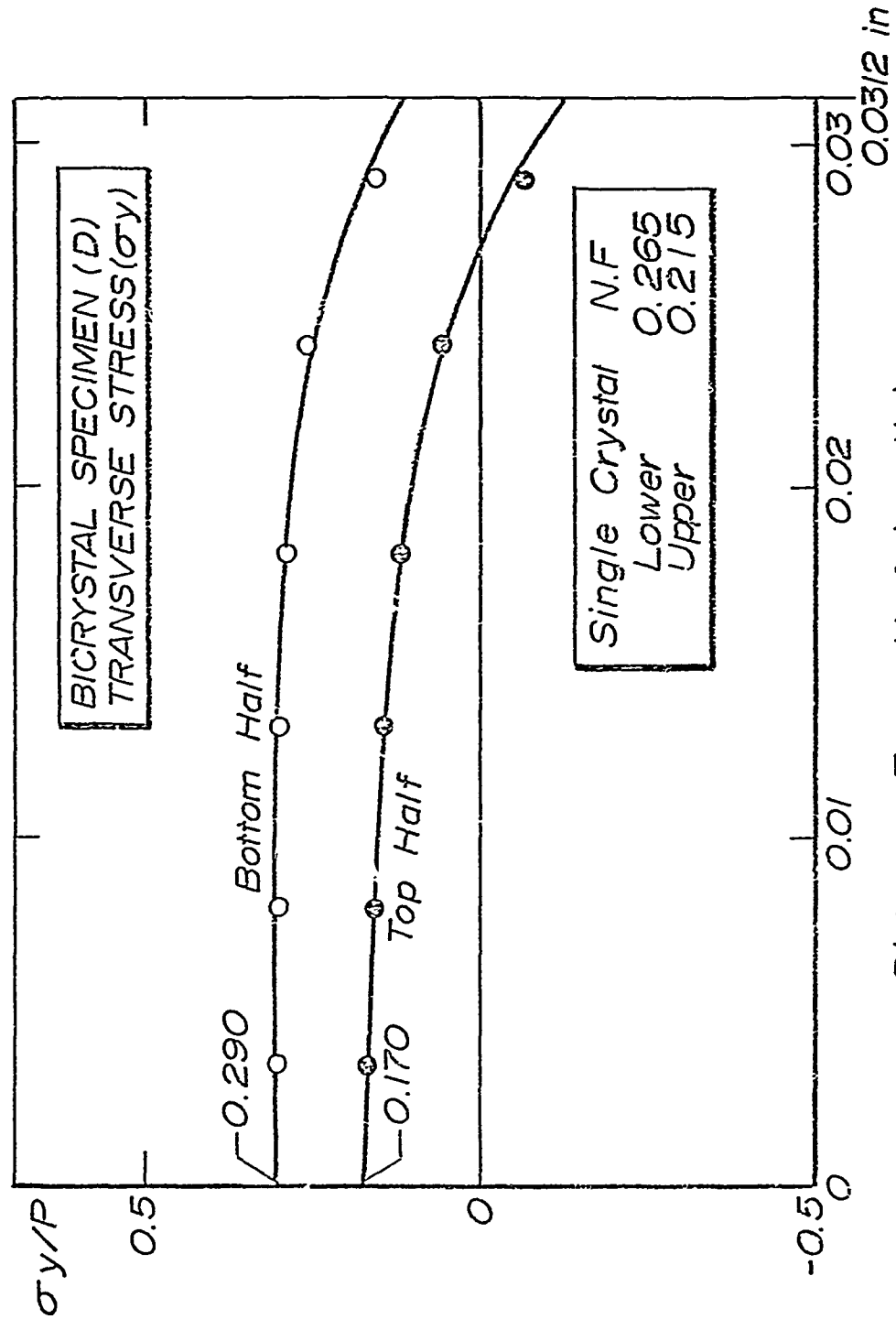

Fig. 9c: Transverse stress distribution of the flat-hyperbolic specimens of alumina. The materials are identifications E and F of Table 1.

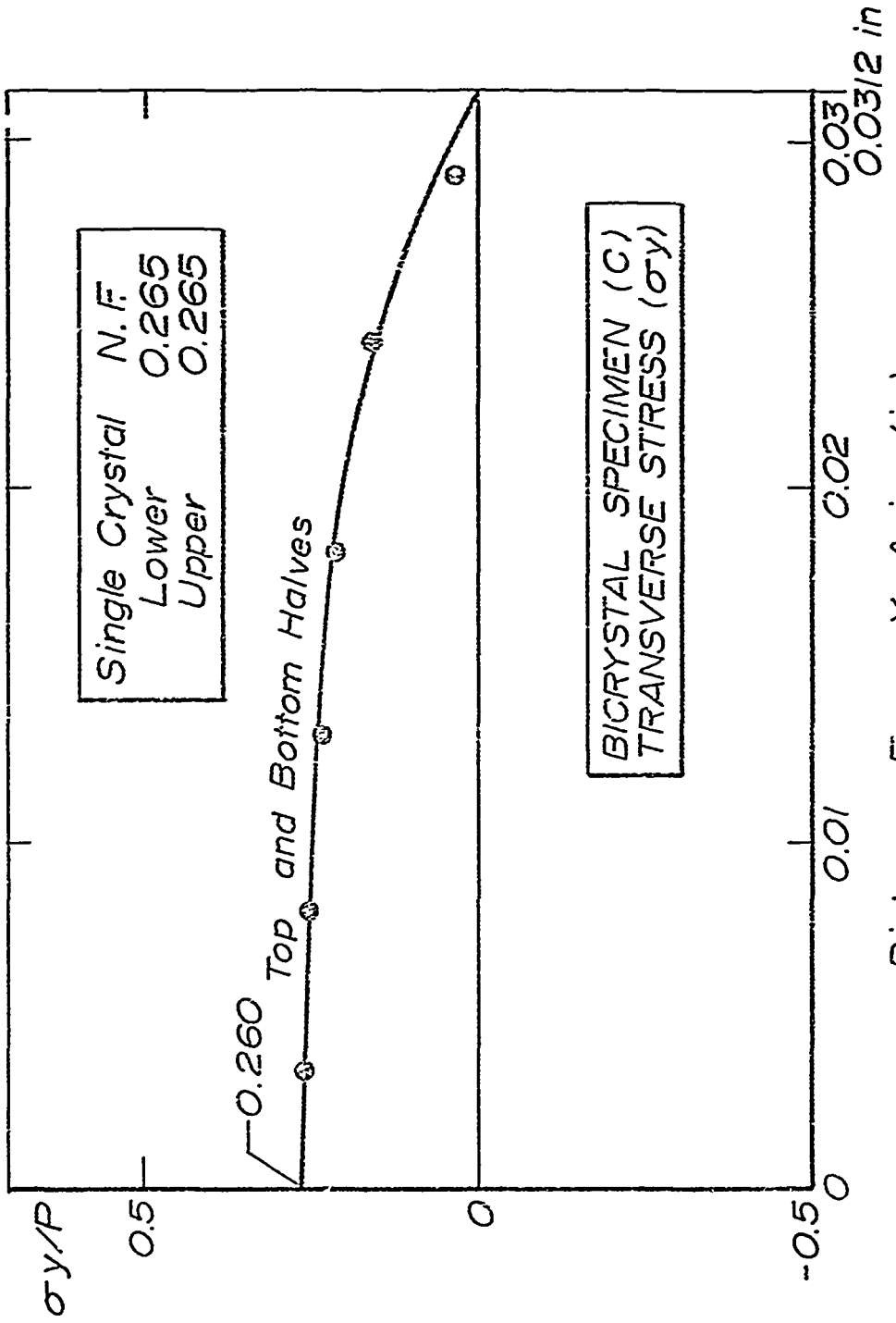

Fig. 9d: Transverse stress distribution of the flat-hyperbolic specimens of alumina. The materials are identifications B and F of Table 1.

Security Classification

DOCUMENT CONTROL DATA - R & D

Security classification of title, body of abstract and indexing annotation must be entered when the overall report is classified

1. ORIGINATING ACTIVITY (Corporate author) The Pennsylvania State University	2a. REPORT SECURITY CLASSIFICATION Unclassified 2b. GROUP

3. REPORT TITLE

Stress Concentration in Elastically Anisotropic Bicrystal Tensile Specimens.

4. DESCRIPTIVE NOTES (Type of report and inclusive dates)

Technical Report # 3

5. AUTHOR(S) (First name, middle initial, last name)

Thomas Kovacs, Herbert A. McKinstry and W. R. Buessem

6. REPORT DATE	7a. TOTAL NO. OF PAGES	7b. NO. OF REFS
March 30, 1972	62	15

8a. CONTRACT OR GRANT NO. N00014-67-A-0385-0004 b. PROJECT NO. ONR 032-509 c. d.	9a. ORIGINATOR'S REPORT NUMBER(S) 9b. OTHER REPORT NO(S) (Any other numbers that may be assigned this report)

10. DISTRIBUTION STATEMENT

Distribution of this document is unlimited; reproduction in whole or in part is permitted for any purpose of the United States Government.

11. SUPPLEMENTARY NOTES	12. SPONSORING MILITARY ACTIVITY
	Department of the Navy Office of Naval Research, Metallurgy Program Washington, D. C. 20360

13. ABSTRACT

The finite element method is used to study the effect of elastic anisotropy in the stress distribution of a hyperbolic shaped crystal. The notch factor is increased by anisotropy for single crystals in this configuration to about the same extent as for a bicrystal.

Preceding page blank

DD FORM 1 NOV 65 1473 (PAGE 1)

S/N 0101-807-6811

Security Classification

A-31408

Security Classification

KEY WORDS	LINK A		LINK B		LINK C	
	ROLE	WT	ROLE	WT	ROLE	WT
Finite element method						
Bicrystal of alumina						
Alumina						
Anisotropy						
Elastic anisotropy						

DD FORM 1 NOV 65 1473 (BACK)

Security Classification

STRESS DISTRIBUTIONS IN Al_2O_3 BICRYSTAL TENSILE SPECIMENS

J. E. Gagorik, R. A. Queeney and H. A. McKinstry

Technical Report Number 4

Office of Naval Research, Metallurgy Program
Contract No. N00014-67-A-0385-0004, ONR 032-509

30 March 1972

Materials Research Laboratory
The Pennsylvania State University
University Park, Pennsylvania 16802

62a

Reprinted from the Journal of The American Ceramic Society, Vol. 54, No. 12 December, 1971

Stress Distributions in Al_2O_3 Bicrystal Tensile Specimens

J. E. GAGORIK, R. A. QUEENEY, and H. A. McKINSTRY

Departments of Engineering Mechanics and Ceramic Science,
The Pennsylvania State University, University Park, Pennsylvania 16802

Stress distributions in Al_2O_3 bicrystals were analyzed for certain misorientations across the grain boundary in straight-sided tensile specimens with the grain boundary normal to the tensile axis. Stresses were found using the numerical analysis technique of direct stiffness calculations or by finite element analysis. When the anisotropy in elastic constants of the bicrystals was considered, misorientation of principal axes yielded stress concentrations at the boundary as high as 1.5σ. The assumption of uniform stress states in bicrystal mechanical response studies, therefore, is not generally accurate.

I. Background

The role of grain boundaries in determining the strength parameters of polycrystalline solids has been investigated extensively. For polycrystalline bodies of low or vanishing ductility, fracture strengths are affected strongly by the presence of grain boundaries. Many of the known facts about the effects of grain boundaries on the mechanical properties of ceramics are reviewed in Ref. 1.

One method of studying the strength characteristics of grain boundaries is through the use of bicrystal specimens. In principle, the misorientation of the adjoining crystals and the orientation of the boundary can be controlled to provide a rational program of strength testing. The definition of bicrystal geometry and characterization of fracture strength of MgO bicrystals was studied by Lange and Buessem.[2,3] Similar studies have been conducted on NaCl bicrystals.[4] The high-temperature creep resistance of grain boundaries in pressure-sintered Al_2O_3 bicrystals has been investigated.[5]

A common feature of these studies was the assumption of uniform stress states at and near the bicrystal boundary. That this assumption is not exact can be seen qualitatively by considering a soft material joined to a stiffer one with a tensile load applied normal to the boundary. The larger tensile strains in the softer material will produce larger transverse strains as well, assuming roughly equal Poisson's ratio effects. A transverse stress field near the boundary, therefore, is necessary to preserve compatibility of deformation. This result is not predicted when a continuously uniform stress field at the boundary is assumed.

Bicrystal specimens can be treated similarly because the misorientation of the components generally results in a change in elastic properties along a given direction at the boundary. The non-nominal stress states developed during loading should be defined before mechanical strength measures can be specified accurately.

II. Method of Analysis

A closed-form analytical solution to the stress field near the transverse grain boundary in a bicrystal tensile specimen is a formidable problem because of the finite width of real specimens. Expanding the specimen geometry to two joined half-spaces might simplify the analytical solution, but this approach would not be applicable to the finite-width real geometry. Furthermore, the most extreme values of the stress distribution may be developed at the specimen edges. This information would be of prime importance in mechanical strength studies.

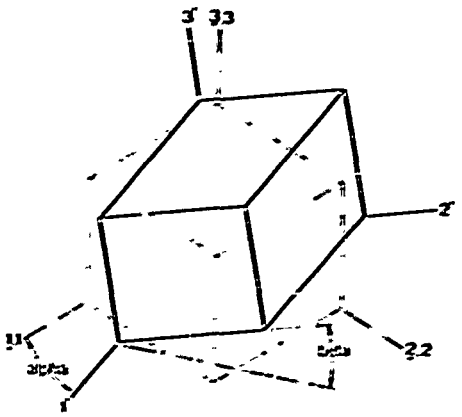

Fig. 1. Generation of crystallographic mismatch between halves of bicrystal by rotation through Euler angles α and β.

To circumvent these problems, the numerical calculation method of finite-element analysis was used. The continuous structure (bicrystal) is subdivided into a set of elastic finite elements (triangles in the present work). The triangles are joined discreetly at the nodes. A complete stiffness matrix for the structure can be assembled by adding the stiffnesses of each element at the nodes. The stiffness matrix relates forces on the nodes to nodal displacements by:

$$[F]=[K][\delta] \tag{1}$$

By inverting the stiffness matrix, the nodal displacements can be related to the nodal forces by:

$$[\delta]=[K]^{-1}[F] \tag{2}$$

The stress in each element can be found from the nodal displacements according to:

$$[\sigma]=[S][\delta] \tag{3}$$

Thus, the components of the stress tensor $[\sigma]$ in any element can be found from the stiffness matrix for the element, $[S]$, and the nodal displacements calculated in Eq. (2). An amplification of the finite-element method is given by Zienkiewicz.[6] The method of analysis has been applied to the interfacial stress states in bicrystals.[7]

III. Bicrystal Geometry and Properties

The specification of crystalline misorientation across the grain boundary is shown in Fig. 1, in which the unprimed axes are the principal axes of the unit cell; coincident with these are the underlined Euler axes. The primed axes define rotations from the principal frame through Euler angles α and β, as indicated.

Received April 5, 1971; revised copy received June 14, 1971.

Supported in part by the United States Office of Naval Research under Grant No. N0014-67-A-0385-0004.

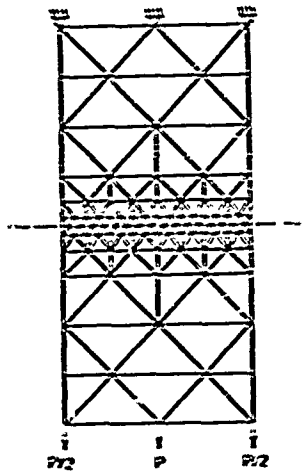

Fig. 2. Tensile specimen showing decomposition into finite elements; grain boundary located at *dashed line*.

For the purposes of the present study, a plane-stress, straight-sided tensile specimen 0.950 in. long, 0.480 in. wide, and 0.033 in. thick was chosen. The specimen and its breakdown into triangular elements are shown in Fig. 2. This specimen and the boundary conditions imposed on it correspond to a plane stress configuration. The choice of a 170-element mesh was arrived at by trial and error. The goal was to achieve a specimen in which a nominal uniform stress state was realized near the specimen ends. Accumulated calculation error, monitored in the form of departure from load equilibrium, was maintained at <1%.

The element stiffnesses [S] were formulated from the single-crystal elastic-constant stiffness components C_{ijkl}. If C_{ijkl} are the principal axes components of the stiffness coefficients, the components in a new, primed axis frame are:

$$C'_{ijkl}=a_{mi}a_{nj}a_{ok}a_{pl}C_{mnop} \qquad (4)$$

with the summation convention observed. The transformation coefficients a_{ij} are the direction cosines between the new and old axes frames. The isothermal stiffnesses used for Al_2O_3 were those of Aleksandrov and Ryzhova.[3]

IV. Results and Discussion

Changes in stress states caused by misorientations between the upper and lower halves of the bicrystal were examined. To discuss these changes over the nominal state, the stress concentration factor, K_σ, may be used, where

$$K_\sigma=\frac{\text{actual axial stress state}}{\text{nominal axial stress state}}$$

Since the total principal stress state determines mechanical response in general, the development, with misorientation, of transverse stresses should also be characterized. Since there is no nominal or average transverse stress, the usual definition of stress concentration factor cannot be used. Instead, a transverse stress concentration factor is defined as the ratio of the transverse stress to the nominal axial stress.

Results obtained are shown in Figs. 3 and 4. Two types of misorientations were studied.

Case A: The plane of the specimen has its normal in the 3-direction of the unit cell with tension applied in the 1-direction. The bottom half of the bicrystal remains stationary for all calculations, whereas the top half is rotated through various α angles, with the angle β held constant at zero. Figure 3(*A*) indicates that, for a 40° α rotation of the upper half, an axial stress concentration factor of $\simeq$1.4 is achieved at the specimen side edge. This figure also indicates a monotonically increasing stress concentration factor as misorientation is increased. Figure 3(*B*) demonstrates the tendency of the stress concentration factor to return to unity as one moves away from the grain boundary, as expected. Figure 3(*C*) demonstrates the development of transverse stresses with increasing misorientation. The transverse stresses decrease rapidly with distance from the grain boundary and do not vary appreciably with distance along the interface.

Case B: The top half of the specimen was originally oriented as in Case A. The bottom half is oriented with 3-direction in the tensile direction, 1-direction in the transverse sense, and 2-direction normal to the plane of the specimen. The bottom half was held fixed for all calculations, whereas the upper half was rotated as indicated in Fig. 4.

Axial stress concentration factors as large as 1.5 were found at the specimen edge (Fig. 4(*A*)). Figure 4(*B*) indicates that these values tend quickly toward unity away from the grain boundary. Large transverse stresses which were highly localized at the grain boundary also developed (Fig. 4(C)); they did not change appreciably across the specimen width.

These results indicate that, as a generality, misorientation between the halves of an Al_2O_3 bicrystal tends to develop more severe stress states at the grain-boundary–specimen-edge intersection than were previously thought to exist. The present calculations found, for certain selected misorientations, stresses 50% higher than those predicted by the assumption of average nominal axial stress for the specimen. Transverse stresses, which naturally affect the mechanical response of the bicrystal, were also found to be present and large enough to be sometimes non-negligible.

Figures 3 and 4 indicate that the calculated axial stresses are not identical at the interface, in apparent violation of force equilibrium. This discrepancy is an intrinsic characteristic of the numerical technique used. The finite-element method averages the stresses over the entire element and associates the average value with the element centroid. Although the particular programing arrangement used in the present study ensured nodal equilibrium to within 1.0%, no such demands can be imposed on these average values for the entire element. The use of element average stresses poses no problem unless the analysis is concerned with abrupt changes in geometry or elastic properties. A finer mesh choice at the interface would undoubtedly indicate equilibrated axial stresses there. However, the present study was designed to draw attention to the necessity of more accurate stress analyses for anisotropic bodies, not to characterize given experimental specimens thoroughly.

It is not possible to draw firm conclusions about the relative effects of variations in specific elastic constants at the interface on the stress distribution there. While variations in e.g. the axial stiffness differences across the boundary are being investigated, the other elastic constants are also changing, and the stress distribution (Eq. (3)) depends on all of these.

In view of the results of the present study, experiments involving the stress-dependent properties of bicrystal grain boundaries must include an analysis of the stress state that accounts for the rapid change in elastic properties at the interface. This requirement would apply to all symmetry classes of crystal structure, not the trigonal class to which Al_2O_3 belongs only. The stress analysis would be viewed in the same characterization context as determination of the crystallographic orientations of the crystal halves.

V. Summary

The abrupt change in elastic properties at the grain-boundary interface in bicrystal tensile specimens (Al_2O_3 was investigated) produced changes in the nominal stress state there. These new stresses are highest at the specimen edge, localized near the boundary, and vary with crystallographic mismatch.

References

[1] Materials Science Research, Vol. 3. Edited by W. W. Kriegel and Hayne Palmour III. Plenum Press, New York, 1966.
[2] F. F. Lange, "Mathematical Characterization of a General Bicrystal," *Acta Met.*, 15 [2] 311–19 (1967).

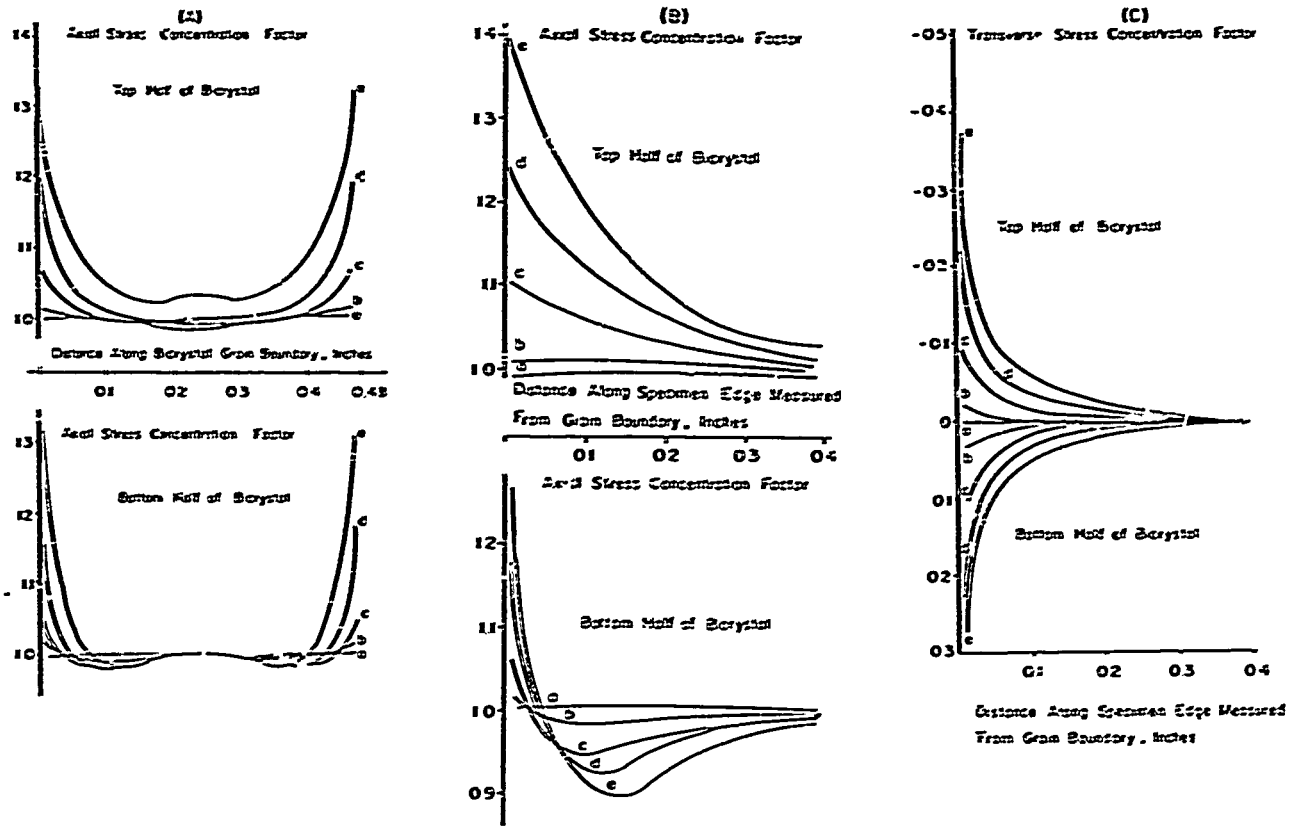

Fig. 3. Stress concentration factors for $\beta=0°$ with $\alpha=$ (*a*) 0°, (*b*) 10°, (*c*) 20°, (*d*) 30°, and (*e*) 40°.

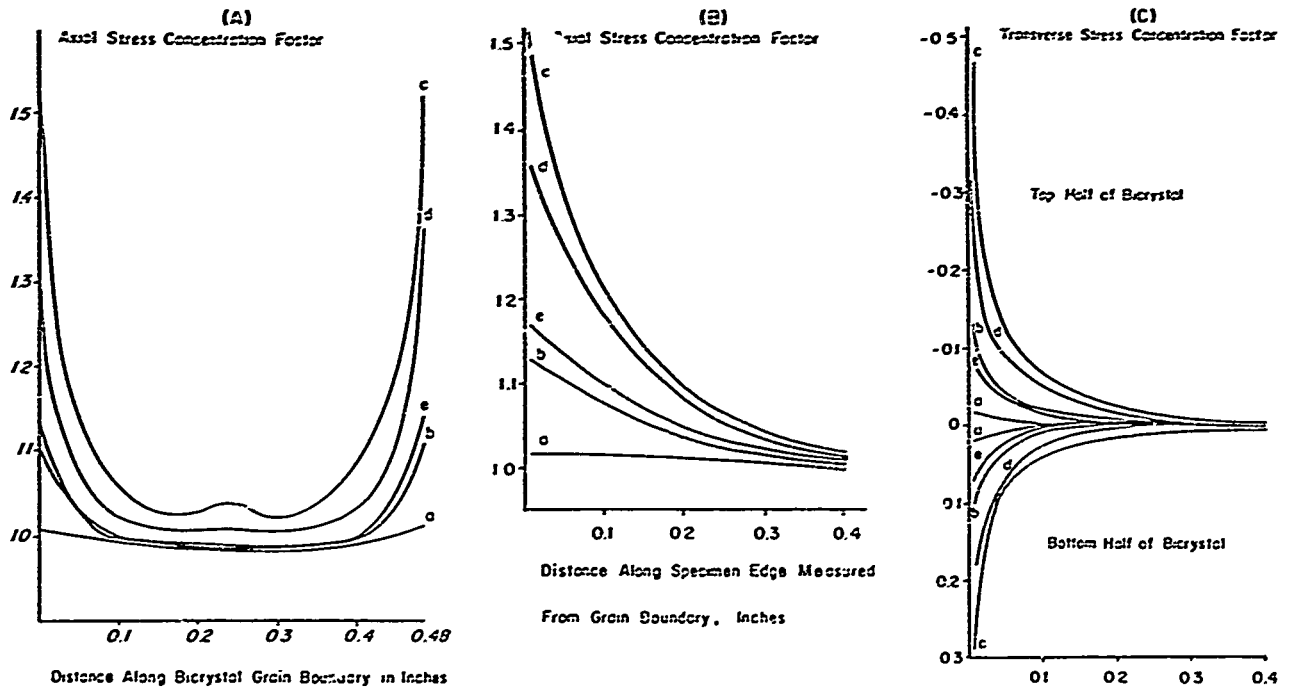

Fig. 4. Stress concentration factors for $\beta=0°$ with (*a*) $\alpha=0°$, (*b*) $\alpha=20°$, and (*c*) $\alpha=45°$ and for $\alpha=45°$ with (*d*) $\beta=20°$ and (*e*) $\beta=55°$.

[3] F. F. Lange and W. R. Buessem, "Intrinsic Brittle Strength of Magnesium Oxide Bicrystals," *J. Appl. Phys.*, 38 [5] 2013–19 (1967).

[4] M. L. Gimpl, A. D. McMaster, and N. Fuschillo, "Influence of Orientation on Properties of Grain Boundaries in NaCl," *J. Amer. Ceram. Soc.*, 51 [11] 655–60 (1968).

[5] M. P. Davis and Hayne Palmour III; pp. 265–83 in Ref. 1.

[6] O. C. Zienkiewicz. The Finite Element Method in Structural Continuum Mechanics. McGraw-Hill Book Co., New York, 1967.

[7] H. Y. B. Mar and W. D. Scott, "Fracture Induced in Al_2O_3 Bicrystals by Anisotropic Thermal Expansion," *J. Amer. Ceram. Soc.*, 53 [10] 555–58 (1970).

[8] K. S. Aleksandrov and T. V. Ryzhova, "Elastic Properties of Crystals," *Sov. Phys.-Crystallogr.*, 6, 228–52 (1961).

Security Classification

DOCUMENT CONTROL DATA - R & D

Security classification of title, body of abstract and indexing annotation must be entered when the overall report is classified

1. ORIGINATING ACTIVITY (Corporate author)	2a. REPORT SECURITY CLASSIFICATION
The Pennsylvania State University	Unclassified
	2b. GROUP

3. REPORT TITLE

Stress Distributions in Al_2O_3 Bicrystal Tensile Specimens.

4. DESCRIPTIVE NOTES (Type of report and inclusive dates)

Technical Report # 4

5. AUTHOR(S) (First name, middle initial, last name)

J. E. Gagorik, R. A. Queeney and H. A. McKinstry

6. REPORT DATE	7a. TOTAL NO. OF PAGES	7b. NO. OF REFS
March 30, 1972	5	8

8a. CONTRACT OR GRANT NO.	9a. ORIGINATOR'S REPORT NUMBER(S)
N00014-67-A-0385-0004	
b. PROJECT NO. ONR 032-509	
c.	9b. OTHER REPORT NO(S) (Any other numbers that may be assigned this report)
d.	

10. DISTRIBUTION STATEMENT

Distribution of this document is unlimited; reproduction in whole or in part is permitted for any purpose of the United States Government.

11. SUPPLEMENTARY NOTES	12. SPONSORING MILITARY ACTIVITY
	Department of the Navy Office of Naval Research, Metallurgy Program Washington, D. C. 20360

13. ABSTRACT

Stress distributions in Al_2O_3 bicrystals were analyzed for certain misorientations across the grain boundary in straight-sided tensile specimens with the grain boundary normal to the tensile axis. Stresses were found using the numerical analysis technique of direct stiffness calculations or by finite element analysis. When the anisotropy in elastic constants of the bicrystals was considered, misorientation of principal axes yielded stress concentrations at the boundary as high as 1.50. The assumption of uniform stress states in bicrystal mechanical response studies, therefore, is not generally accurate.

DD FORM 1 NOV 65 1473 (PAGE 1)

S/N 0101-807-6811

Security Classification

A-31408

Security Classification

14 KEY WORDS	LINK A		LINK B		LINK C	
	ROLE	WT	ROLE	WT	ROLE	WT
Anisotropy						
Finite Element Method						
Alumina						
Stress Concentation						
Elasticity: anisotropic						

DD FORM 1 NOV 65 1473 (BACK)

Security Classification

A STUDY OF A TWO-DIMENSIONAL FINITE ELEMENT MODEL OF A CERAMIC BODY

H. A. McKinstry, H. E. Shull, and W. R. Buessem

Technical Report Number 5

Office of Naval Research, Metallurgy Program
Contract No. N00014-67-A-0385-0004, ONR 032-509

30 March 1972

Materials Research Laboratory
The Pennsylvania State University
University Park, Pennsylvania 16802

A Study of a Two-Dimensional Finite Element Model of a Ceramic Body

ABSTRACT

The elastic behavior of a ceramic body has been modeled by use of the finite element method. The model simulates a set of nineteen hexagonal crystals whose elastic and thermal properties can be independently varied. Several different configurations of the elastic properties of the crystals were evaluated under conditions of isostatic, uniaxial and thermal loadings. The effect of anisotropy shifts the position where the maximum shear acts in the model, under isostatic and thermal loadings.

INTRODUCTION

The finite element method of analysis has been growing rapidly in application to widely varying subjects: from earth dams, to whole steamships to pressure valves (Refs. 1,2). The present study may be an application to the smallest objects yet studied: the grains of a ceramic body.

The model for study was taken to be the simplest two-dimensional representation of a ceramic body. Buessem and Lange (Ref. 3) proposed a hexagonal model in which the forces due to thermal expansion anisotropy might be considered. In his discussion of the microstructure of ceramics p. 409 (Ref. 4), Kingery states, "if we restrict the structure to one with the simplest corners with three grains meeting, the average polygon must be a hexagon." The model designed for this study consists of nineteen hexagon-shaped crystals as shown in Fig. 1. Each of these hexagons can be given specific anisotropic elastic constants and anisotropic thermal expansion coefficients. In this way the model can simulate the random orientation of crystals in a polycrystalline ceramic body.

This model was further subdivided into 366 triangles with 199 nodes as shown in Fig. 2, in order to be compatible with the computer program available.

The computer program was written by Dahl (Ref. 5) and has been modified by Gagorik (Ref. 6) and T. Kovacs (Ref. 7).

Alumina Model

The elastic constants of alumina were used to obtain the values assigned to each of the nineteen hexagonal crystals of the model. The elastic compliances used were those measured by J. Geiske (Ref. 8). The values used were converted into the English system of units as are given in Table I.

Table I

Elastic Compliances $(\text{inches})^2/\text{pound}$

$S_{11} = 0.01620$	$S_{24} = -S_{14}$
$S_{12} = 0.00480$	$S_{22} = S_{11}$
$S_{13} = 0.00264$	$S_{55} = S_{44}$
$S_{14} = 0.00327$	$S_{56} = -2S_{14}$
$S_{33} = 0.01500$	$S_{66} = 2\,(S_{11} - S_{12})$
$S_{44} = 0.00478$	

These elastic compliances were first transformed by a computer program written by J. Gagorik (Ref. 6) based on the method of Lieberman and Zirinsky (Ref. 9) which performs the equivalent of a rotation of the crystal. Then, these compliances for the rotated crystal were converted into technical constants. For an anisotropic crystal, technical constants are defined by Lekhnitskii (Ref. 10) to be consonant with the usual elastic constants; Young's modulus, E, the shear modulus G, and Poisson's ratio, ν.

For the two-dimensional plane-stress problem considered, the technical constants are obtained from the value of the rotated elastic compliances by the following relationships:

$$E_x = 1/S_{11}$$

$$E_y = 1/S_{22}$$

$$\nu_{xy} = -S_{12}/S_{11}$$

$$\nu_{yx} = -S_{12}/S_{22}$$

$$G_{xy} = 1/S_{66}$$

Hooke's law in plane stress is then expressed as:

$$\begin{pmatrix} E_x \\ E_y \\ E_{xy} \end{pmatrix} = \begin{pmatrix} 1/E_x & -\nu_{yx}/E_y & 0 \\ -\nu_{xy}/E_x & 1/E_y & 0 \\ 0 & 0 & 1/G_{xy} \end{pmatrix} \begin{pmatrix} \sigma_x \\ \sigma_y \\ \sigma_{xy} \end{pmatrix}$$

Configurations

A set of six different configurations was processed using four different types of loading.

In the first configuration, each of the nineteen crystals was given isotropic constants corresponding to the orientation of each crystal with the c-axis perpendicular to the plane of the model.

The second, third and fourth configurations were obtained by assigning to the center crystal technical constants corresponding to the rotation of an alumina crystal about an axis parallel to the x-axis by amounts of 40, 90 and 140 degrees respectively. The rest of the constants were given the same isotropic values as in the first configuration.

The fifth configuration was composed of three different sets of constants. The center crystal was oriented so that the c-axis lies in the plane of the paper and points in the x-direction. The a-axis was supposed to have been placed in the y-direction. However, a value for the direction

corresponding to the maximum anisotropy was selected instead. The remaining eighteen crystals were divided in such a way that for the top half of the crystals all had the same orientation, and the bottom half crystals all were given constants corresponding to a ninety degree rotation from the other half of the crystals. The constants for these two halves were selected to correspond to the orientation found by Kovacs (Ref. 7) to possess the maximum anisotropy for alumina. This corresponds to a rotation of the c-axis of the crystal about an axis perpendicular to an a-axis. The rotation for maximum anisotropy was fifty-five degrees. In the model, constants were used corresponding to a rotation of fifty degrees.

The sixth configuration was an arrangement designed to represent, as well as possible, a polycrystalline ceramic body with anisotropic constituents. The constants were chosen to produce a random arrangement of the crystals. The center crystal was fixed in its orientation so that the c-axis was placed in the x-direction and the a-axis in the y-direction. A two-angle rotational matrix with ten-degree intervals in both angles was used as the population from which to choose the appropriate constants randomly.

Loadings

Each of the six configurations was subjected to four different loadings. The first loading corresponded to an isostatic loading. Force components were placed on each external node in such a way that the resultants would point to the center of the model. This type of loading produces some shear in the outermost elements but is evened out before reaching the second layer of crystals.

The second and third loadings were uniaxial tensions, applied at the external nodes. In the second type the forces act vertically in the y-direction and in the third type, the forces act horizontally in the x-direction. Hence, the y-direction loading is uniform. The x-direction loading is slightly non-uniform. In the fourth type of loading, the forces generated by the thermal expansion of the crystals, with each expansion determined by its appropriate anisotropic thermal expansion coefficients, were placed on the external nodes. The system was then allowed to adjust internally under these forces. For the isotropic case, it was found that the forces were not identical with those used for the isostatic case. The

forces were calculated, however, so that no shear strains were generated at any point within the model.

Finite Element Method

The finite element method provides a means of obtaining the solution of elastic problems which are not directly soluble by standard elastic mathematical analysis. The structure to be analyzed in divided into a set of small units, usually triangles, to which the standard elastic theory can be applied. Each triangle is linked with the triangles surrounding it. The displacements of the connecting nodes then must be related to the other in a compatible way, and the computer program finds the answer as a solution of simultaneous equations.

The time required for computer solution varies with the parameters assigned to the model and ranges from 60 seconds to 120 seconds. The lower time is the more common. The program uses a Gauss-Seidel iterative method for solution, and there is a variation in the number of iterations required to reduce the error to an acceptable level.

Representation

The figures (Figs. 3-10) which present the results of these analyses show on one page all six configurations. For each different type of loading there are two pages; one showing the principal stresses, and the other showing the maximum shear stress.

In the figures presenting the principal-stress data, the length of the half arrow represents the magnitude of the maximum tensile stress at the center of each element, and the magnitude of the second principal-stress is indicated by a line perpendicular to and crossing it. The direction in which these stresses act is also indicated. In the figures showing the maximum shear stress (τ_{max}), the direction indicated is forty-five degrees to the principal stresses, and the magnitudes of both members of the cross are equal. In order to show the variations in τ_{max} more clearly for the isostatic and thermal loading cases, a scale factor was used to increase the size by about 16% over that used for the principal stresses.

The computer output consists of a tabulation of the stress and strain components at the center of each triangle.

DISCUSSION

Isostatic Loading

One of the interesting features is evident in comparing the τ_{max} plots, Figs. 4b, c and d for the 40°, 90° and 140° rotation. The maximum shear stress lies outside the central crystal for rotations of 40 and 90 degrees. It lies inside for the 140° rotation. The effect of the anisotropy is to vary the position in the sample where τ_{max} will have its largest value.

In the bicrystal with a central inclusion, Fig. 4e, the distribution of τ_{max} has a semblance of a 2-fold symmetry axis outside the central crystal. The greatest shear lies inside. Its magnitude is approximately 10% of the principal stresses. The central crystal is anisotropic, and this adds an additional complication to the interpretation of the source of the shear intensification.

The random-orientation model gives a maximum shear stress near a corner of the central crystal. The magnitude of the τ_{max} is a little more than 6% of the principal stresses.

Uniaxial Loadings

Two different, compressional uniaxial loadings were used, since their action at different faces of a hexagon would be different. The figures (Figs. 5,6,7,8) offer little help in an interpretation of the effects of anisotropy. The lines of principal stress align themselves with the external loads. There is some evidence of a slight turning but, as read from the computer output, the variation of the angle of principal stress varies by not more than ± 2 degrees. (It is interesting to note that the direction of principal stress coincides with the principal strain in the isotropic media and deviates a little in anisotropic media). By extrapolating the principal stresses to the faces of the central crystal, a maximum variation of 6% in the different models is observed in the face normal stress and the face shear stress.

The changes in the normal force on faces one and four for the case of vertical uniaxial loading can be obtained from the computer output. The stresses normalized in terms of the applied stress for the 40°, 90° and 140° rotations are 1.5, 0.3 and -5.0 percent respectively. The effect of the anisotropy is sufficient to change the sign of the stress from tension to compression.

In an attempt to gain more information about the uniaxial loadings, a different method of presenting the data has been shown. The results shown in Figs. 11-19 will be discussed under the heading of SYMAP contour maps.

Thermal Loading

For the isotropic case, thermal loading of the model produced absolutely no internal stresses, (Fig. 9a). With the rotation of the central crystal about an axis parallel to the x-axis, interesting differences can be noted. The principal stresses maximize inside the center crystal for the 40° rotation case and, as can be seen in Fig. 9b, there is a tendency for uniaxial stressing on the left, outside the center crystal boundary. They maximize outside and to the left of the center crystal for the 90° rotation, (Fig. 9c). For the 140° rotation, (Fig. 9d), the principal stresses become almost uniaxial on the right side of the crystal just inside the boundary. The trajectories, as indicated by the arrows, show that in addition to the anisotropy, the geometrical shape of the boundary also has a strong effect. The high τ_{max} near the boundaries of the center crystal emphasizes the alteration of the distribution of stresses as the anisotropic character of the crystal is changed, (Figs. 10b,10c and 10d). The distributions are clearly different in the three cases.

The normal and tangential stresses on each face of the center crystal were calculated by extrapolating the stresses to the boundary. Parabolic extrapolation functions were used to find the best fit from four nearest layers both inside and outside the center crystal. The inner and outer extrapolations do not always agree. For Table II, which gives the values for these three rotation models, the maximum deviation for inner and outer extrapolations was approximately 50% with the average deviation about 10%. For the isotropic case these stresses would be zero.

Table II

The normal and tangential stresses (psi) on the faces of the center crystal

	40 degrees		90 degrees		140 degrees	
Face	σ_N	σ_T	σ_N	σ_T	σ_N	σ_T
1	3800	-70	4400	-65	-1466	0.2
2	15015	+2810	14876	2900	-2670	-994
3	10430	-1475	10350	-1681	-6200	1800
4	9010	+35	9700	24	4074	-70
5	10400	1500	10360	1720	-6150	-1790
6	14940	-2794	14810	-2905	2650	1000

The values for the 40° and 90° rotations are much more similar than the diagrams indicate. The 140° rotation is, however, markedly different. Whereas the first two leave the center crystal in tension, the third case has it in a somewhat more complicated state, with four faces experiencing compression and two faces under tension. As indicated, these stresses should not be regarded as having precision. Since some of the inner and outer extrapolation values deviate by as much as 50%, it must be assumed that the model is not sufficiently subdivided to take into account the rapidly changing stress. With the stress gradient so high in the region of interest, a new model would be indicated as necessary. Unfortunately, time and funds do not permit such an extension.

Although the deviations of the stresses for the maximum anisotropy case vary on an average of 45%, all of them have the same sign. This is not the situation for the random orientation model. Here, the deviations may be as large as 500% and the extrapolated values are of opposite sign. Clearly, a finer mesh model is needed for this case. The normal and tangential stresses range from plus or minus zero to thirty thousand psi. It is unfortunate that our present model does not give reasonable values for this nearest approach to the real ceramic body.

SYMAP Contour Map

Another method for presenting the data from the FEM program is to make use of an available computer program SYMAP (Ref. 11) which prints out an

interpolated contour map.

The computer over-prints characters to vary the darkness of the printing, and thus a contour map is developed for visual inspection. The results for the uniaxial loadings of the rotated center crystal are presented in Figs. 11-16. The maximum values do not appear in these figures, because only the region of and near (four layers out) the center crystal are presented. Where the maxima lie within this region, the figures are easily interpreted since they are the plot of a single variable only. However, as an aid to interpretation, contour lines separating the different stress fields have been hand-drawn.

The data plotted in Figs. 11-16 are the maximum principal stress, σ_1. Since the uniaxial loading was compressional, the second principal stress will be negative and of larger magnitude. Thus the σ_1 plotted here will be a sensitive measure of the deviation from a uniform uniaxial stress distribution. For a completely uniaxial distribution, σ_1 should be zero.

A scale that can be used to describe the maps was obtained by dividing the calculated value for σ_1 by the absolute value of σ_2. This will produce a ratio of values from -0.22 to +0.08 on a scale of 8 as listed in Table III. In Figs. 11-16, the scale number is produced at the center of each triangle in the finite element model.

Table III

Scale for SYMAP Contour Plots

Scale Number	L	1	2	3	4	5	6	7
$\frac{\sigma_1}{\lvert\sigma_2\rvert}$	-0.28	-0.22	-0.18	-0.12	-0.08	-0.02	+0.02	+0.08

Figs. 11, 12 and 13 correspond to the plots in Figs. 5b,c and d, for the rotation of the center crystal by 40°, 90° and 140° respectively.

For the 40° rotation, σ_1 has its largest magnitude, -0.28, to the right and to the left of the center crystal in two places adjacent to the corners. The pattern of the stress distribution for the 90° rotation is similar. The appearance of the 140° rotation is considerably different. The maximum compression is shifted to the top and bottom of the center crystal. The compression at the center of the center crystal changes from -0.12 to -0.18 to -0.22, respectively, for the three rotations.

The uniaxial vertical loadings show a considerably different pattern. Figs. 14, 15 and 16 correspond to the plots in Figs. 7b,c, and d for the rotation of the center crystal by 40°, 90° and 140°, respectively. The σ_1 is slightly in tension, +0.02 for the 40° and 90° cases, but it is compressional for the 140° case, -0.08. There is a corresponding build-up of compressional stress, top and bottom in these cases, perpendicular to the uniaxial stress, but it achieves a maximum value of only -0.12 for the 40° case.

Off Center Models

A slightly different set of models is presented in Fig. 17. The crystal to the right of the center one has been rotated 40°, 90° and 140°, respectively, in Figs. 17a,b and c, and subjected to isostatic loading. Both τ_{max} and the principal stresses are presented on the same page. The τ_{max} plots show much more variation than do the plots of the principal stresses. The distribution of the maximum shear stresses indicates a rather profound effect of anisotropy. The larger values of the shear for the 40° case are outside of and to the left of the rotated crystal, with a considerable build-up on the slant faces.

The 90° case shows a similar distribution, though the magnitude of the τ_{max} is not as large.

The distribution of τ_{max} in the 140° case is markedly different, with the larger values lying inside the boundaries of the rotated crystal. Similar behavior was observed in Figs. 4b,c and d, when the rotated crystal was the center crystal.

Simplified Models

The results of the finite element analysis, are plotted in a slightly different form in Figs. 18c, d and 19. Each principal stress and τ_{max} are plotted separately. The first principal stress (maximum tension) is plotted on the left as a single half arrow at the center of each triangle of the model. The length of the arrow is proportional to the magnitude of the stress it represents. The magnitude of the maximum arrow length is indicated in this figure for each stress. The second principal stress (maximum compression) is plotted similarly in the center, and the maximum shear stress, τ_{max}, is plotted on the right. Only isostatic loading is considered.

In the case of Model A, a hard isotropic inclusion is inserted into the system. The Young's modulus of the center crystal is ten times larger than the surrounding crystals. The stresses on all faces are essentially equal and raised by the factor 1.36 over that of the completely homogeneous model. At the boundary the stress is seen to be predominantly radial. The extrapolated normal stress at the boundary is consistently 3% higher inside than outside. The shear at the boundary has increased from zero for the homogeneous case to 50% of the normal stress, and, as seen in Fig. 18a, it is concentrated outside the center crystal.

For the case of Model B, a soft isotropic inclusion is enclosed in a system ten times stiffer. The stresses on each face are reduced by a factor of 0.27. The surrounding structure could sustain a hole, and so this reduction is easily understood. The principal compressional stresses inside the center crystal are less than 0.20 times the compressional stresses outside. The shear is raised to 75% of the average normal stress, and from Fig. 18b it can be seen to be confined to the region outside the center crystal. The shear inside the center crystal is essentially zero. The boundary outside the center crystal is loaded predominately circumferentially.

The other four models are anisotropic. Because of the relationship $\nu_{xy}E_x=\nu_{yx}E_y$ for orthotropic materials, a limit is imposed on the degree of anisotropy. The ratio of 3/1 permits reasonable values of Poisson's ratio.

Model C was given technical constants so that in the y-direction the constants are continuous. In the x-direction the modulus is three times greater than the matrix. It might be expected that the stresses would be increased on faces one and four (faces perpendicular to the x-axis) and that the other faces would be affected relatively little. The finite element analysis shows that a stress increase of 1.32 occurs for the x-faces and 1.20 for the other faces. The geometric effect of the crystal shape on the trajectories is evident in Fig. 18c, and it is evident that τ_{max} has its largest values outside of and all the way around the center crystal.

Model D has technical constants such that only the y-direction is different from the matrix and the modulus in that direction is 1/3 that of the matrix. It might be anticipated that there would be no alteration in stress at the x-faces and a reduction on the other faces. The analysis shows that there is a stress increase on the x-faces of 1.16 and for the other faces a reduction of 0.93. In Fig. 18d, the plot of the principal stresses at the center of each finite element triangle shows an unusual behavior near the x-faces. The principal-stress axes are rotated nearly 90 degrees. The values for the principal stresses are lower inside the center crystal, but τ_{max} is nearly uniformly large inside the center crystal. The direction of principal-stress axes coincides with that of the principal strain axes outside the center crystal, but inside they do not.

There is very little difference between Model A (hard isotropic) and Model E (hard anisotropic). Figures 18a and 18c are essentially identical. The stresses extrapolated to the boundary differ by about 2%.

It appears that the large change (x10) in modulus is the dominating factor. The stress-increase noted for the anisotropic case, where the inner elastic modulus was three times greater than the matrix, was 1.32 (Model C). For Model A, where the modulus change was ten times, the stress increase was 1.36. Therefore, the three-fold increase in the elastic constant is seen to be almost as effective as the ten-fold increase. Hence, the anisotropic effect of the center crystal is masked to a large extent by the larger change of both moduli.

There is also little to distinguish Model B (soft isotropic) and Model F (soft anisotropic), by examination of Figs. 18b and 18f. The stresses at

the boundary are, however, reduced on all faces for Model F and on the faces perpendicular to the x-axis, the forces were reduced to less than half the value they were subjected to for Model D.

Six Random Orientation Models

In Fig. 19 six different random orientations under thermal loading are given. The center crystal is maintained constant in all of the figures with the c-axis in the direction of the x-axis and the a-axis in the y-direction.

The position of the maximum stresses varies from one different random arrangement to the next. There is a tendency for maximum stresses to develop near the corners of the crystals. The stresses extrapolated to the boundaries from the inside did not compare well with the extrapolation from the outside. In some instances the extrapolations from one side of the boundary were large and negative and from the other side were large and positive. A finer-mesh model seems indicated.

CONCLUSIONS

The elastic behavior of an alumina ceramic body has been modeled by the use of the finite element method. It is found that:

1) The anisotropic characteristics of the material alter the position in the model where the magnitude of the shear stress is maximum under isostatic, uniaxial, and thermal loadings.

2) Under uniaxial loading, the effect of anisotropy under the conditions examined was to alter the stresses acting on the faces perpendicular to the loading forces from compression to tension by about 6% of the applied loading.

3) The inclusion of a crystal with elastic constants ten times greater or less than the matrix makes such a difference that the effect of a three fold anisotropy is nearly masked.

4) Stress gradients generated in a model with random orientation of the crystals is very high. Further conclusions about the effect of random orientation would require a model better adapted to the high-stress gradient.

REFERENCES

1. O. C. Zienkiewicz, "The Finite Element Method in Engineering Science," McGraw-Hill, London, 1971.

2. Papers presented at International Symposium on Numerical and Comp[illegible] Methods in Structural Mechanics, sponsored by the Office of Naval Research and the University of Illinois at Urbana, Illinois, September 8-10, 1971.

3. W. R. Buessem and F. F. Lange, "Residual Stresses in Anisotropic Ceramics," Interceram., Vol. 15, No. 3, 229-231 (1966).

4. W. D. Kingery, "Introduction to Ceramics", John Wiley & Sons, Inc., 1960.

5. H. D. Dahl, "A Finite Element Model for Anisotropic Yielding in Gravity Loaded Rock", Ph.D. Dissertation, The Pennsylvania State University, 1969.

6. J. E. Gagorik, R. A. Queeney and H. A. McKinstry, "Stress Distributions in Alumina Bicrystal Tensile Specimens," J. Amer. Ceram. Soc., 54, (12) 625-627, (1971).

7. T. Kovacs, "Stress Concentration in Elastically Anisotropic Bicrystal Tensile Specimens", paper in final report, The Pennsylvania State University, 1972.

8. J. H. Gieske, "The Third Order Elastic Coefficients and Some Anharmonic Properties of Aluminum Oxide," Ph.D. Dissertation, The Pennsylvania State University, 1968.

9. D. S. Lieberman and S. Zirinsky, "A Simplified Calculation for the Elastic Constants of Arbitrarily Oriented Single Crystals," Acta Cryst. 9, 431-436, (1956).

10. S. G. Lekhnitskii, "Theory of Elasticity of an Anisotropic Elastic Body", Translation from Russian by P. Fern, Holden Day, San Francisco, 1963.

11. L. O. Degelman, G. E. Edwards, R. J. Masters and L. O. Sinkey, SYMAP-5, Introductory Manual for Synagraphic Computer Mapping, Department of Architectural Engineering, The Pennsylvania State University, Report No. 69-4, 1969. (SYMAP was developed for the Laboratory for Computer Graphics, Harvard University).

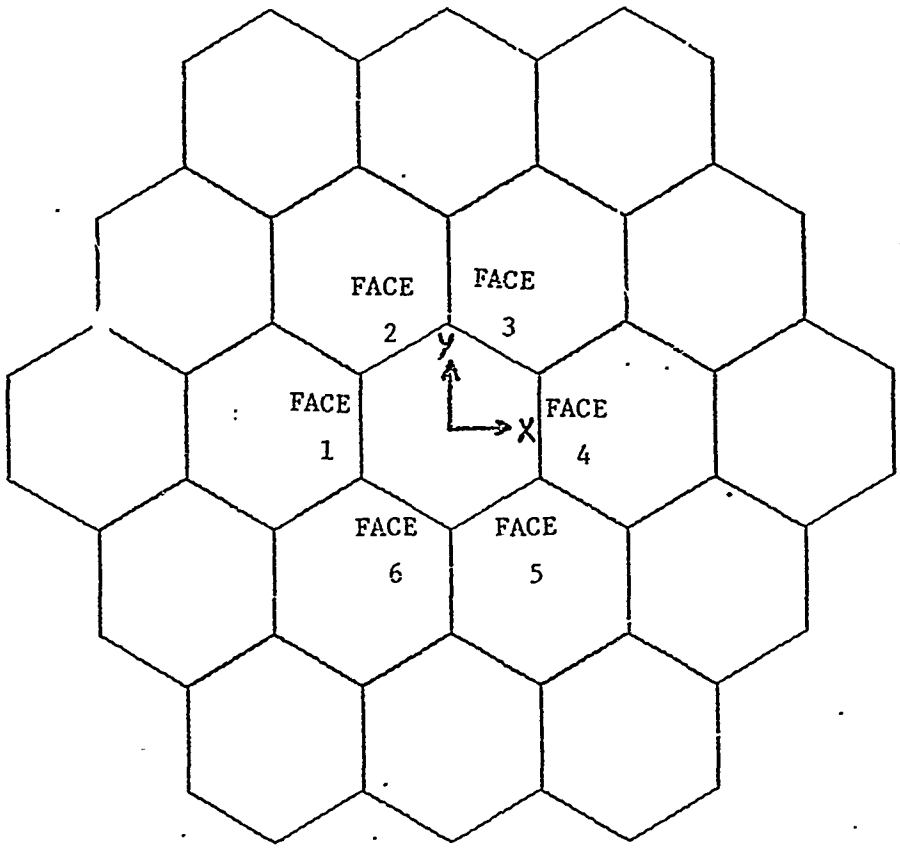

Fig. 1. Nineteen crystal model of a two dimensional ceramic body. Each hexagon can be given independent anisotropic elastic and thermal constants. The orientation of the axes are shown. The faces of the center crystal are numbered.

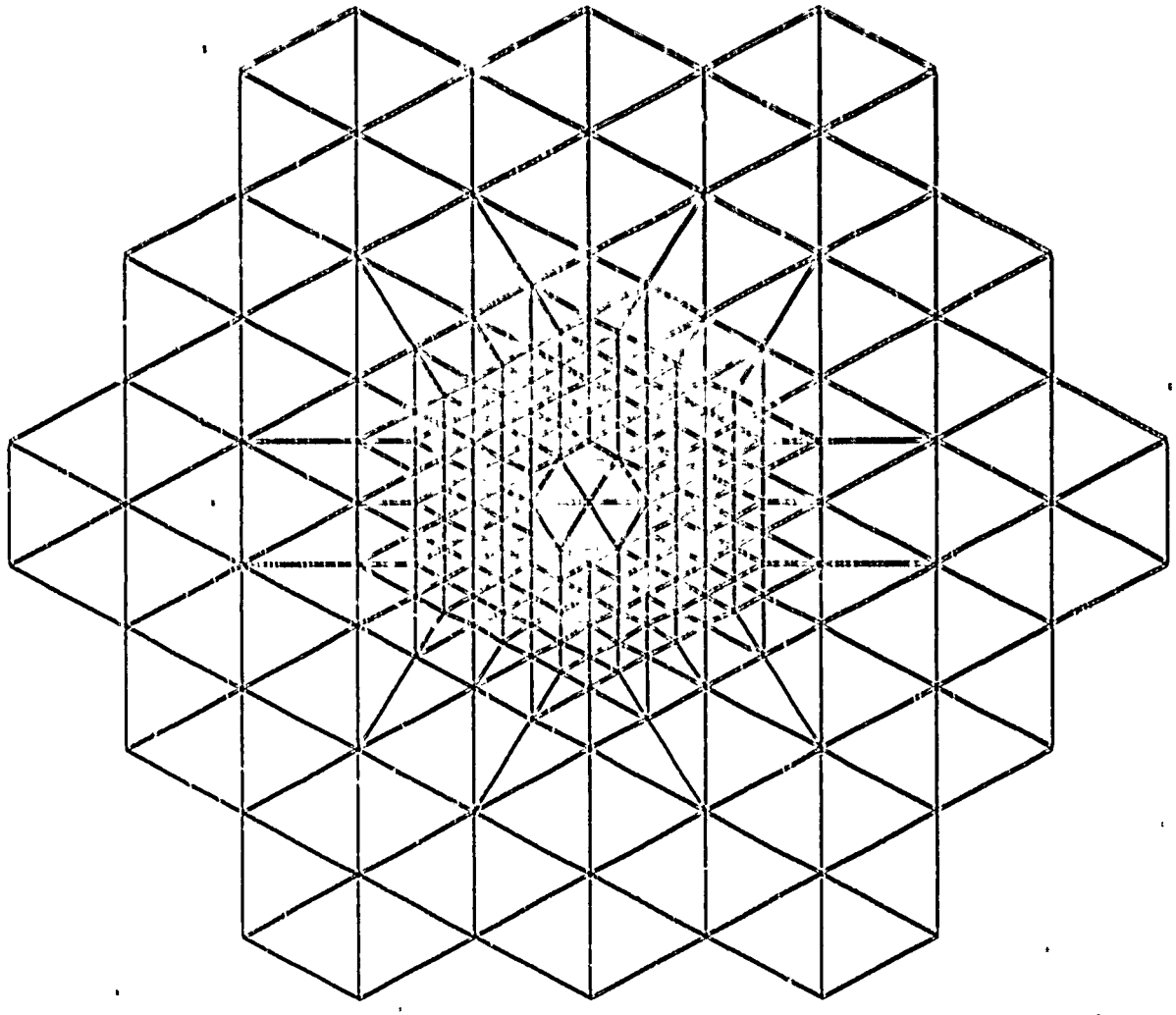

Fig. 2. Finite element model for nineteen crystal model of a ceramic body. The model has 366 triangles and 199 nodes.

FIG 3 PRINCIPAL STRESS: ISOSTATIC LOADING

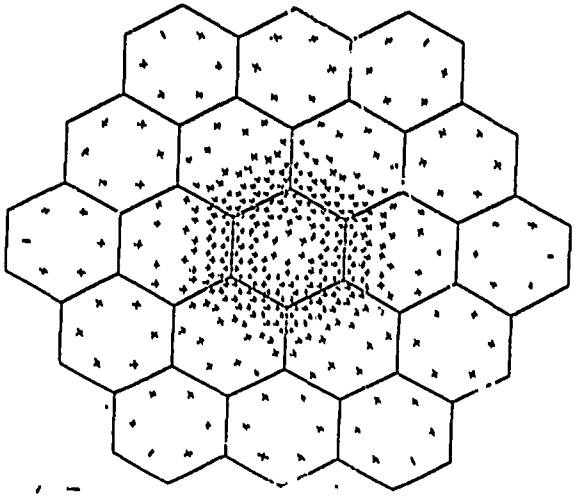

a ISOTROPIC

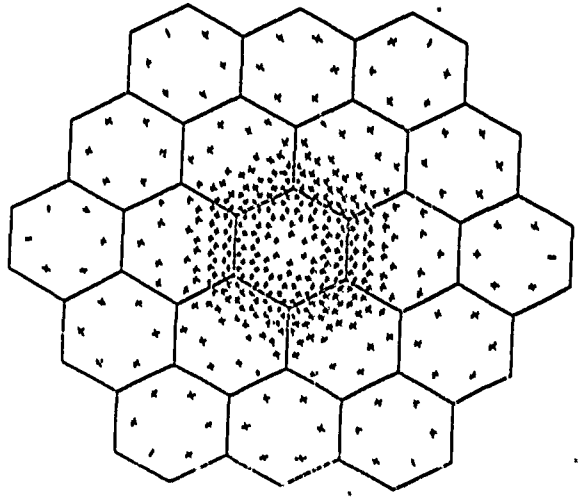

b CENTRAL CRYSTAL ROTATED $\beta = 40°$

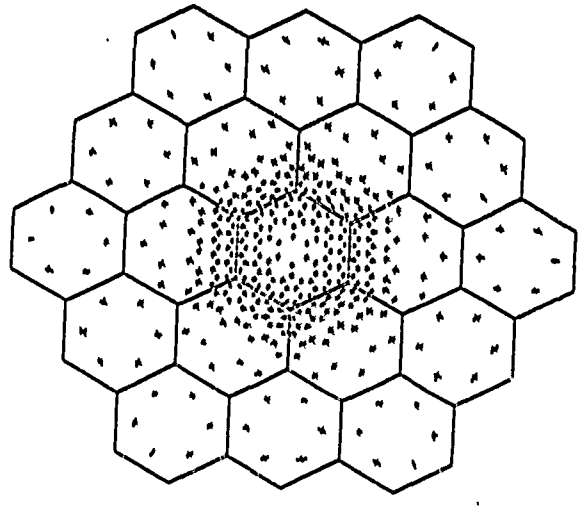

c CENTRAL CRYSTAL ROTATED $\beta = 90°$

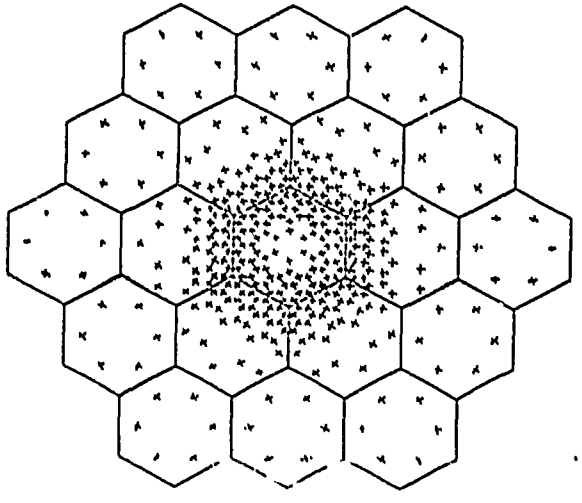

d CENTRAL CRYSTAL ROTATED $\beta = 140°$

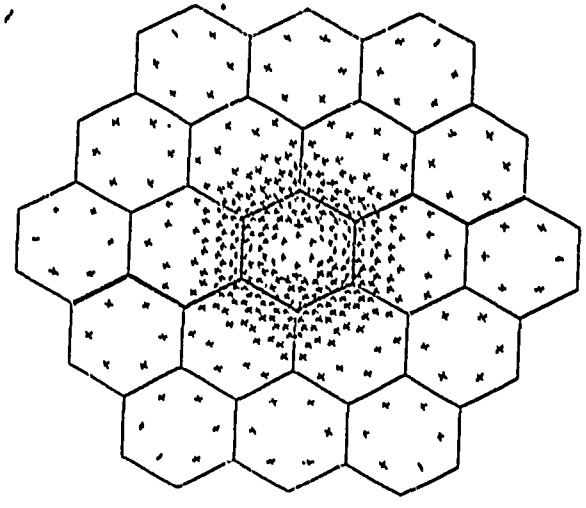

e MAXIMUM ANISOTROPY

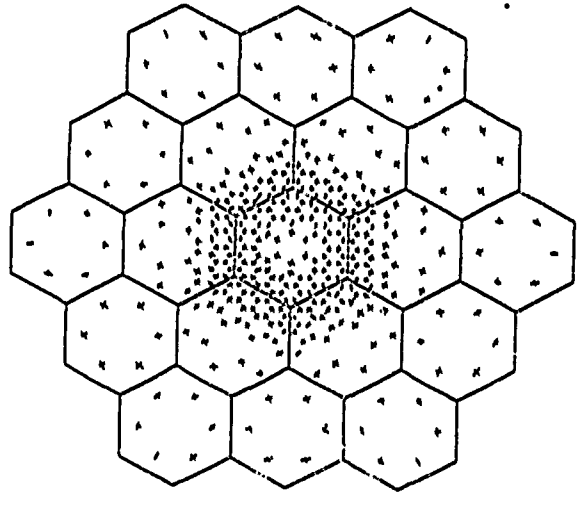

f RANDOM ORIENTATION

85.

FIG 4 TAU MAX: ISOSTATIC LOADING

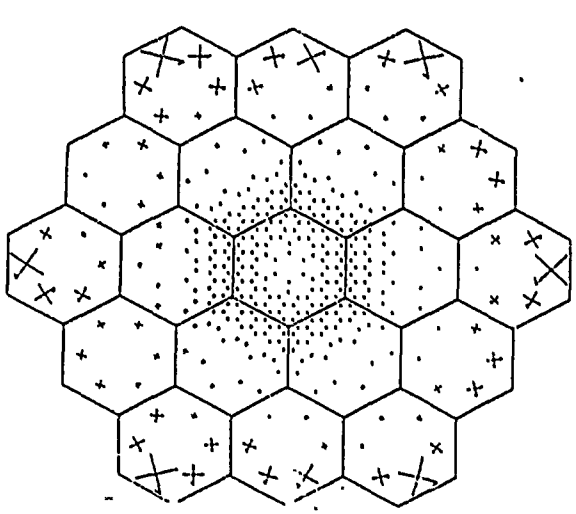

a ISOTROPIC

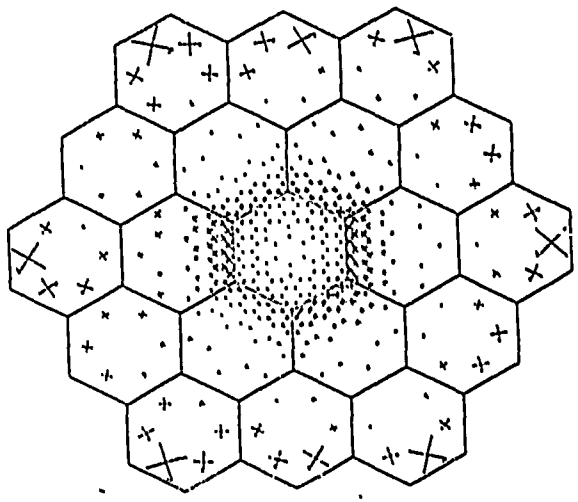

b CENTRAL CRYSTAL ROTATED β = 40°

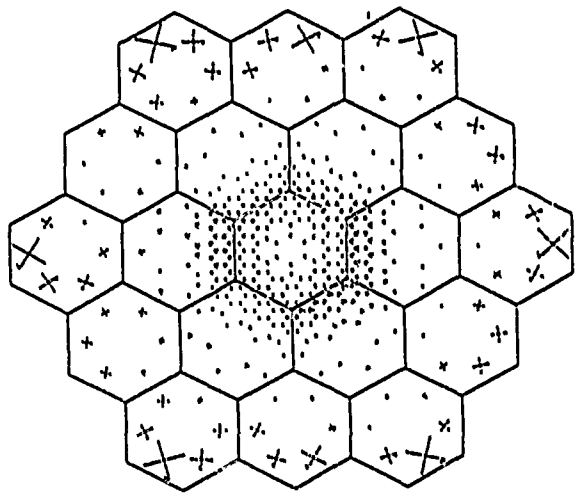

c CENTRAL CRYSTAL ROTATED β = 90°

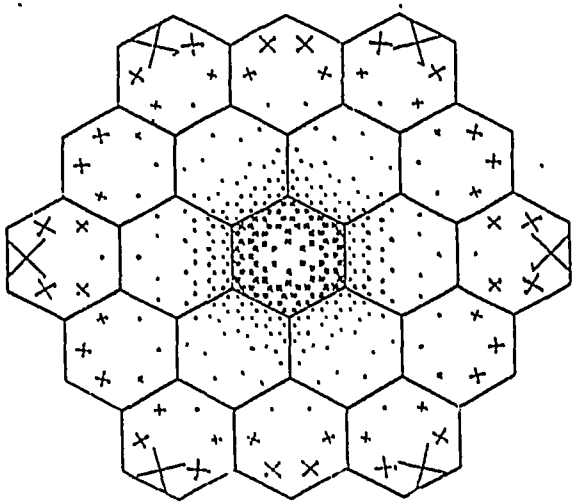

d CENTRAL CRYSTAL ROTATED β = 140°

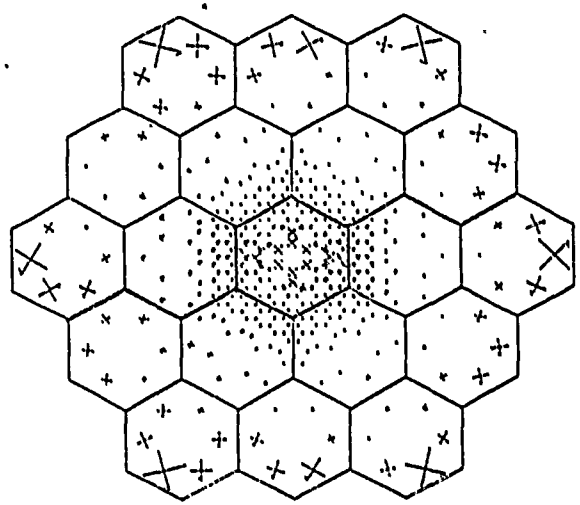

e MAXIMUM ANISOTROPY

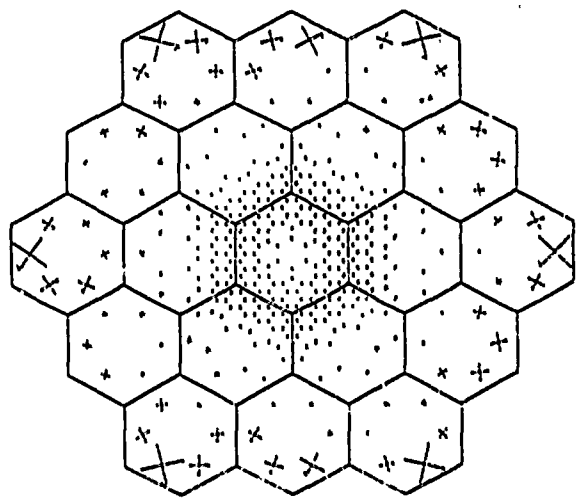

f RANDOM ORIENTATION

FIG 5 PRINCIPAL STRESS: UNIAXIAL-1 LOADING

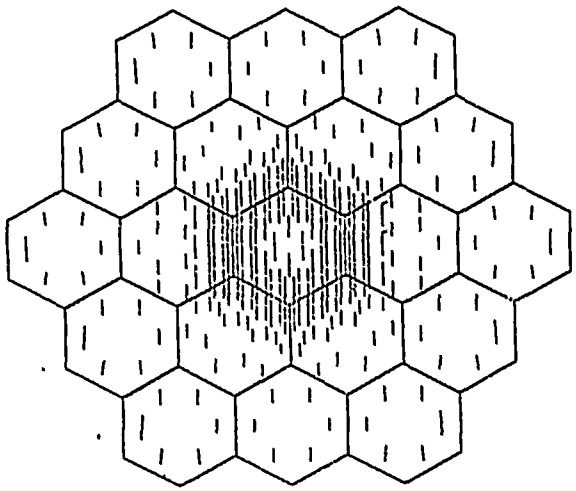

a ISOTROPIC

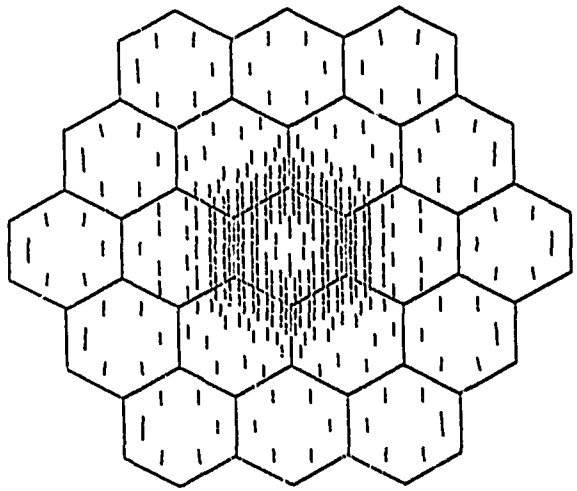

b CENTRAL CRYSTAL ROTATED $\beta = 40°$

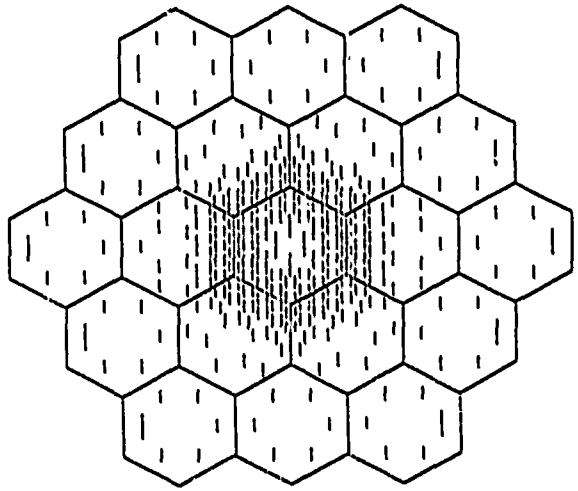

c CENTRAL CRYSTAL ROTATED $\beta = 90°$

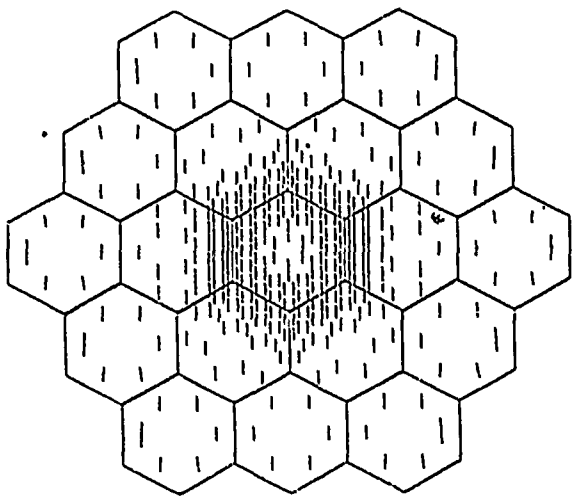

d CENTRAL CRYSTAL ROTATED $\beta = 140°$

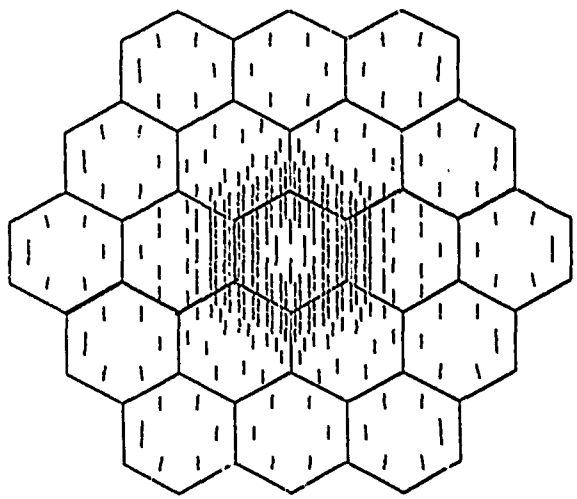

e MAXIMUM ANISOTROPY

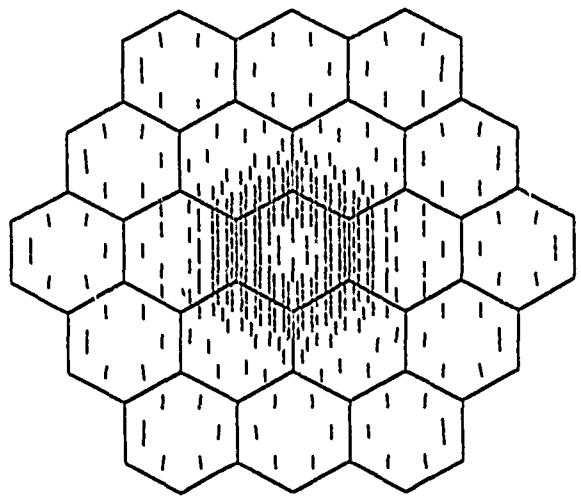

f RANDOM ORIENTATION

18

FIG 6 TAU MAX: UNIAXIAL-1 LOADING

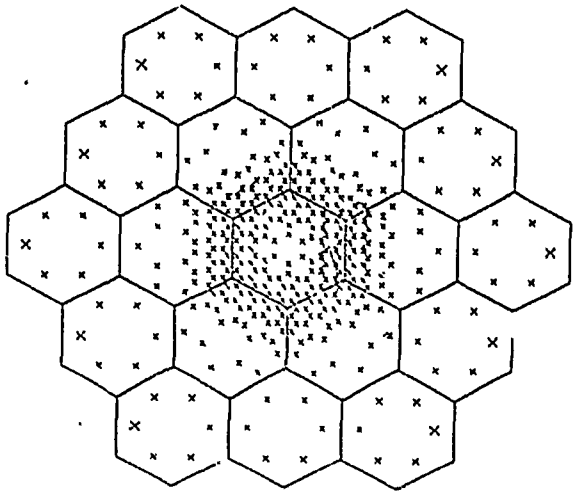

a ISOTROPIC

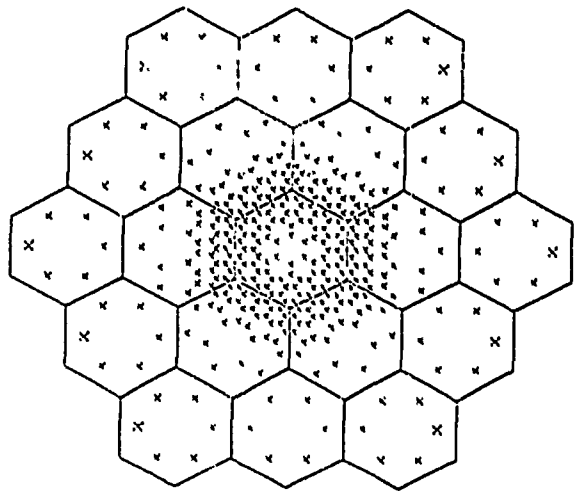

b CENTRAL CRYSTAL ROTATED θ = 40°

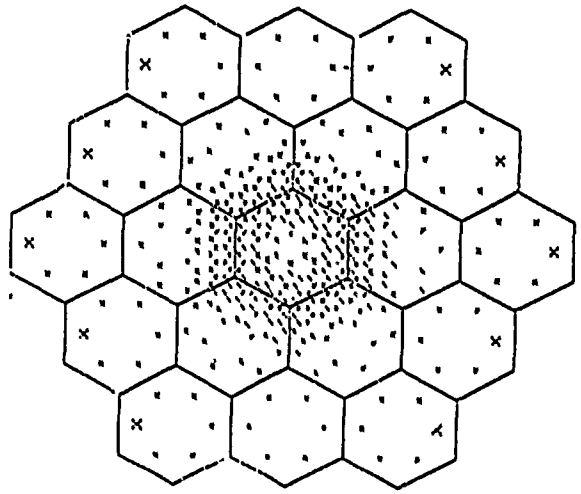

c CENTRAL CRYSTAL ROTATED θ = 90°

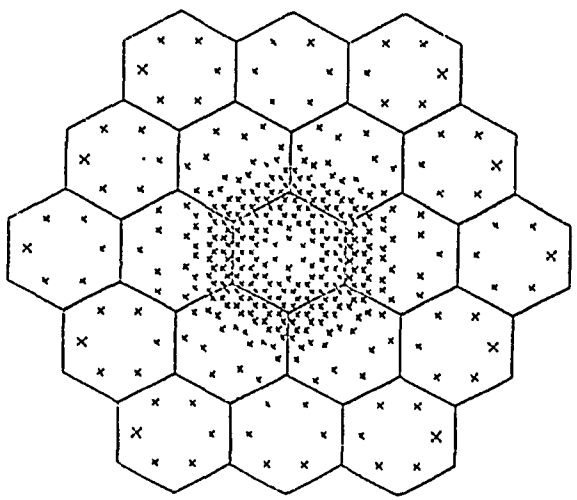

d CENTRAL CRYSTAL ROTATED θ = 140°

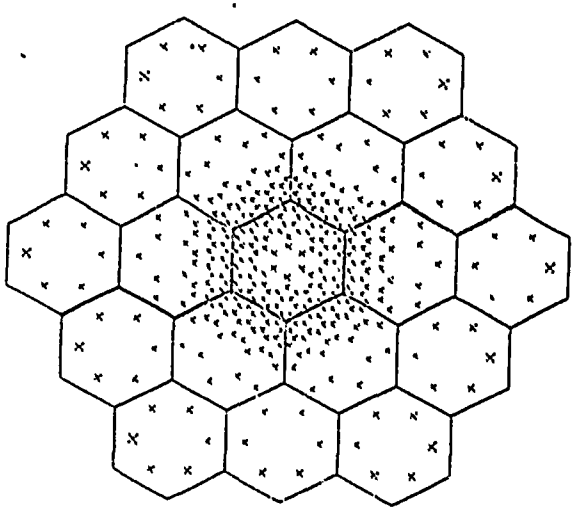

e MAXIMUM ANISOTROPY

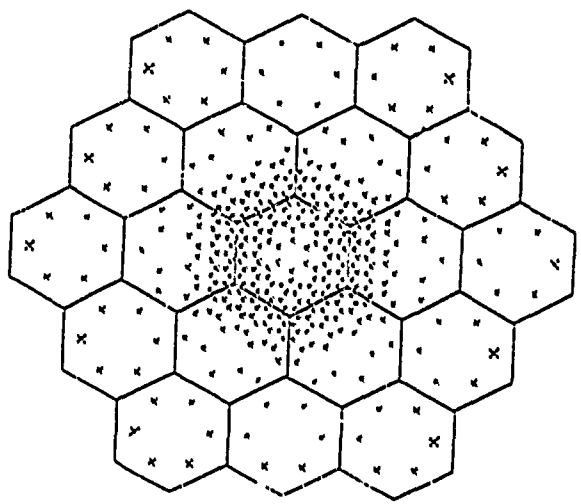

f [illegible]

FIG 7 PRINCIPAL STRESS: UNIAXIAL-2 LOADING

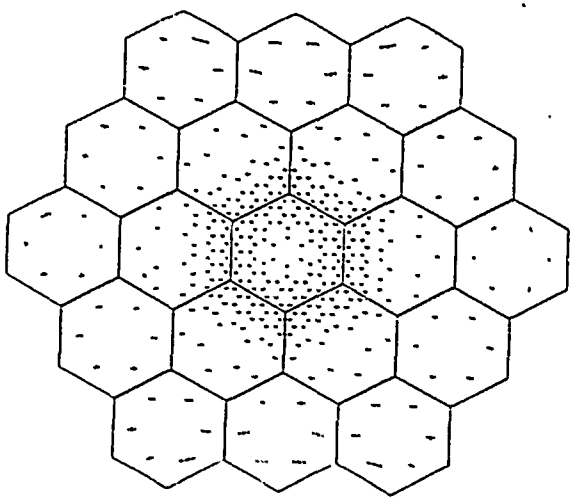

a ISOTROPIC

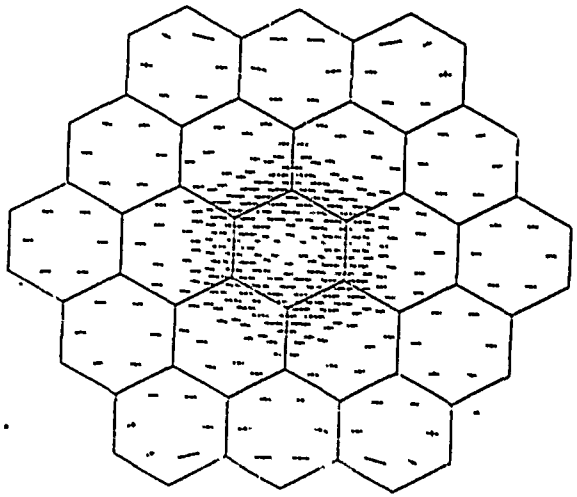

b CENTRAL CRYSTAL ROTATED β = 40°

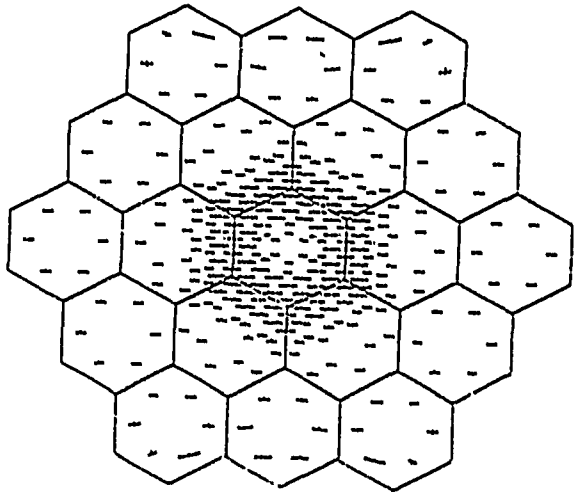

c CENTRAL CRYSTAL ROTATED β = 90°

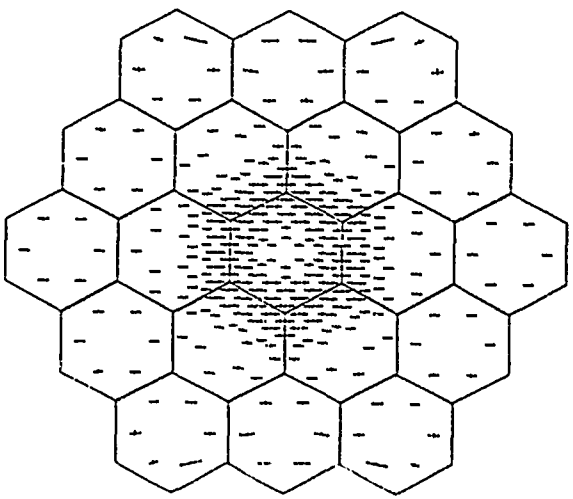

d CENTRAL CRYSTAL ROTATED β = 140°

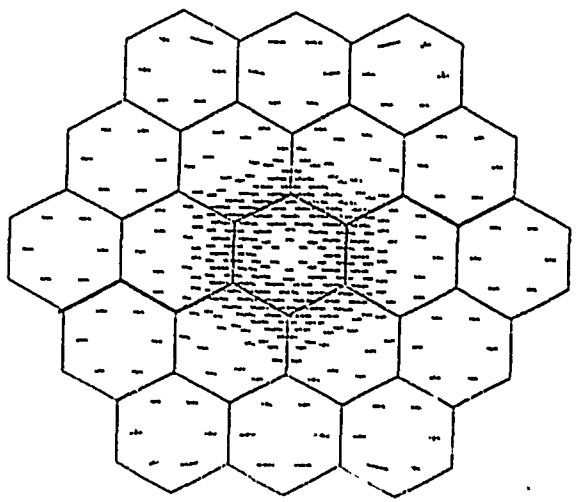

e MAXIMUM ANISOTROPY

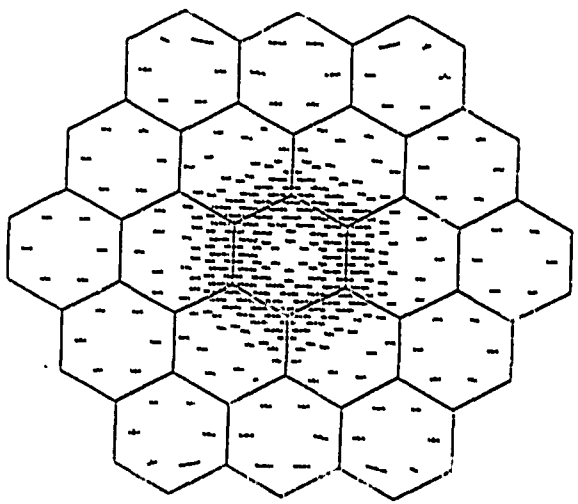

f RANDOM ORIENTATION

FIG 8 TAU MAX: UNIAXIAL-2 LOADING

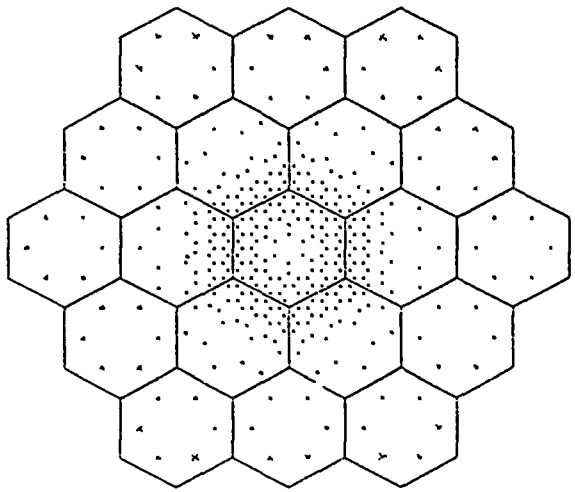

a ISOTROPIC

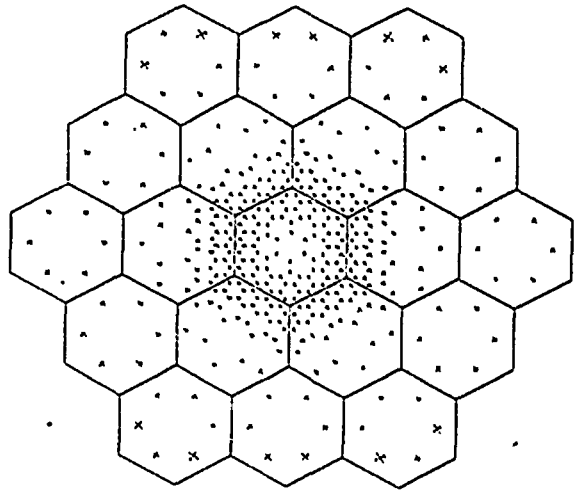

b CENTRAL CRYSTAL ROTATED $\beta = 40°$

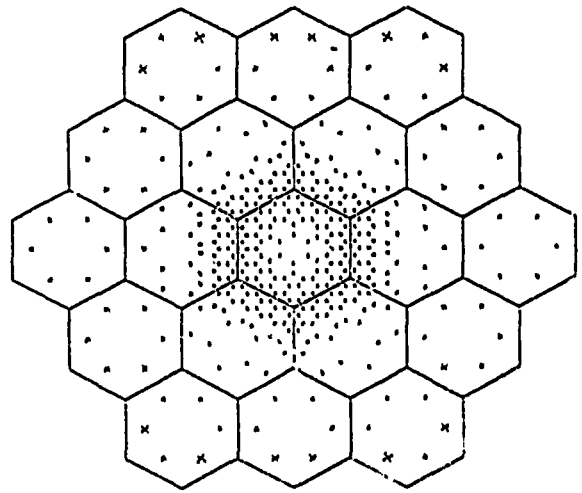

c CENTRAL CRYSTAL ROTATED $\beta = 90°$

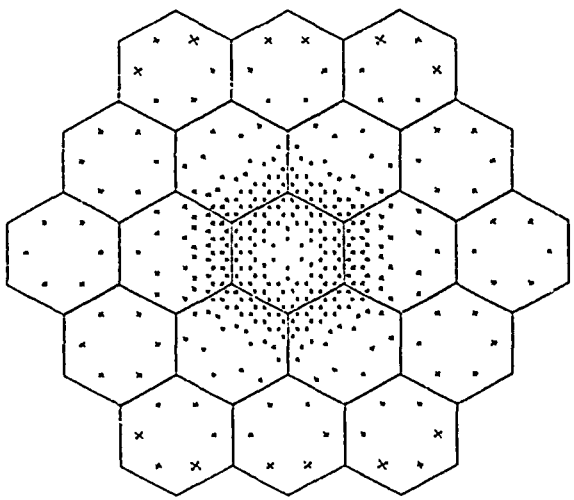

d CENTRAL CRYSTAL ROTATED $\beta = 140°$

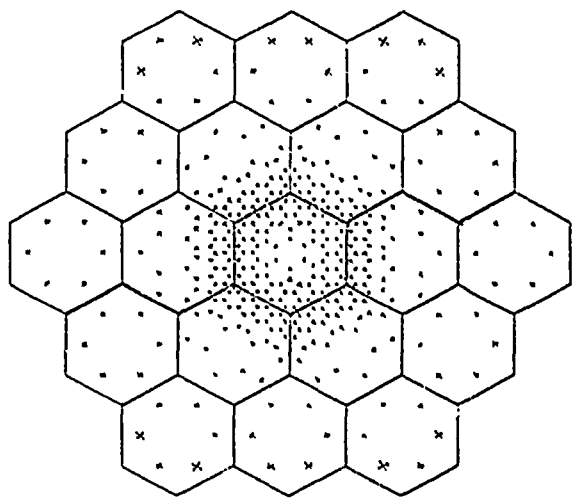

e MAXIMUM ANISOTROPY

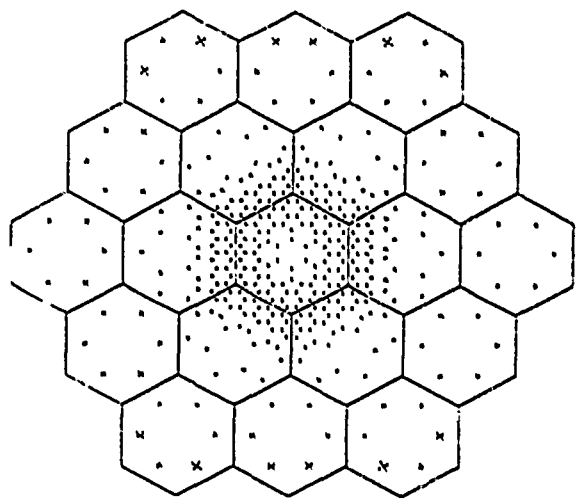

f [illegible]

96

FIG 9 PRINCIPAL STRESS: THERMAL LOADING

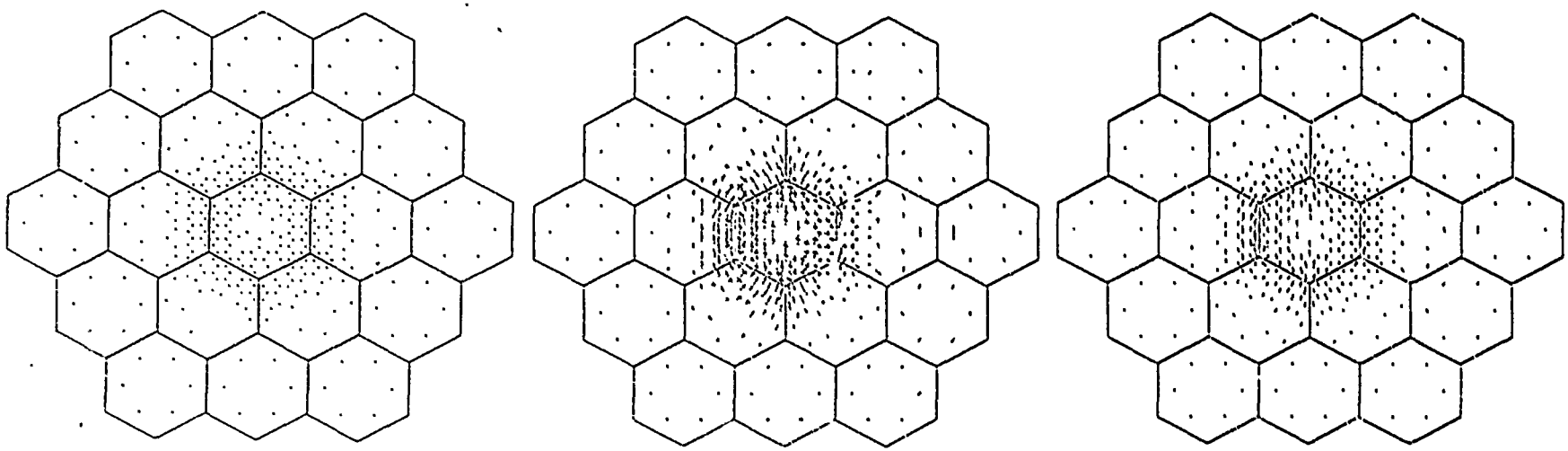

a ISOTROPIC

b CENTRAL CRYSTAL ROTATED $\beta = 30°$

c CENTRAL CRYSTAL ROTATED $\beta = 90°$

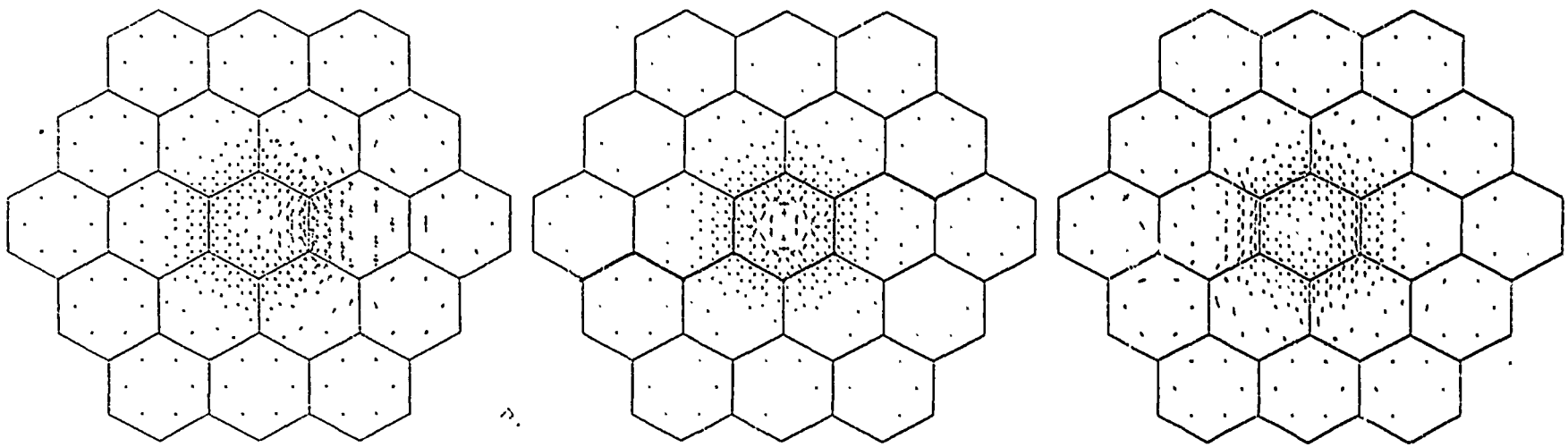

d CENTRAL CRYSTAL ROTATED $\beta = 140°$

e MAXIMUM ANISOTROPY

f RANDOM ORIENTATION

16

FIG 10 TAU MAX: THERMAL LOADING

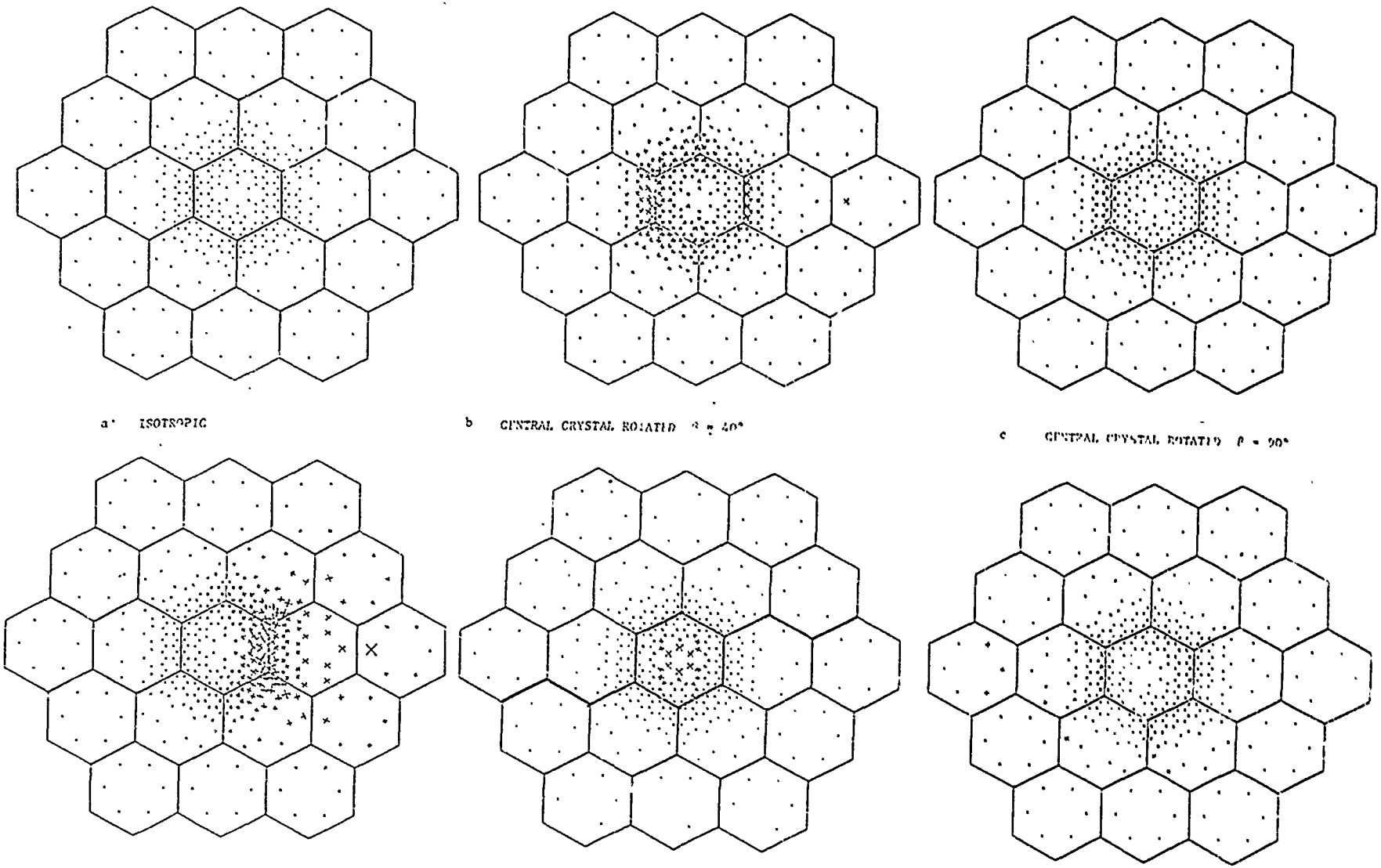

a ISOTROPIC

b CENTRAL CRYSTAL ROTATED $\theta = 40°$

c CENTRAL CRYSTAL ROTATED $\theta = 90°$

d CENTRAL CRYSTAL ROTATED $\theta = 140°$

e MAXIMUM ANISOTROPY

f RANDOM ORIENTATION

92

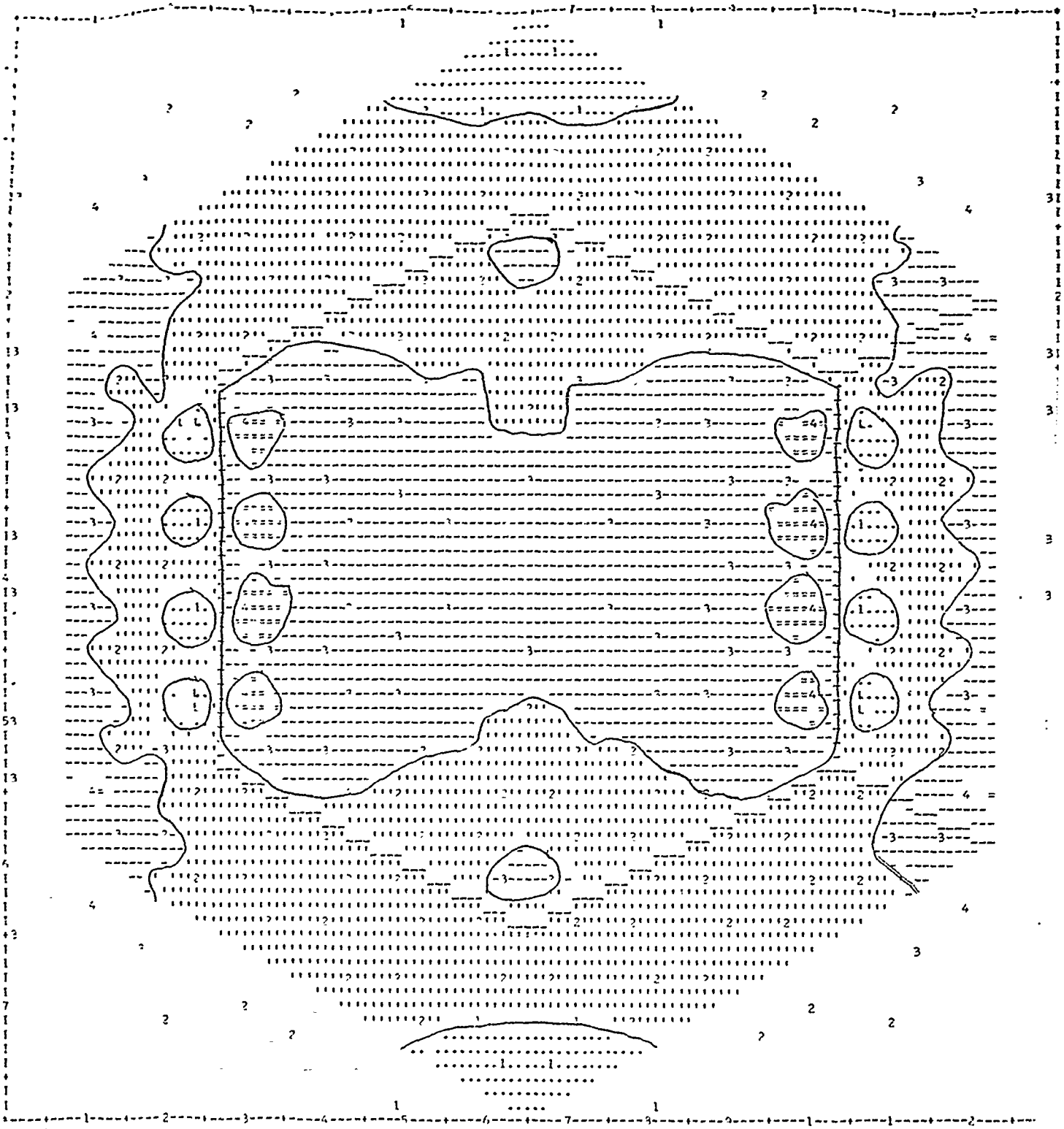

SYMAP

TIME = 09:39:46.44

ELAPSE TIME = 92.73 SECONDS FOR MAP

FIG. 11 SYMAP PLOT OF MINIMUM PRINCIPLE STRESS FOR THE REGION OF THE CENTRAL CRYSTAL WHICH IS ROTATED 45 DEGREES. HORIZONTAL UNIAXIAL LOADING

C 45 ROTATED CENTER CRYSTAL WITH UNIAXIAL (2) LOADING SIG-1

C CENTRAL CRYSTAL AND EIGHT LAYERS PLOTTED, CENTRAL CRYSTAL DRAWN IN.

C NUMBERS DENOTE ACTUAL DATA POINTS

DATA VALUE EXTREMES ARE -1.29 130.54

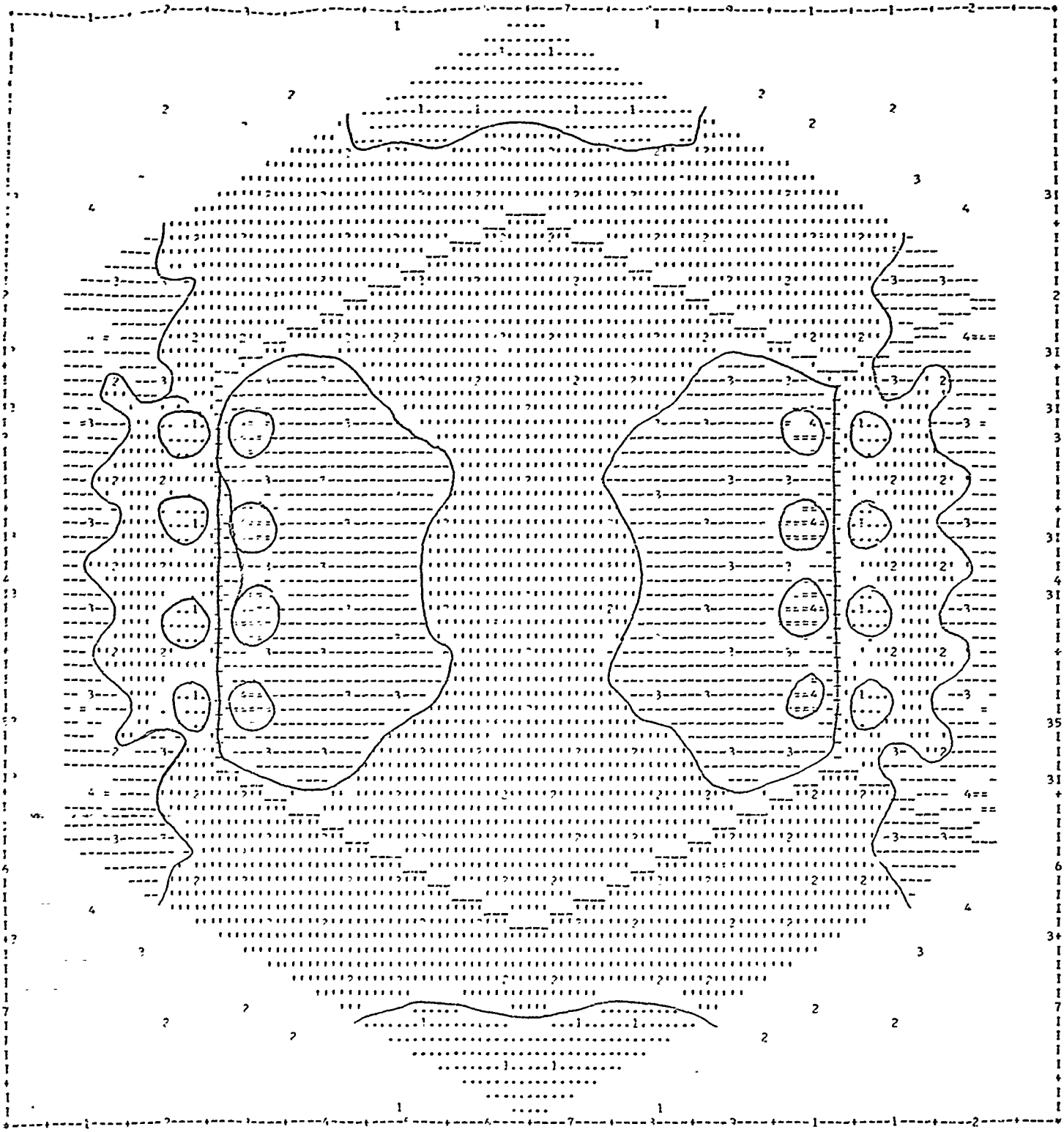

SYMAP

TIME = 10:07:41.41

ELAPSE TIME = 130.27 SECONDS FOR MAP

FIG. 12 SYMAP PLOT OF MINIMUM PRINCIPLE STRESS FOR THE REGION OF THE CENTRAL CRYSTAL WHICH IS ROTATED 90 DEGREES. HORIZONTAL UNIAXIAL LOADING

C 90 ROTATED CENTER CRYSTAL WITH UNIAXIAL (2) LOADING SIG=1

C CENTRAL CRYSTAL AND EIGHT DAYS ELIMINATED. CENTRAL CRYSTAL DRAWN IN.

C NUMBERS DENOTE ACTUAL DATA POINTS

DATA VALUE EXTREMES ARE -41.44 130.65.

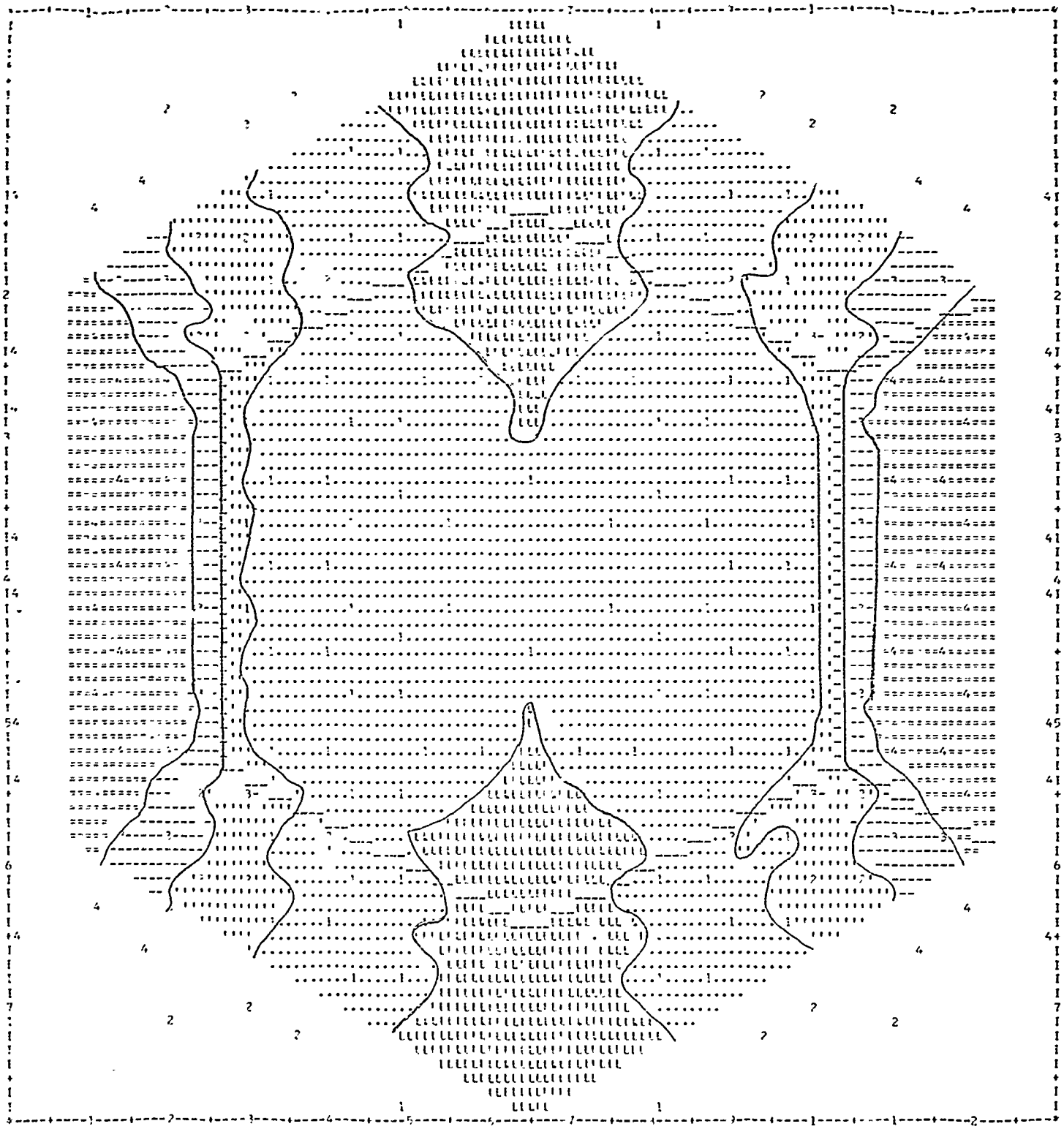

SYMAP

TIME = 10:45:45.18

ELAPSE TIME = 74.32 SECONDS FOR MAP

FIG. 13 SYMAP PLOT OF MINIMUM PRINCIPLE STRESS FOR THE REGION OF THE CENTRAL CRYSTAL WHICH IS ROTATED 140 DEGREES. HORIZONTAL UNIAXIAL LOADING

C 140 ROTATED CENTER CRYSTAL WITH UNIAXIAL (X) LOADING. SIG-1

C CENTRAL CRYSTAL AND EIGHT LAYERS PLOTTED, CENTRAL CRYSTAL DRAWN IN.

C NUMBERS DENOTE ACTUAL DATA POINTS

DATA VALUE EXTREMES ARE -41.41 131.71

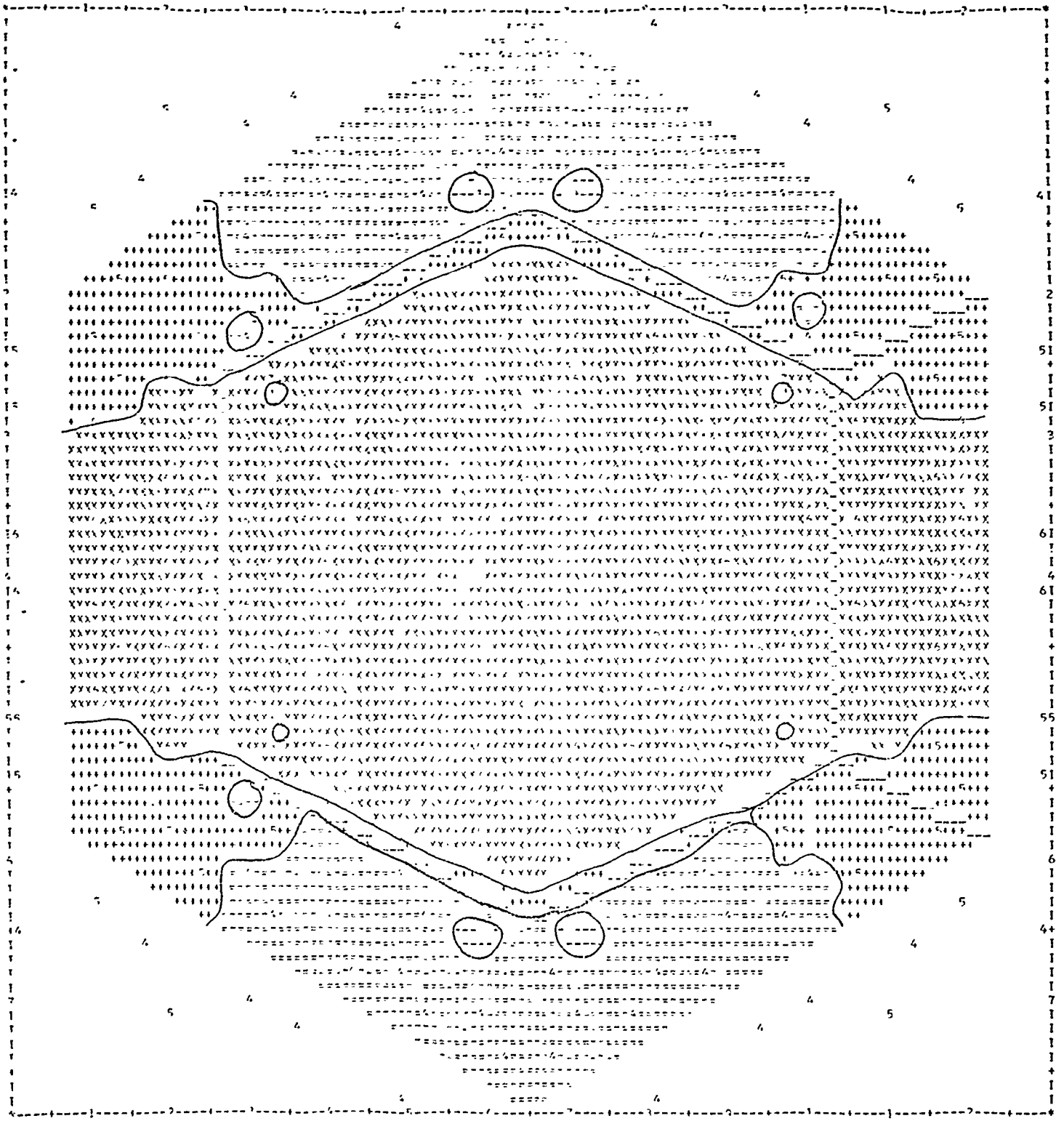

SYMAP

TIME = 10:59:54.33

ELAPSE TIME = 1[illegible] SECONDS FOR MAP

FIG. 14 SYMAP PLOT OF MINIMUM PRINCIPLE STRESS FOR THE REGION OF THE CENTRAL CRYSTAL WHICH IS ROTATED 40 DEGREES. VERTICAL UNIAXIAL LOADING

C 40 DEGREE ROTATION OF CENTER CRYSTAL [illegible] SIG1

C CENTRAL CRYSTAL AND EIGHT LAYERS PLOTTED, CENTRAL CRYSTAL [illegible]

C NUMBERS DENOTE ACTUAL DATA POINTS

DATA VALUE EXTREMES [illegible]

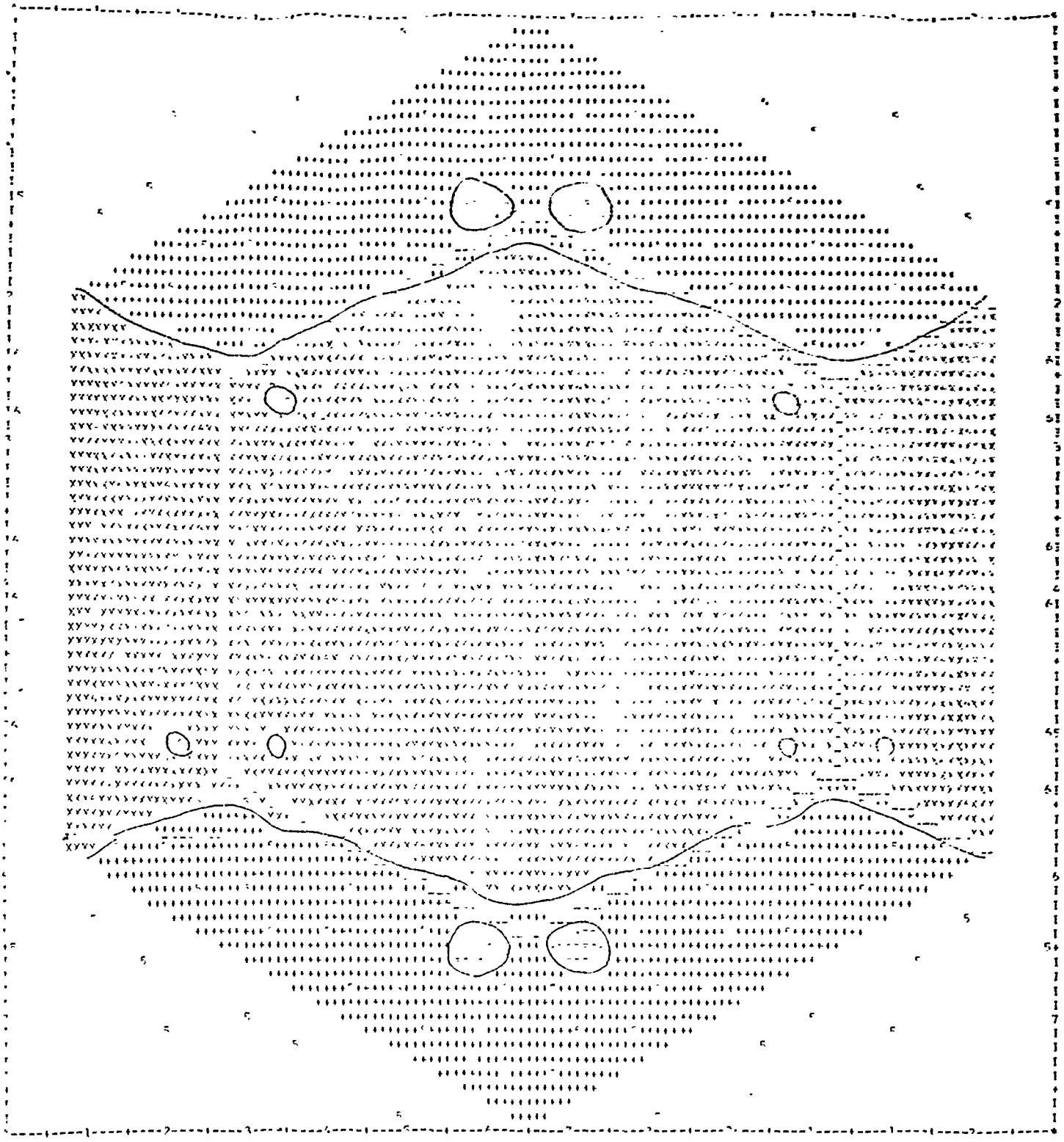

SYMAP

TIME = 20:12:21.33

ELAPSE TIME = 345.36 SECONDS FOR MAP

FIG. 15 SYMAP PLOT OF SECTION PRINCIPLE COMPONENT FOR THE REGION OF THE CENTRAL CRYSTAL WHICH IS CONTAINED IN 90 PLANES. VERTICAL EXPANSION FOUR-FOLD.

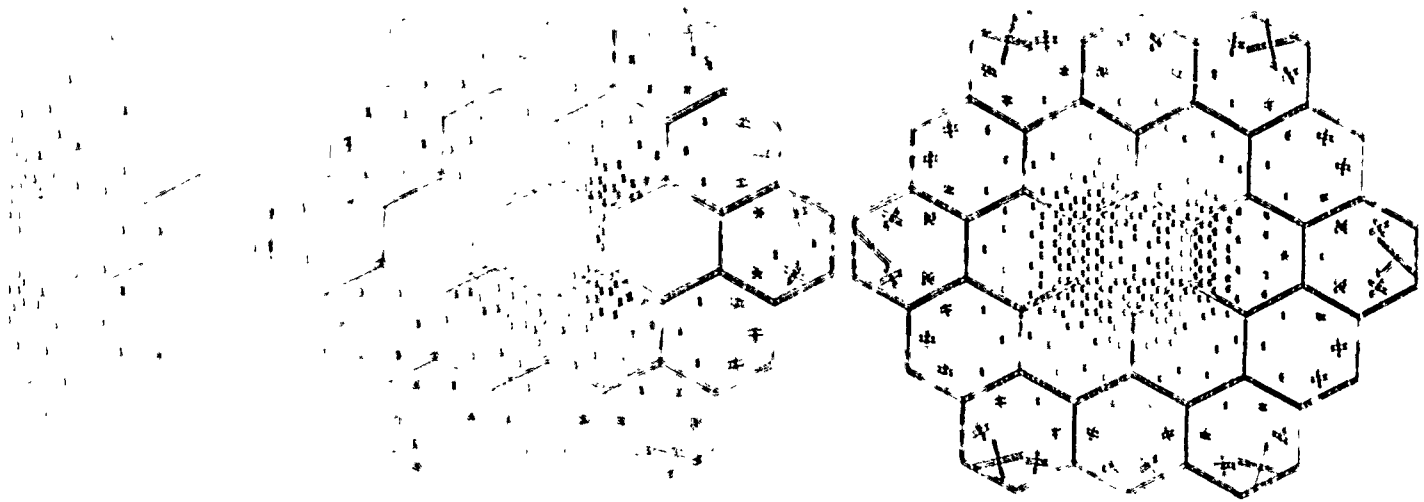

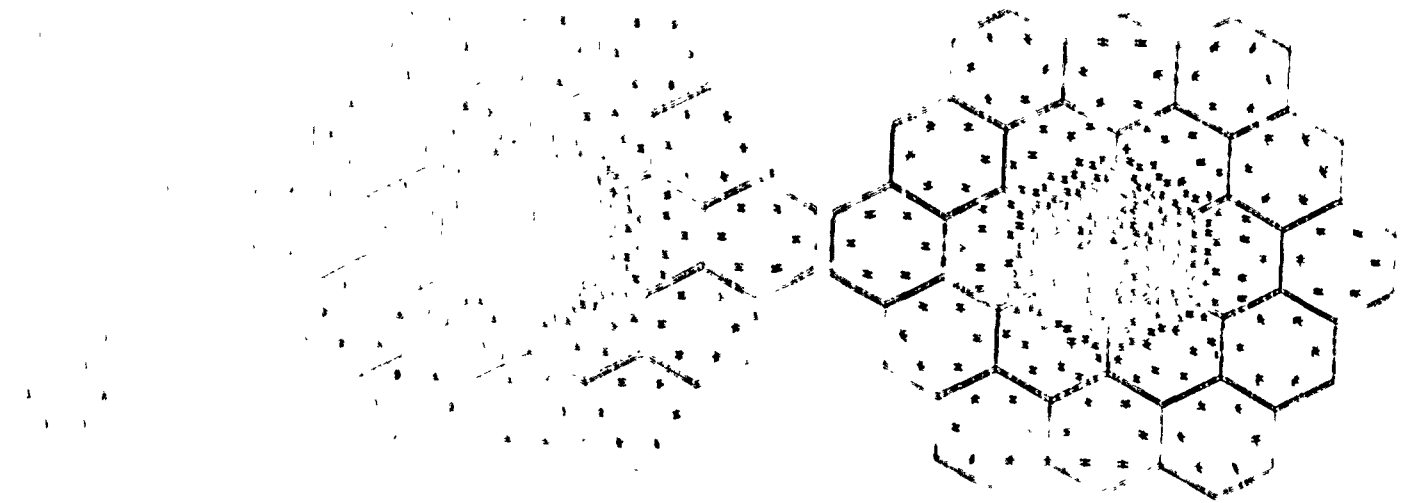

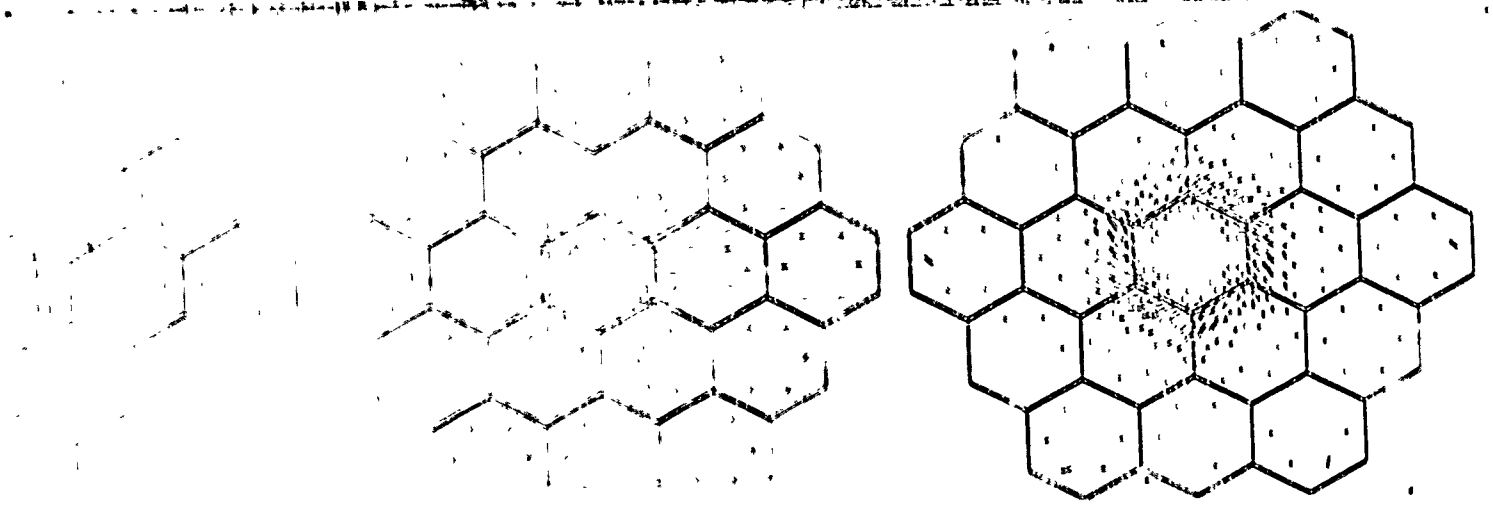

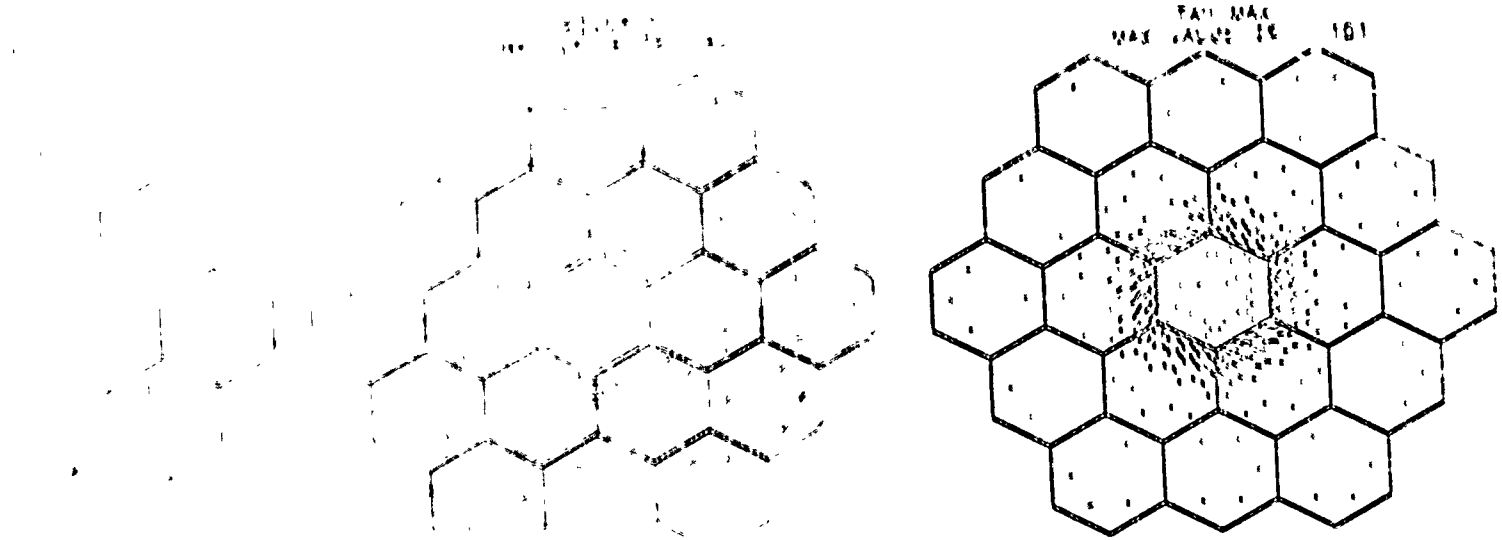

Fig. 1

TAU MAX
MAX VALUE IS 169

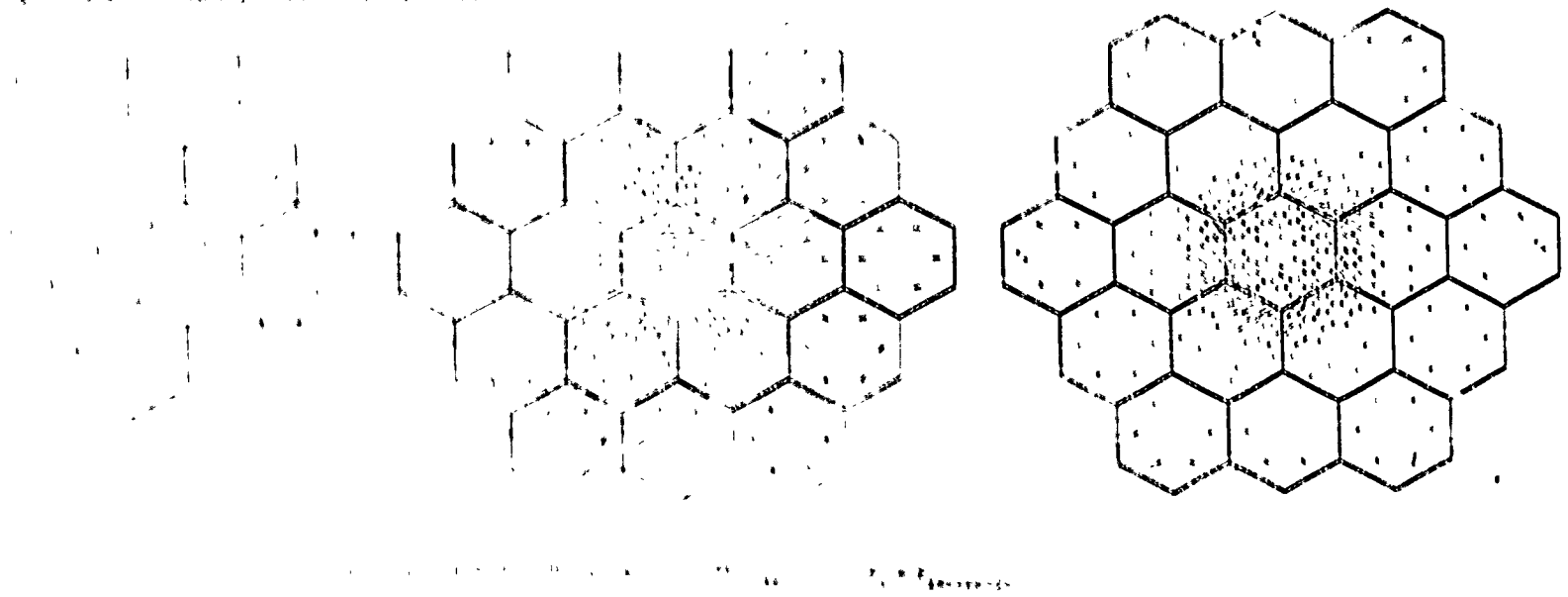

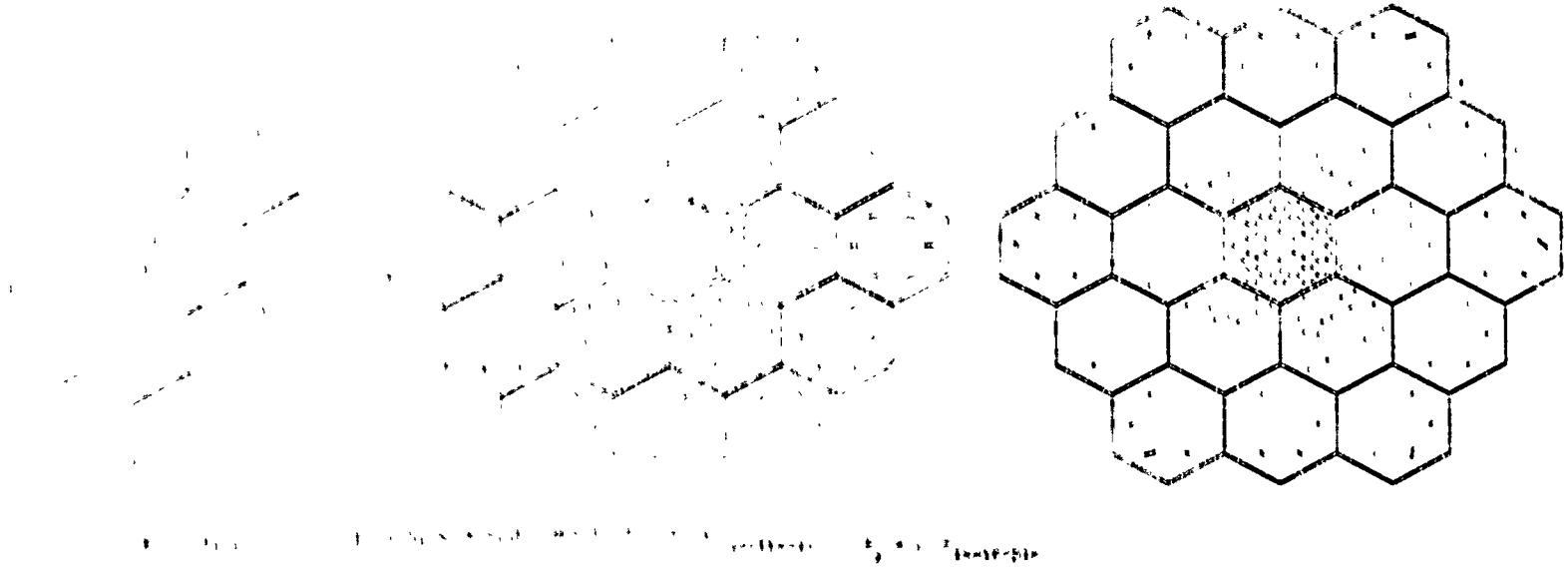

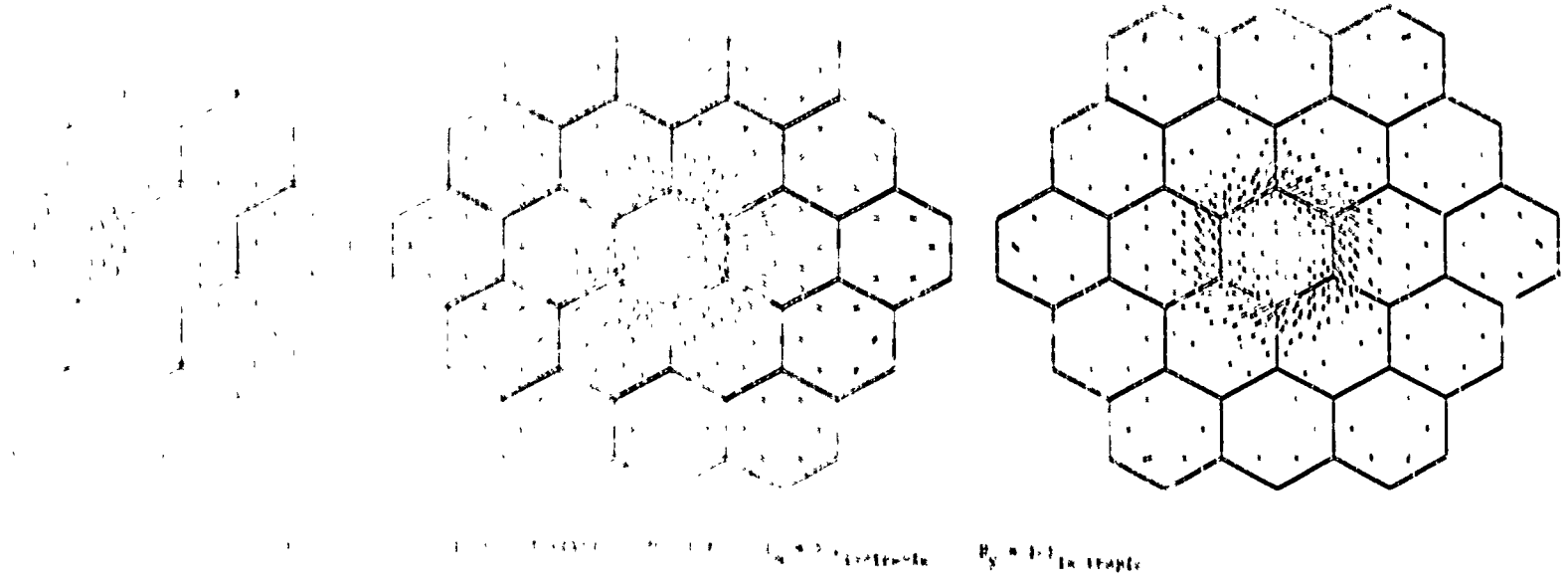

TAU MAX
MAX VALUE IS 119

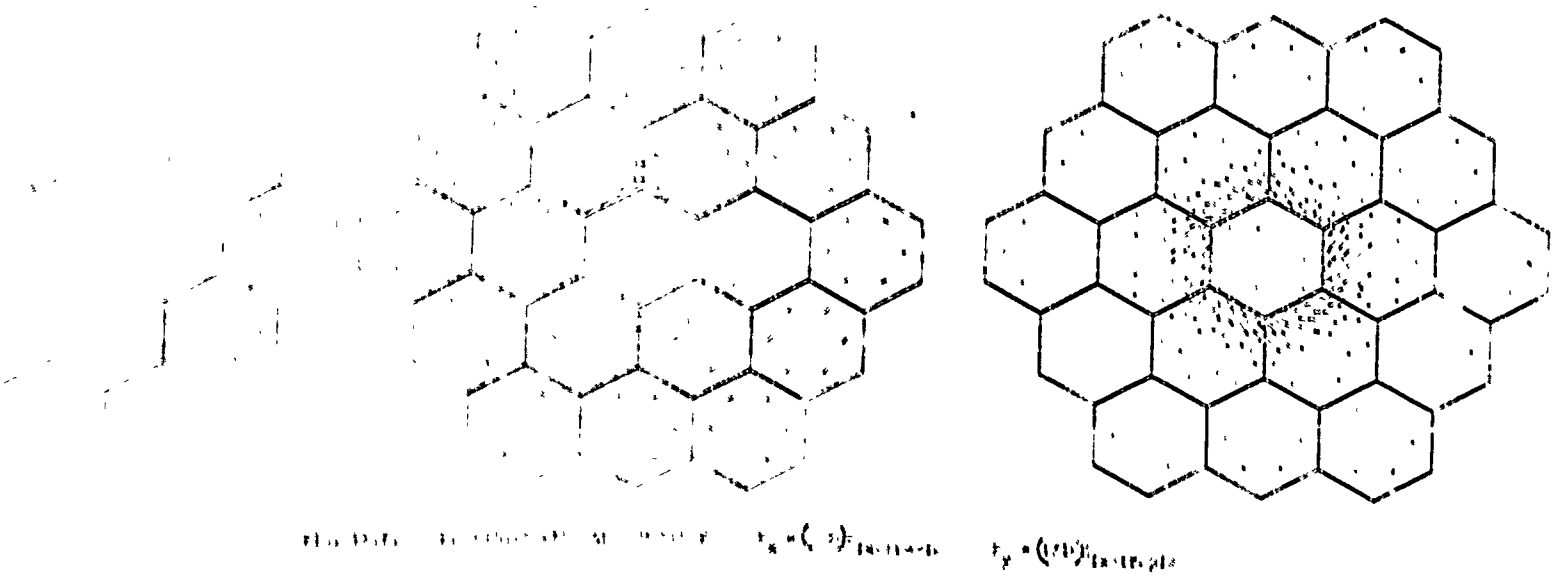

TAU MAX
MAX VALUE IS 207

102

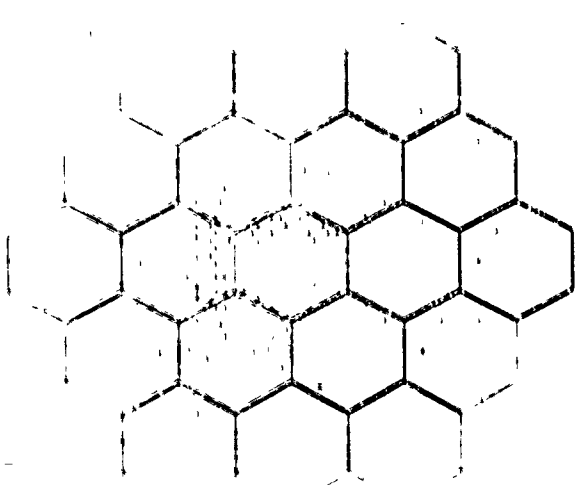

SIGMA 2
MAX VALUE IS 153764

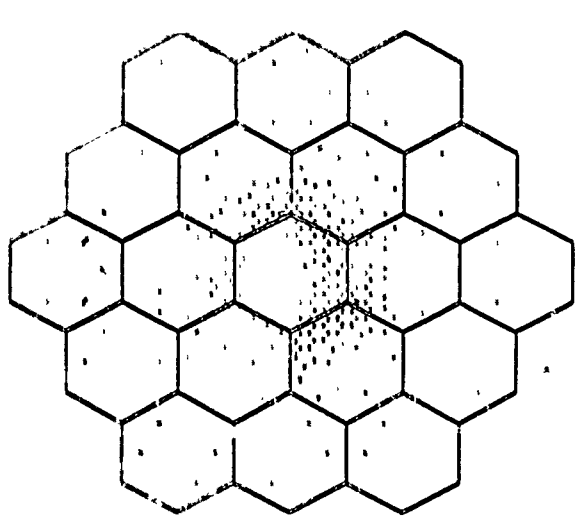

TAU MAX
MAX VALUE IS 70615

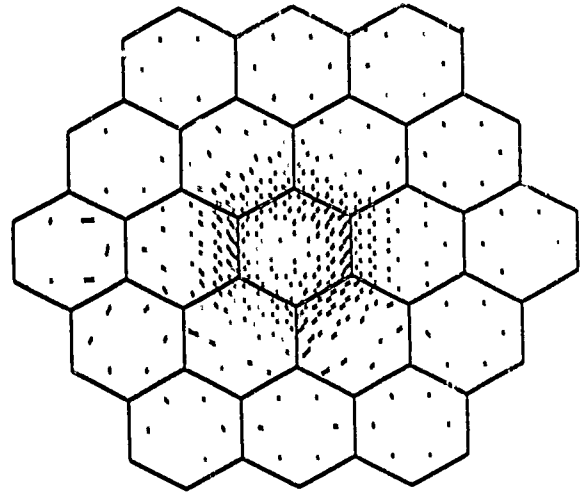

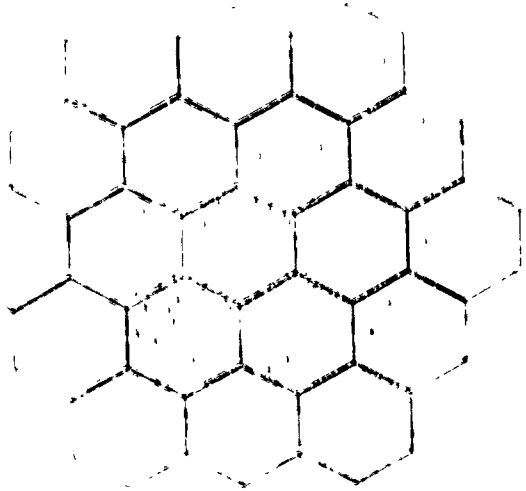

SIGMA 3
MAX VALUE IS 153701

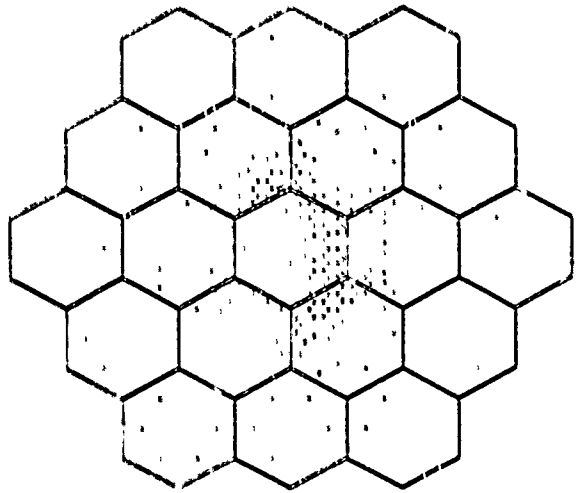

TAU MAX
MAX VALUE IS 65395

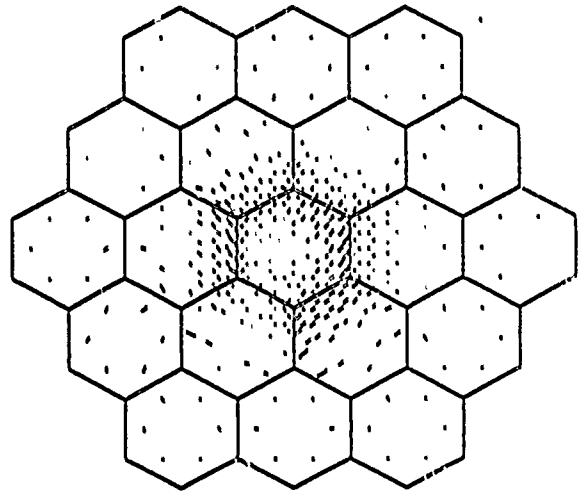

FIG. 19

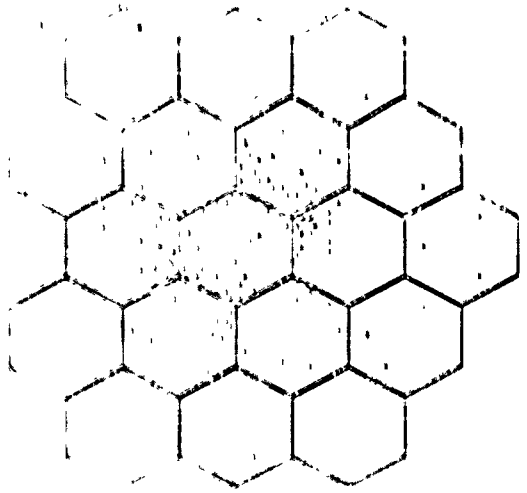

SIGMA 1
MAX VALUE IS [illegible]

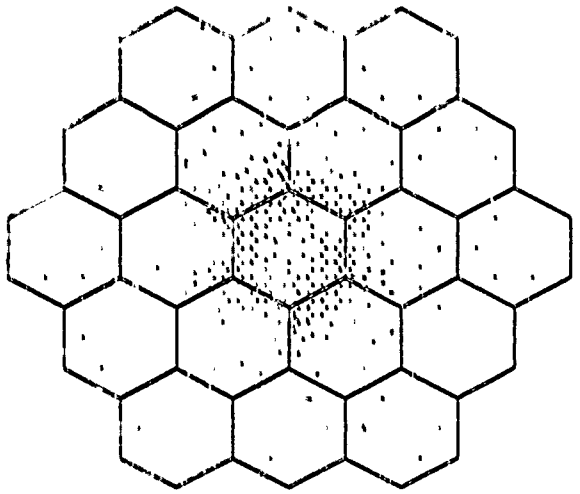

SIGMA 2
MAX VALUE IS 90742

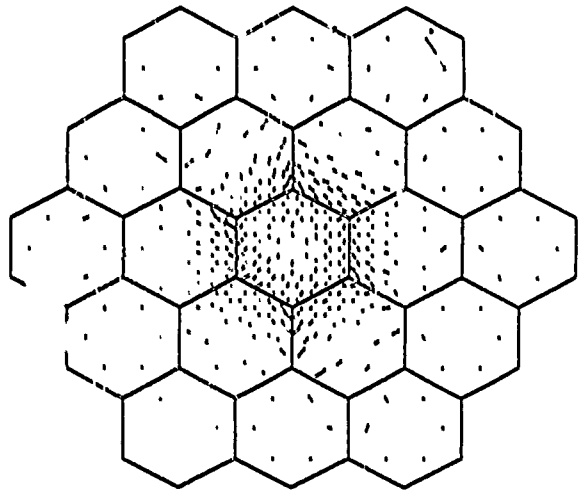

TAU MAX
MAX VALUE IS 50184

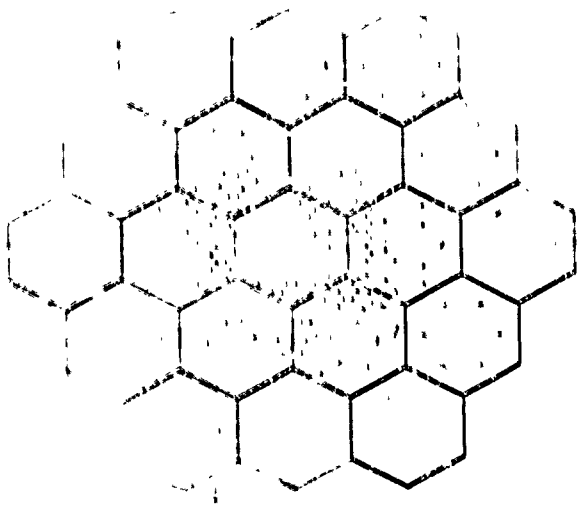

SIGMA 1
MAX VALUE IS 79720

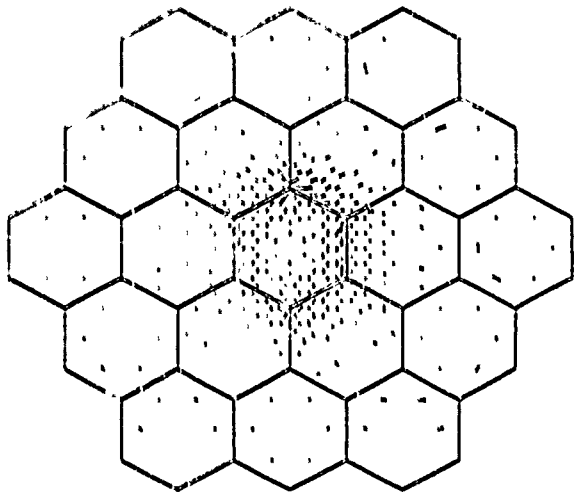

SIGMA 2
MAX VALUE IS 86494

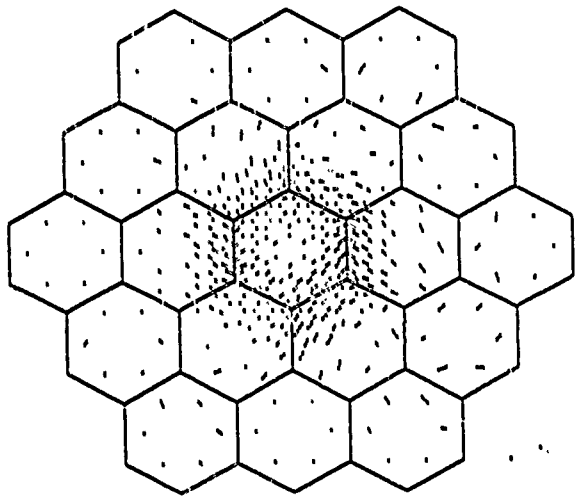

TAU MAX
MAX VALUE IS 42792

FIG. 26

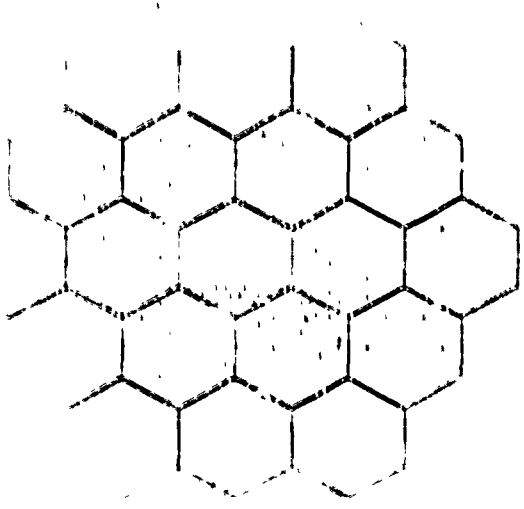

SIGMA 2
MAX VALUE IS .99667

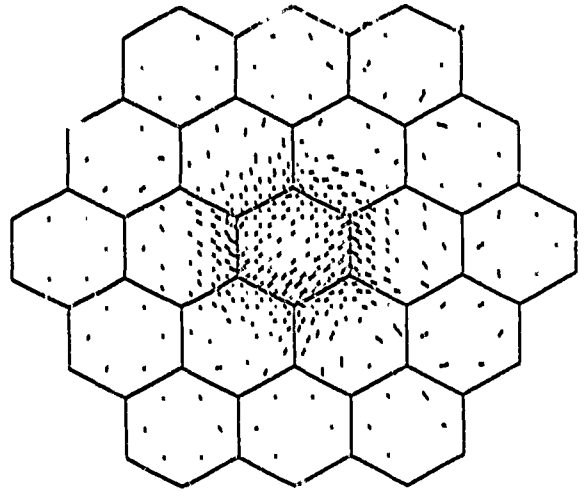

TAU MAX
MAX VALUE IS .49976

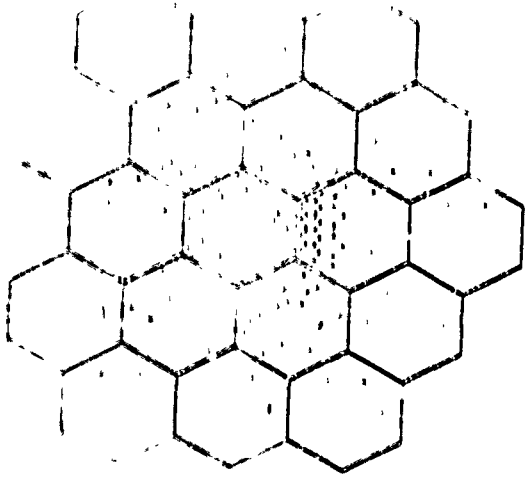

SIGMA 2
MAX VALUE IS .97164

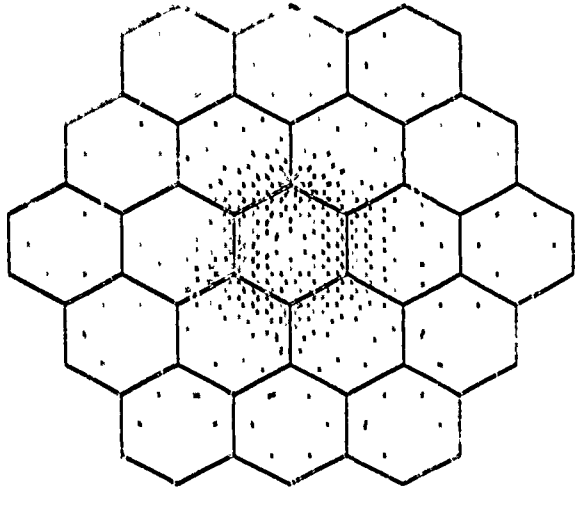

TAU MAX
MAX VALUE IS .53957

R

FIG. 21

105

Security Classification

DOCUMENT CONTROL DATA - R & D

Security classification of title, body of abstract and indexing annotation must be entered when the overall report is classified

1. ORIGINATING ACTIVITY (Corporate author)	2a. REPORT SECURITY CLASSIFICATION
The Pennsylvania State University	Unclassified
	2b. GROUP

3. REPORT TITLE

A Study of a Two-Dimensional Finite Element Model of a Ceramic Body.

4. DESCRIPTIVE NOTES (Type of report and inclusive dates)

Technical Report # 5

5. AUTHOR(S) (First name, middle initial, last name)

H. A. McKinstry, H. E. Shull, and W. R. Buessem

6. REPORT DATE	7a. TOTAL NO. OF PAGES	7b. NO. OF REFS
March 30, 1972	62	11

8a. CONTRACT OR GRANT NO.	9a. ORIGINATOR'S REPORT NUMBER(S)
N00014-67-A-0385-0004	
b. PROJECT NO. ONR 032-509	
c.	9b. OTHER REPORT NO(S) (Any other numbers that may be assigned this report)
d.	

10. DISTRIBUTION STATEMENT

Distribution of this document is unlimited; reproduction in whole or in part is permitted for any purpose of the United States Government.

11. SUPPLEMENTARY NOTES	12. SPONSORING MILITARY ACTIVITY
	Department of the Navy Office of Naval Research, Metallurgy Program Washington, D. C. 20360

13. ABSTRACT

The elastic behavior of a ceramic body has been modeled by use of the finite element method. The model simulates a set of nineteen hexagonal crystals whose elastic and thermal properties can be independently varied. Several different configurations of the elastic properties of the crystals were evaluated under conditions of isostatic, uniaxial and thermal loadings. The effect of anisotropy shifts the position where the maximum shear acts in the model, under isostatic and thermal loadings.

DD FORM 1473 (PAGE 1)

S/N 0101-807-6801

Security Classification

A-31408

14 KEY WORDS	LINK A		LINK B		LINK C	
	ROLE	WT	ROLE	WT	ROLE	WT
Model of ceramic body						
Anisotropy						
Thermal loading and anisotropy						
Thermal anisotropic forces						